

https://dspace.org/

Alternatives to distillation: multi-membrane permeation and petrol pre-blending for bio-ethanol recovery

Stacey, Neil Thomas

2016

http://hdl.handle.net/10539/20993

Stacey, Neil Thomas (2016) Alternatives to distillation: multi-membrane permeation and petrol pre-blending for bio-ethanol recovery, University of Witwatersrand, Johannesburg, <http://wiredspace.wits.ac.za/handle/10539/20993>

Downloaded from a DSpace repository. https://dspace.org/

Alternatives to Distillation:

Multi-membrane permeation and petrol pre-blending for bio-ethanol recovery

By

Neil Thomas Stacey

A thesis submitted for the degree of Doctor of Philosophy

To

The Department of Chemical and Metallurgical Engineering

Faculty of Engineering, University of the Witwatersrand,

Johannesburg

Copyright Notice

The copyright of this thesis vests in the University of the Witwatersrand, Johannesburg, South Africa, in accordance with the University's Intellectual Property Policy. No portion of the text may be reproduced, stored in a retrieval system, or transmitted in any form or by any means, including analogue and digital media, without prior written permission from the University. Extracts of or quotations from this thesis may, however, be made in terms of Sections 12 and 13 of the South African Copyright Act No. 98 of 1978 (as amended), for non-commercial or educational purposes.

Full acknowledgement must be made to the author and the University.

An electronic version of this thesis is available on the Library webpage (www.wits.ac.za/library) under "Research Resources".

For permission requests, please contact the University Legal Office or the University Research Office (www.wits.ac.za).

Abstract

Separation of materials is crucial to the operation of the majority of chemical processes, not only for the purification of final products but also for the processing of feed-stocks prior to chemical reaction. The most commonplace method of materials separation is distillation which, unfortunately, is often an energy-intensive process and contributes significantly to mankind's energy consumption and carbon dioxide emissions.

Alternative approaches to separation are therefore a crucial element of the ongoing pursuit for sustainability in chemical industries. There are two principal ways of going about this. The first is to replace distillation units with alternative unit operations that can achieve the same separation with less energy expenditure. The second approach is overall flowsheet revision, fundamentally changing a separation cycle to minimize its energy requirements.

The greatest improvements to energy efficiency will be achieved by applying both approaches in tandem. However, each must be developed separately to make that possible.

This thesis lays the groundwork for radical revision of major separation operations by showcasing a new overall flowsheet for bioethanol separation that promises tremendous improvements in separation efficiency, reducing the energy usage involved in ethanol purification by as much as 40% in some scenarios.

It also develops a novel method for the design of multi-membrane permeation units, showing how area ratio can be manipulated to fundamentally alter separation performance from such units, resulting in superior separation performance to conventional units, achieving higher recoveries than conventional setups.

With membranes being an increasingly popular separation method, the potential for superior performance from multi-membrane units promises improvements in separation efficiency.

Keywords

Fuels, Biofuels, Ethanol, Bio-ethanol, Process Synthesis, Sustainability, Green Technology, Separation, Membranes, Multi-Membrane Permeation, Residue Curve Maps

Declaration

I declare that except where acknowledged, this thesis is my own un-aided work.

It is being submitted for the degree of Doctor of Philosophy in Engineering at the University of the Witwatersrand, Johannesburg. It has not been submitted before for any degree or examination in any other University.

_____

Neil Stacey

_____day of _____year_____

Publications emanating from this research

Patents

N.T. Stacey, A. Hadjitheodorou, and D. Glasser. Patent application SA 2015/02097: "petrol-ethanol mixtures", filed in April 2015 with the South African patent office

Peer-reviewed journal articles

N. T. Stacey, M. Peters, D. Hildebrandt, and D. Glasser, "Synthesis of Two-Membrane Permeation Processes Using Residue Curve Maps and Node Classification," *Ind. Eng. Chem. Res.*, vol. 52, no. 41, pp. 14637–14646, 2013.

Conference presentations

N. T. Stacey, A. Hadjitheodorou, M. Peters, D. Hildebrandt, and D. Glasser, "Energy-efficient bio-ethanol recovery", AIChE annual meeting, 2012.

N. T. Stacey, A. Hadjitheodorou, M. Peters, D. Hildebrandt, and D. Glasser, "Obtaining a petrol/ethanol blend from a fermentation liquor with reduced energy", SAIChE annual meeting 2012.

N. T. Stacey, M. Peters, D. Hildebrandt, and D. Glasser,
Gas separation of ternary systems in a single permeator with two membranes using residue curve maps", AIChE Spring Meeting 2011.

Acknowledgments

This thesis is a product of tumultuous times. While writing it, I have seen the closure of my research group and departure of my supervisors, as well as the appointment of a new Head of School and a new Dean of Faculty amidst departmental strife.

Any obstacle can be overcome by sufficient stubbornness, however, and my time as a free-range postgrad turned out to be productive, leading to Wits filing a patent on the bioethanol separation process detailed in this thesis. I also managed to procure corporate investment in a project to further develop and commercialize the technology just in time to capitalize on new legislation mandating ethanol blending in petrol.

The combination of South Africa's worst drought in two decades and record low oil prices has since led to the shelving of most prospective projects for ethanol production in South Africa, making for a difficult market for new bioethanol technology. However, market conditions will doubtless change in coming years and I am confident that our technology has the capacity to contribute meaningfully to the pursuit of the region's environmental and economic goals. It took the efforts of many to make the development of this technology possible in such difficult circumstances.

First and foremost, I would like to thank my supervisors, Prof. David Glasser, Prof. Diane Hildebrandt and Dr. Mark Peters. Without them I would never have had the opportunity to pursue this degree and its completion would have been impossible without their encouragement.

Next I would like to offer my thanks to the Vice-Chancellor and Principal of the university, Prof. Adam Habib, along with Deputy Vice-Chancellor, Prof. Rob

Moore. Their timely intervention ensured that that the postgraduate students from the COMPS research group, including myself, were not left without funding and support following the closure of the research group. I hope and believe that we have, as a group, rewarded the faith shown in us under difficult circumstances.

Finally I would like to acknowledge the gratefully appreciated financial contributions of the National Research Foundation (NRF).

Contents

Copyright Notice i
Abstract ii
Keywords iii
Declaration iv
Publications emanating from this research v
Acknowledgments vi
List of Figures xi
List of Tables xiii
Nomenclature xiv
Chapter 1. Introduction and literature review 1
1.1 Background 1
1.2 Objectives of thesis 3
1.3 Conventional bioethanol purification processes 3
1.4 Membrane processes 6
1.4.1 Membrane Residue Curve Maps (M-RCMs) 7
1.4.2 Stationary points 8
1.4.3 Multi-membrane separation 9
1.4.4 Asymmetric configuration of two-membrane permeator 11
1.4.5 Internally-staged membrane separators 12
1.4.6 Physical equipment 13
1.4.7 Combined-permeate two-membrane permeator 14
CHAPTER 2. Pre-blending for energy-efficient bioethanol recovery 16
2.1 Introduction 16
2.2 Flow-sheeting 17
2.2.1 Conventional approach; purify then blend 17
2.2.2 Revised overall flowsheet 18
2.3 Phase behaviour 19
2.3.1 Requirements for useable fuel 22
2.4 Process flow-sheeting and modelling 23
2.5 Results and discussion 28

2.6 Conclusions 32
Chapter 3. Detailed investigation of process variables for direct blending of ethanol and petrol 34
3.1 Stability requirements 35
3.2 Modelling 36
3.3 Process Variables 40
3.3.1 Blending ratio 41
3.3.2 Pressure 41
3.3.3 Temperature 41
3.3.4 Number of stages 41
3.4 Context 42
3.4.1 The South African context 42
3.4.2 The American context 43
3.5 Effects of individual parameters: results and discussion 44
3.5.1 Blending ratio and number of stages 44
3.5.2 Pressure 46
3.5.3 Temperature 46
3.6 Improvements to basic process 48
3.6.1 Temperature Swing process 48
3.6.2 Lower ethanol content for South African context 51
3.7 Conclusions 53
Chapter 4. Multi-membrane Residue Curve Maps 56
4.1 Introduction 56
4.2 Derivation of Residue Curve Equation and choice of flux model 60
4.3 Permeation modeling 62
4.4 Simple permeation model 63
4.5 Location of Stationary points 66
4.6 Manipulation of RCM topography and classification of nodes 66
4.6.1 Vector notation for relative permeability 66
4.6.2 Plotting of residue curve maps 67
4.7 Effect of varying area ratio on topography 71
4.8 Classification of nodes and use of eigenvalue plots for synthesis 72
4.9 Comparison of continuous processes 76
4.9.1 Separate permeate streams 81

4.10 Conclusions....89
Chapter 5. Quaternary mixtures and complex permeation....92
5.1 Complex permeation modelling....92
5.2 Additional stationary points....93
5.3 Complex behaviour....94
5.3.1 Combination of two membranes with complex permeation....98
5.4 Qaternary mixtures....99
5.5 Shortcut node classification: flux criterion....102
5.5.1 Implications of shortcut node classification....113
5.5.2 Shortcut node classification with complex permeation....115
5.6 Discussion....118
Chapter 6. Concluding Remarks....120
6.1 Energy-efficient bioethanol recovery....120
6.2 Multi-membrane permeation design methodology....123
References....126
Appendix A: Raw stream data....132

List of Figures

Figure 1.1:Typical bioethanol purification process using three distillation columns in sequence. 4
Figure 1.2: Schematic of single-membrane permeator 9
Figure 1.3: Two-membrane permeator in asymmetric configuration 11
Figure 1.4: Internally-staged membrane setup....12
Figure 2.1: Flowsheet for ethanol purification and 2.1b: extended flowsheet for actual ethanol useage....18
Figure 2.2: Revised overall flowsheet for bioethanol separation....19
Figure 2.3: Liquid phase behaviour of Gasoline/Ethanol/Water mixture at 25°C and 1atm temperature, using the UNIQUAC model, fitted to experimental results from Rahman et al. [24]. This experimental data can be viewed in Figure 3.3. *Phase behaviour diagram provided by Aristoklis Hadjitheodorou, additional notations by Neil Stacey 21
Figure 2.4: Conventional distillation Process Flowsheet. One primary disitillation column is depicted for convenience. In practice, multiple columns in sequence are often used. 23
Figure 2.5: Proposed alternative process: conventional separation methods are used to produce an azeotropic mixture which is then blended in a two-stage liquid-liquid extraction process....26
Figure 2.6: Single-stage petrol pre-blending flowsheet for simulation....27
Figure 2.7: Two-stage petrol pre-blending flowsheet for simulation 27
Figure 2.8: Flowsheet for a two-stage petrol blending process with blending ratio of 7.1. Flow-rates are given on a volumetric basis as a ratio to the initial flow-rate of the ethanol feed stream. 28
Figure 2.9: Flowsheet for a two-stage petrol blending process with blending ratio of 7.1. Flow-rates are given on a volumetric basis as a ratio to the initial flow-rate of the ethanol feed stream. 29
Figure 2.10: Two-stage petrol pre-blending separation process represented on triangular composition diagram. Feed compositions are pure petrol and an azeotropic ethanol blend, respectively.....30
Figure 3.1: Overall process flowsheet for efficient bioethanol separation using ethanol pre-blending....34
Figure 3.2: Process flowsheet for ethanol/petrol blending step 35
Figure 3.3: Phase equilibrium diagrams for water/ethanol/iso-octane and water/ethanol/petrol systems. Source: Rahman et al. (2007)....37
Figure 3.4: Single-stage process flowsheet for simulation 39
Figure 3.5: Two-stage process flowsheet for simulation 39
Figure 3.6: Multi-stage column process flowsheet for simulation....40

Figure 4.1: sketch of a batch, two-membrane permeator in an asymmetric configuration 60
Figure 4.2: Simple M-RCM with α= [0.7, 1, 4] 67
Figure 4.3: Simple M-RCM with α= [2, 1, 0.4] 68
Figure 5.1: Single-membrane M-RCM with complex permeation. α = [10, 1, 0.1], γ_(C,B) = 3 94
Figure 5.2: Single-membrane M-RCM with α = [0, 1, 0.3] 95
Figure 5.3: Two-membrane M-RCM; Membrane One: α = [10, 1, 0.1] and γC,B = 3; Membrane Two: α = [0.1, 1, 0. 3], E=1 96
Figure 5.4: Two-membrane MM-RCM; Membrane One: α = [10, 1, 0.1] and γC,B = 3; Membrane Two: α = [0.1, 1, 0. 3], E=5 97
Figure 5.5: M-RCM with complex behaviour. α = [0.1, 1, 0. 3] and γA,C = 1 98
Figure 5.6: Two-membrane M-RCM; Membrane One: α = [10, 1, 0.1] and γC,B = 3; α = [0.1, 1, 0. 3] and γA,C = 1, E=2 99
Figure 5.7: Eigenvalue method and Flux criterion plotted on same axes: Membrane One: α = [1, 1.5, 2, 4]; Membrane Two: α = [1,0.8,0.63,0.37] 110
Figure 5.8: Eigenvalue method and Flux criterion plotted on same axes: Membrane One: α = [6, 1.5, 2, 4]; Membrane Two: α = [2, 1.8, 0.63, 0.37] 112
Figure 5.9: Total flux along B-C axis of a membrane permeation system with α = [10, 1, 0.1] and $\boldsymbol{\gamma C, B}$ = 3. Dashed lines to indicate location of additional node 117

List of Tables

Table 2.1: Structural parameters of Pure Components for UNIQUAC model 20
Table 2.2: Binary interaction parameters for UNIQUAC model 20
Table 2.3: Energy requirements of azeotropic distillation 24
Table 3.1: Effect of blending ratio on ethanol recovery and content 44
Table 3.2: Effect of pressure on process performance 46
Table 3.3: Effect of temperature on liquid-liquid phase-split 47
Table 3.4: Performance of three-step, two-step and single-step decanting processes producing fuel mixture at ambient temperature 50
Table 3.5: Effect of lower initial ethanol content on 2-stage counter-current liquid-liquid extraction 52
Table 4.1: Properties of nodes in different operating regions 75
Table 5.1: relative permeabilities for polyethylene, 4-methylpentene and cellulose acetate 100
Table 5.2: Node classification for Silicone rubber and Cellulose Acetate 100
Table 5.3: Node classification for 4-methylpentene and Cellulose Acetate 101
Table 5.4: Relationship between total flux and relative permeability vector 104
Table 5.5: relationship between eigenvalue properties and relative permeability vector 106
Table 5.6: Comparison of node properties predicted by different methods for two membranes with α = [1, 1.5, 2, 4] and α = [1,0.8,0.63,0.37] respectively 110
Table 5.7: Comparison of node properties predicted by different methods for two membranes with α = [6, 1.5, 2, 4] and α = [2, 1.8, 0.63, 0.37]] respectively 112

Nomenclature

Scalar quantities represented in *italics*

Vector quantities represented in **bold**

When membrane or phase numbers are given as a superscript, they are given in **bold** so as to distinguish them from exponents

Symbols

A	Membrane area [m^2]
E	Relative ease of permeation
F	Feed flow-rate [*mol/s*]
J	Membrane flux $\left[\frac{mol}{s.m^2}\right]$
J^r	Relative Membrane flux $\left[\frac{mol}{s.m^2}\right]$
J_i	Flux of component i through membrane [*mol/s*]
$\boldsymbol{J^{mn}}$	Flux through membrane n $\left[\frac{mol}{s.m^2}\right]$
L	(distillation; continuous) Liquid flow-rate [*mol/s*]
L	(distillation; batch) Liquid hold-up [*mol*]
R	(membrane; continuous) Retentate flow-rate [*mol/s*]
R	(batch; membrane) Retentate hold-up [*mol*]

p_i^0	Saturation pressure of component i [bar]
P^{mj}	(membrane; continuous) Permeate flow-rate in permeate phase j [mol/s]
$\dot{P}^{mj}$	(membrane; batch) Permeate Removal rate through membrane j [mol/s]
r	Pressure ratio
s	Membrane split ratio
V	(distillation; continuous) Vapour flow-rate [mol/s]
$\dot{V}$	(distillation; batch) Vapour Removal rate
x	Fluid molar composition
$\mathbf{x}$	(membrane) molar composition vector of Retentate
$\mathbf{x}$	(distillation) molar composition vector of liquid
y_i	(distillation) mole fraction of component i in vapour
y_i	(membrane) mole fraction of component i in permeating material
$\mathbf{Y}^{mj}$	(membrane) molar composition vector of Permeate phase j
$\mathbf{y}$	(distillation) molar composition vector of vapour
$\mathbf{y}^{mj}$	(membrane) molar composition vector of material permeating through membrane j

$\boldsymbol{K}$	Molar composition vector of intermediate phase in internally-staged permeator

Greek Letters

α_i^D	Relative volatility for distillation
$\boldsymbol{\alpha}_i^D$	Relative volatility vector for distillation
$\alpha_{i,n}^M$	Relative permeability of component i through membrane n for membrane separation
$\boldsymbol{\alpha}_{i,n}^M$	Relative permeability vector of membrane n for membrane separation
δ	Membrane thickness $[m]$
π_L	Retentate (high) pressure $[bar]$
$\pi_{V,n}$	Permeate (low) pressure in phase n $[bar]$

Subscripts

D	Referring to distillation
i	Referring to component i
L	(membrane) Referring to Retentate
B	Referring to bottom of column
n	Referring to component n

Superscripts

T	Referring to top of column
M	Referring to membrane
$\boldsymbol{mn}$	Referring to permeate phase n, or to membrane n

Abbreviations

CPM	Column Profile Map
RCM	Residue Curve Map
D-RCM	Distillation Residue Curve Map
M-RCM	Membrane Residue Curve Map
MM-RCM	Multi-Membrane Residue Curve Map
DE	Differential Equation
CS	Column Section
M-RCM	Membrane Residue Curve Map
VLE	Vapour-Liquid Equilibrium
MBT	Mass Balance Triangle

Chapter 1. Introduction and literature review

1.1 Background

Rising energy costs and growing environmental consciousness have spurred a drive toward sustainability and energy efficiency in all aspects of chemical engineering processes. The need to alleviate fossil fuel dependency has driven the development of new processes with minimal environmental impact.

Renewability and energy efficiency have become key targets throughout the chemical engineering industry. This thesis serves to address this need by investigating alternatives to one of the most energy-intensive chemical processes: distillation. Distillation is the most widespread separation process in chemical engineering and represents a sizeable fraction of global energy usage, as much as 3% according to Hewitt et al [1].

Distillation depends on the evaporation of liquids and formation of gaseous products, making it an inherently demanding process in terms of energy usage. The development and optimization of alternatives promises to reduce the energy consumption of existing and future chemical processes. Thorough optimization of any chemical process involving distillation separation process must give due consideration to alternative separation methods.

One approach to alleviating fossil fuel dependency is the use of renewable biofuels to directly replace liquid fuels used in transportation. However, economic viability has proven a barrier to the widespread adoption of biofuels, even with the price of crude oil having risen sharply in recent decades.

Ethanol is the most commonly-used biofuel, with over 50 billion litres produced annually in the United States alone[2]. The distillation of a single litre of ethanol typically requires

between 4.6MJ and 9MJ, depending on the specifics of the process [3-6]. Considering that the combustion of a litre of ethanol produces around 20MJ of energy, this represents a significant total energy usage, amounting to almost half of the energy yield of the ethanol when burnt as a fuel. This doesn't even factor in energy inputs in other stages of the process, such as in the planting and harvesting of raw materials and the transportation of both raw materials and products. With such quantities of energy devoted to distillation, seeking alternative separation approaches is a clear avenue in the pursuit of cleaner and cheaper chemical processes.

If the energy consumption and cost of distillation can be reduced, the environmental impact of fuel usage will be directly reduced by cutting the carbon emissions involved in producing that energy. Beyond that, reducing the cost of bioethanol production promises to encourage increased implementation of bioethanol usage, further reducing carbon emissions.

The large scale of existing bioethanol production offers a ready market for new separation processes for bioethanol, and improvements to the bioethanol purification process promise to yield significant financial and environmental benefits. In light of this, Chapters 2 and 3 of this thesis develop and examine a radical new approach to bioethanol recovery which has the potential to significantly reduce the energy consumption and cost of the process.

Chapters 4 and 5, on the other hand, deal with separation technology in a more general sense by examining multi-membrane permeation, an under-utilised separation technique that makes use of multiple membranes in a single unit in order to perform separations for which those membranes in isolation are not suitable. In this way, challenging separations can be performed using relatively simple equipment.

1.2 Objectives of thesis

This thesis aims to reduce energy consumption in the chemical industry by improving the efficiency of separation processes.

This will be achieved firstly through the examination of petrol pre-blending for bio-ethanol recovery, a concept capable of significant savings in an energy-intensive process.

By examining separation performance improvements from multi-membrane permeation, this thesis aims to demonstrate that more efficient separations can be achieved using this under-utilized separation technology. Further, by developing a rapid methodology for evaluating and designing multi-membrane permeation processes, this thesis aims to facilitate the adoption of this separation technology for applicable chemical processes.

With membrane permeation becoming an increasingly widespread separation method, the development of more sophisticated and efficient membrane units promises to improve separation efficiency in key areas of the chemical industry.

1.3 Conventional bioethanol purification processes

Ethanol cannot be fully purified using conventional distillation because of the existence of a binary azeotrope between ethanol and water. The azeotrope occurs at a composition of approximately 95% ethanol and 5% water by volume, and limits the purification to this composition when only conventional distillation is used.

Consequently, additional process complexity is required to produce ethanol of higher purity. A commonly-used method for this is to add an additional chemical species to the mixture to act as an entrainer, eliminating the azeotrope by altering the phase equilibrium behaviour. This makes it possible to obtain pure ethanol as a distillation product. However, the other product stream from such a process will contain a mixture of that entrainer and water, and the entrainer must then be separated from water in order to be recycled to the process. This results in a process with a number of distillation columns. A typical configuration is shown in Figure 1.1.

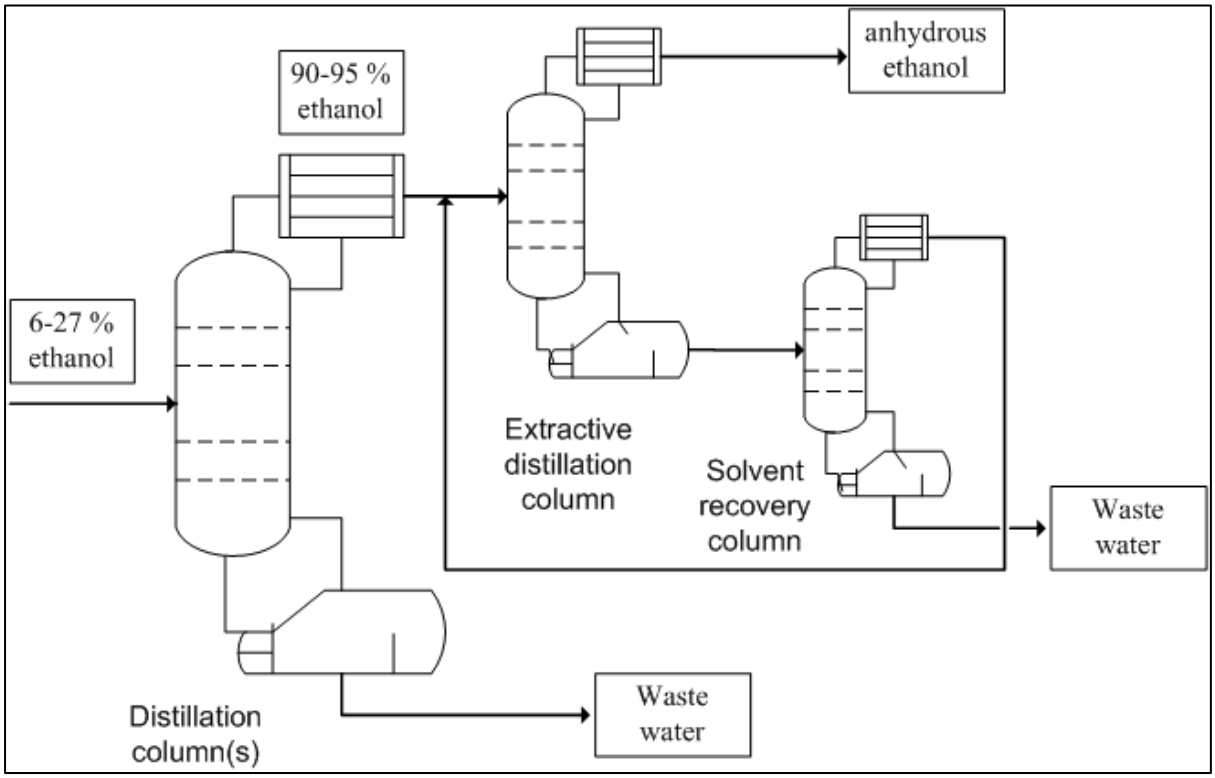


Figure 1.1:Typical bioethanol purification process using three distillation columns in sequence.

The first distillation column serves to purify ethanol to the azeotropic composition. While one column can be used for the initial purification as shown in Figure 1-1, in some processes, more than one column is used for this step [3-7].

The primary separation step typically uses between 2.8MJ and 7MJ per litre of ethanol produced, whereas the extractive distillation, which is eliminating only a small amount of remaining water, typically uses between 0.9MJ and 2.2MJ per litre [2-6]. This means that a sizeable fraction of the total separation energy is used to remove only the last 0.3% to 3.2% of the water.

The final purification step thus exhibits the greatest inefficiency because of the effects of azeotropic phase behaviour. Therefore, it is this step where alternative separations can be implemented most cost-effectively.

Distillation remains in wide use because it is cost-effective and scalable, hence the slow pace of its replacement by more energy-efficient processes. The final and most inefficient distillation step is the portion of the process where an alternative separation method is most likely to outperform distillation.

It seems highly probable that alternative separation methods will for the time being prove to be more efficient than distillation for this final step, but that distillation will remain preferable for the initial separation, resulting in hybrid processes incorporating units of different separation methods.

Consequently, the most likely avenue for introducing new separation methods is to initially replace just the final purification step of the process. Chapters 2 and 3 of this thesis will focus on developing a novel energy-efficient alternative to the purification of the azeotropic ethanol mixture.

1.4 Membrane processes

Separation of materials is critical to any chemical engineering project, not only in obtaining pure products, but also in supplying appropriate feed materials to reactors and in eliminating corrosive substances that may prove harmful to equipment downstream. Improvements in separations equipment offer benefits both direct and indirect.

Membrane permeation has shown great promise as a separation method, and has already been adopted in a number of industries[8]. Membrane technology, therefore, is an area of particular interest to researchers investigating more efficient separation methodologies. Improved membrane performance results in reduced pumping costs and energy utilization, a result with broad implications across each facet of the chemical industry that makes use of membranes.

Membrane research tends to focus on the development of new membranes and of new fabrication techniques for membranes. Utilizing new membrane materials in an existing permeator design will result in improved separation performance.

However, there is an alternative avenue for improvement that has been largely neglected in existing research. In this thesis, I examine ways to achieve better separation performance by using more sophisticated permeator designs. Multi-membrane permeation is one example of a sophisticated membrane setup that is capable of achieving better performance using the same membranes.

I intend to demonstrate that the use of more sophisticated membrane setups offers the possibility of not only making separation processes more economical but also of making new separations possible using membranes previously considered unsuitable for those separations.

To facilitate implementation of these permeator designs, I also present a rapid design methodology to assist in the design and evaluation of multi-membrane permeator design.

A number of different types of membrane separation processes exist, including reverse osmosis, electrodialysis, pervaporation and gas separation, each applicable to a particular phase or type of material. This thesis focuses on gas-diffusion membranes, but the synthesis methods will be developed in such a way as to be applicable to most, if not all, membrane types.

As with any other piece of equipment, the design of membrane separators requires consideration of capital and running costs. Running costs arise because of the pumping required to maintain a pressure difference between the permeate and retentate phases, as well as replacement of membranes as they are prone to wear.

Capital costs include the cost of the vessel and the cost of membrane material. Highly selective membranes tend to be more costly, and when such are used they tend to dominate the capital cost of the unit. Highly selective membranes also tend to have lower permeability [9], [10], so not only do such membranes cost more per unit area, but larger areas are required when such membranes are used. Aside from the capital costs involved in using high-selectivity membranes, their routine replacement can become a significant running cost.

It is clear, therefore, that capital and operating cost can be significantly reduced if it is possible to achieve a desired separation using cheap membranes of lower selectivity.

1.4.1 Membrane Residue Curve Maps (M-RCMs)

Residue Curve Maps (RCMs) were developed as a synthesis tool in the field of distillation[11]. Residue curves are trajectories mapping the change of liquid composition over time, as vapour is removed in a simple distillation operation. These maps offer insight

into a number of aspects of the separation of a mixture of chemical species, informing one of the feasibility of separation for various splits, and of the position and nature of azeotropes.

Membrane separation can be considered to be in some ways analogous to distillation, and Peters et al. [12] derived a residue curve equation for membrane separations, identical in form to the residue curve equation for distillation. M-RCMs exhibit many of the same properties as RCMs and have proven to be a useful analytical tool for the synthesis of membrane separation operations [13].

In Chapter 4 a residue curve equation is derived for multi-membrane permeators, extending the same simple synthesis techniques to more complicated membrane arrangements.

1.4.2 Stationary points

For a detailed examination of the topological properties of RCMs, the reader is referred to the work of Doherty et al.[14] For the purposes of this thesis it is important that the reader be familiar with some of the basic properties of such maps. In particular, the concept of stationary points and some knowledge of their nature is crucial to understanding the synthesis techniques developed, since they rely upon the classification of stationary points as a source of insight into a system's behaviour. Stationary points are locations on an RCM representing compositions at which the residue curve equation is equal to zero. In other words, these are points at which the composition of the material being studied is not changing, be it the liquid in a batch still or the retentate in a batch membrane operation. These points are of importance because they are nodes which govern the behaviour of the residue curves. These nodes can be classified as either stable, unstable or saddle points. An unstable node serves as the origin of all residue curves, while a stable node is a point where all curves terminate. Curves tend to approach a saddle point, but never reach it, instead moving away towards the stable node. For idealised models such as constant relative volatility (distillation) and constant relative

permeability (membrane separation), these nodes occur on the vertices of the mass balance triangle; in other words, at pure components.

It can be said that, since profiles approach the stable node, and terminate there, that a component which is a stable node can be readily obtained in the retentate, since the composition of the retentate will approach that composition. Similarly, the unstable node will tend to be purified in the permeate. It can also be said that the unstable node is the component which will be most readily removed from the retentate. Therefore, knowing the nature of the nodes offers one substantial insight into the behaviour of a membrane permeator.

1.4.3 Multi-membrane separation

Conventional separations operate on the basic principle of transferring material between two phases which have different compositions. In the case of distillation, these two phases are saturated liquid and vapour in equilibrium.

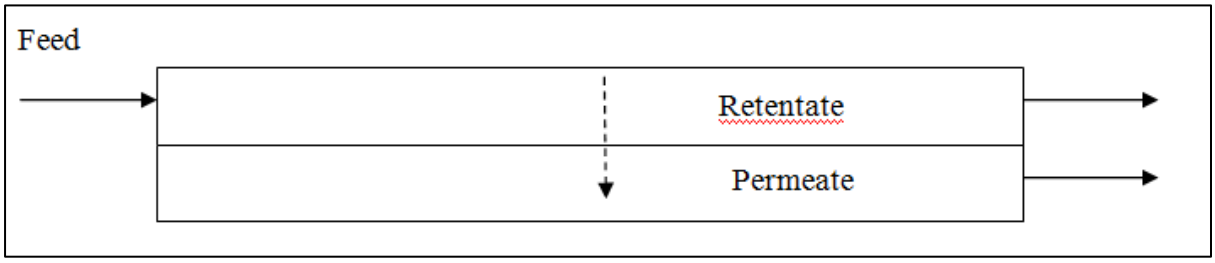


Figure 1.2: Schematic of single-membrane permeator

In the case of a conventional membrane permeator as shown in Figure 1.2, the two phases are the Retentate and Permeate phases, with material transferred by way of permeation through a membrane.

Multi-membrane permeators, however, can operate with three or more phases of material, divided by a sequence of two or more membranes. These membranes can be identical, or they can possess differing permeability flux properties. A number of different multi-membrane setups are possible. Some of these are described hereafter.

A key property of multi-membrane permeators is their capacity to produce three product streams, something which is impossible in a single-membrane unit.

1.4.4 Asymmetric configuration of two-membrane permeator

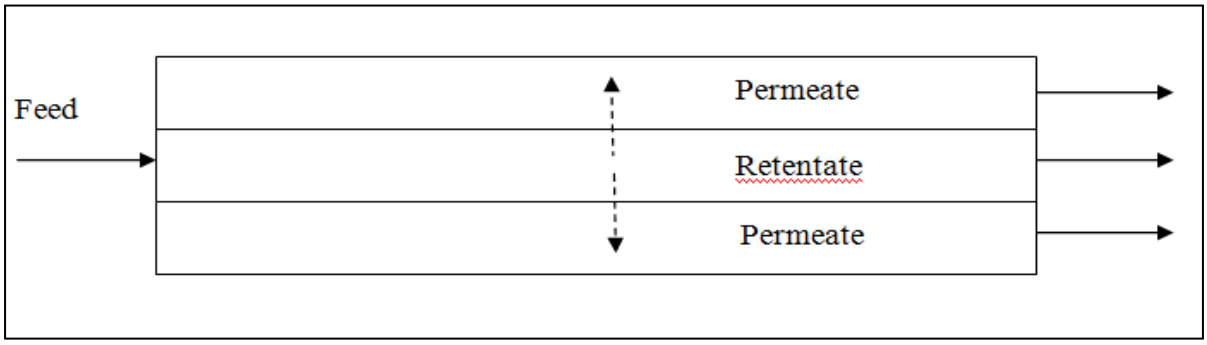


Figure 1.3: Two-membrane permeator in asymmetric configuration

Figure 1.3, where solid arrows show material streams and dotted arrows show the direction of permeation, displays a two-membrane permeator in an asymmetric configuration. A key feature to note is the fact that this membrane setup is capable of producing three separate product streams from a single unit as opposed to the two product streams to which a single-membrane permeator is limited.

Note also that in general, both permeate streams must be at a pressure lower than that of the retentate. Note that this is just one possible configuration of how such a system could be set up; a variety of flow regimes are possible, since it is not necessary for either of the permeate streams to run co-current to the retentate. Also, one is not limited to a single feed stream. Material can be fed to any number of the phases in the system.

Furthermore, such a setup can be readily extended to include more membranes, particularly if hollow membrane fibres are used in a shell and tube arrangement with the retentate stream in the shell. Such a setup makes it possible to increase the number of membrane types used

by simply incorporating additional membrane fibres, which can be withdrawn separately to yield separate permeate streams.

The principal focus of this thesis is on developing a shortcut technique for designing and synthesising two-membrane permeators in the asymmetric configuration and identifying scenarios where they will offer performance benefits over conventional approaches.

1.4.5 Internally-staged membrane separators

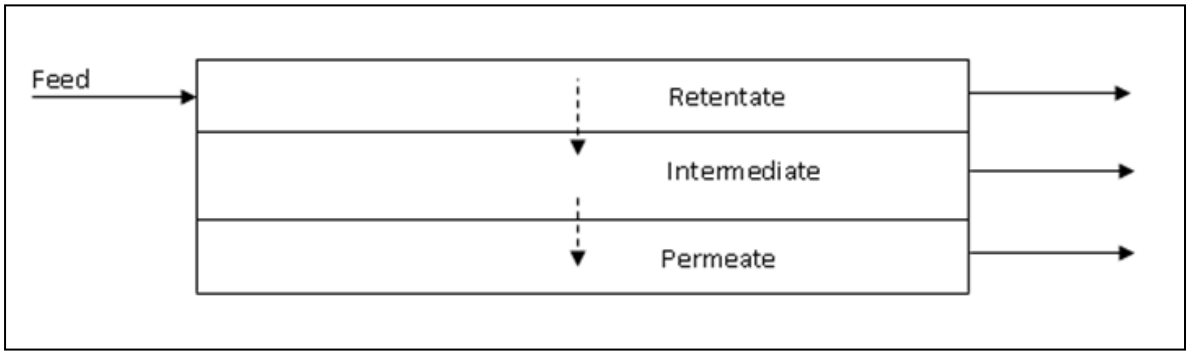


Figure 1.4: Internally-staged membrane setup

Figure 1.4, where solid arrows show material streams and dotted arrows show the direction of permeation, displays a possible configuration for an internally-staged membrane permeator. In this setup, the intermediate phase must be at a pressure higher than that of the permeate but lower than that of the retentate. Once again, one is not limited to this exact configuration, as multiple feed options and flow regimes are available. Although one is once again not limited to two membranes, arrangements with a high number of membranes staged internally are made problematic by the need for a pressure drop with each subsequent stage.

It must also be noted that the need for a pressure drop between each of the stages means that applying the vacuum permeate assumption becomes problematic when dealing with internally-staged setups. It is necessary to specify a non-zero pressure in the intermediate phase. As a result, the separation achieved by the first membrane will tend to be poor, since

the effectiveness of separation by membrane permeation depends on a high pressure ratio across the membrane[12].

This thesis does not examine the properties of internally-staged membrane permeators, but it must be remembered that they may offer high selectivity and should therefore be considered as a possible alternative to conventional membrane separations and to the equipment types which this thesis does examine. Further work investigating their properties is not without merit, and no method for synthesizing sophisticated membrane separations can be considered truly complete without a technique for evaluating the suitability of internally-staged permeators.

1.4.6 Physical equipment

The most common membrane module types are plate and frame, spiral-wound and hollow fibre [8]. A plate and frame setup exposes the retentate to flat sheets of membrane material. A spiral-wound module wraps sheets of membrane material around a central collection pipe through which the permeate stream flows, while a hollow-fibre module utilises a 'shell-and-tube' arrangement with hollow fibres of membrane material as the tubes within a larger shell.

Hollow-fibre modules offer the highest ratio of membrane area to unit volume and lend themselves readily to the asymmetric configuration of multi-membrane processes, since it is possible to simply pack additional fibre types into the shell, and to withdraw them separately in order to obtain separate permeate streams. In some cases, not all of the permeate streams are required and the requirement for multiple membrane types is related only to the effect on the retentate composition. In these cases, multiple permeates can be withdrawn jointly.

Such a setup, with only one permeate stream, would be no more complex than a simple permeator, providing that a hollow-fibre module is used. It is suggested that hollow-fibre

modules are held in mind when conceptualising asymmetric configuration processes described throughout this thesis.

Hollow-fibre modules are not, however, readily adapted to internally-staged permeation, so other module types must be considered. Flat sheet setups are convenient for internal staging, provided that similar areas are required for the two membranes. Concentric spiral-wound membranes and collection pipes would allow for a range of area ratios, but very high area ratios may prove problematic for such setups. Therefore, hybrid arrangements seem most appropriate for internally-staged membrane separations with very high area ratios. One could use a hollow-fibre module, but adapt the shell to serve as the inner pipe of a spiral-wound membrane module. This would yield a far higher area for the membrane used in the hollow-fibre form, allowing for high area ratios.

1.4.7 Combined-permeate two-membrane permeator

If the purification of the retentate is the chief objective of a two-membrane permeator unit, then it will not always be necessary to withdraw two separate permeate streams. Consider a shell-and-tube arrangement using hollow-fibre membranes, with the retentate in the shell, and two different types of membrane fibres forming the tubes. If the material flowing through the different membranes is withdrawn jointly, then the resulting equipment is no different to a single-membrane permeator, except that two different types of fibre are present. The number of inlet and outlet streams and the pumping requirements are all identical. However, two-membrane separation is taking place because separate permeate streams exist within the tubes. If such a system is able to achieve separations which are not possible in single-membrane permeators with existing membranes, then a dramatic simplification of equipment required for that separation is possible.

This setup also offers a convenient basis for comparison. The overall capital and running costs of such a unit can be considered to be more or less equivalent to those of a single-membrane permeator with the same membrane area. Consequently, performance improvements achieved by such a permeator in comparison to a conventional permeator will come without significantly altering the cost of separation.

If the retentate stream is in the tubes and the permeate in the shell, then an interesting scenario arises where two separate retentate streams exist, and only one combined permeate stream. This setup is still technically a form of multi-membrane permeation. However, with the assumption of vacuum permeate the composition of the permeate stream has no effect on permeation (see chapter 4 for a more detailed explanation of the vacuum permeate assumption). Such a setup would perform no differently to a pair of membrane permeators operating in parallel. This kind of process has been examined in prior research considering cascade structures of conventional membrane permeators and is therefore not of interest in this thesis.

Chapter 2. Pre-blending for energy-efficient bioethanol recovery

The contents of this chapter and of chapter 3 are the subject of a provisional patent application filed by the University of the Witwatersrand with the South African Patent Office in April 2015

*The phase equilibrium modelling used in this chapter is provided by Aristoklis Hadjitheodorou, a fellow PhD student at the University of the Witwatersrand. However, the concepts and flowsheets presented in this chapter are my own, and the investigations undertaken in this chapter were done solely by me. I also produced the entirety of the written content.

2.1 Introduction

The most prevalent use of bio-ethanol is not as a fuel in its pure form, but rather as an additive to petrol. Conventional processes, however, fully purify bio-ethanol prior to blending it into petrol. This is an energy-intensive and costly process and is typically achieved through distillation. In this chapter I examine the possibility of blending partially purified fermentation products directly into petrol, allowing the spontaneous liquid phase separation to eliminate the bulk of the remaining water without the addition of separation energy.

Fermentation has long shown promise as an inexpensive process for producing renewable fuel; a wide variety of biomass feed-stocks can be fermented to produce ethanol[15–17], and the process is relatively straightforward and inexpensive. Bio-ethanol is the most widely-used renewable fuel and its production accounts for billions of dollars per year. However, the net energy efficiency of bioethanol usage has been questioned and there remains a considerable need to optimize bioethanol production in order to maximize its energy efficiency and minimize its environmental impact[18], [19].

The nature of the fermentation process dictates that fermentation products are dilute, comprised primarily of water. In order for bioethanol to be used as a fuel, this water must be eliminated. This separation is conventionally achieved using distillation. Since distillation

requires the evaporation of liquids, it tends to require substantial energy inputs. This is exacerbated in this case by the high heat capacity of water and the existence of a binary azeotrope in the ethanol/water mixture, resulting in a particularly energy-intensive separation process. In this chapter I examine the possibility that some of this energy consumption can be alleviated by the use of simple flowsheet improvement.

2.2 Flow-sheeting

The conventional approach to bio-ethanol recovery is to fully purify ethanol from the fermentation products.

2.2.1 Conventional approach; purify then blend

Figure 2.1a shows the conventional approach to this separation: which is to consider pure ethanol as the end-product of the separation circuit. However, ethanol is most commonly used as an additive to petrol rather than as a pure fuel itself. Consequently, the overall process flowsheet can be considered to have an additional step, shown in Figure 2.1b.

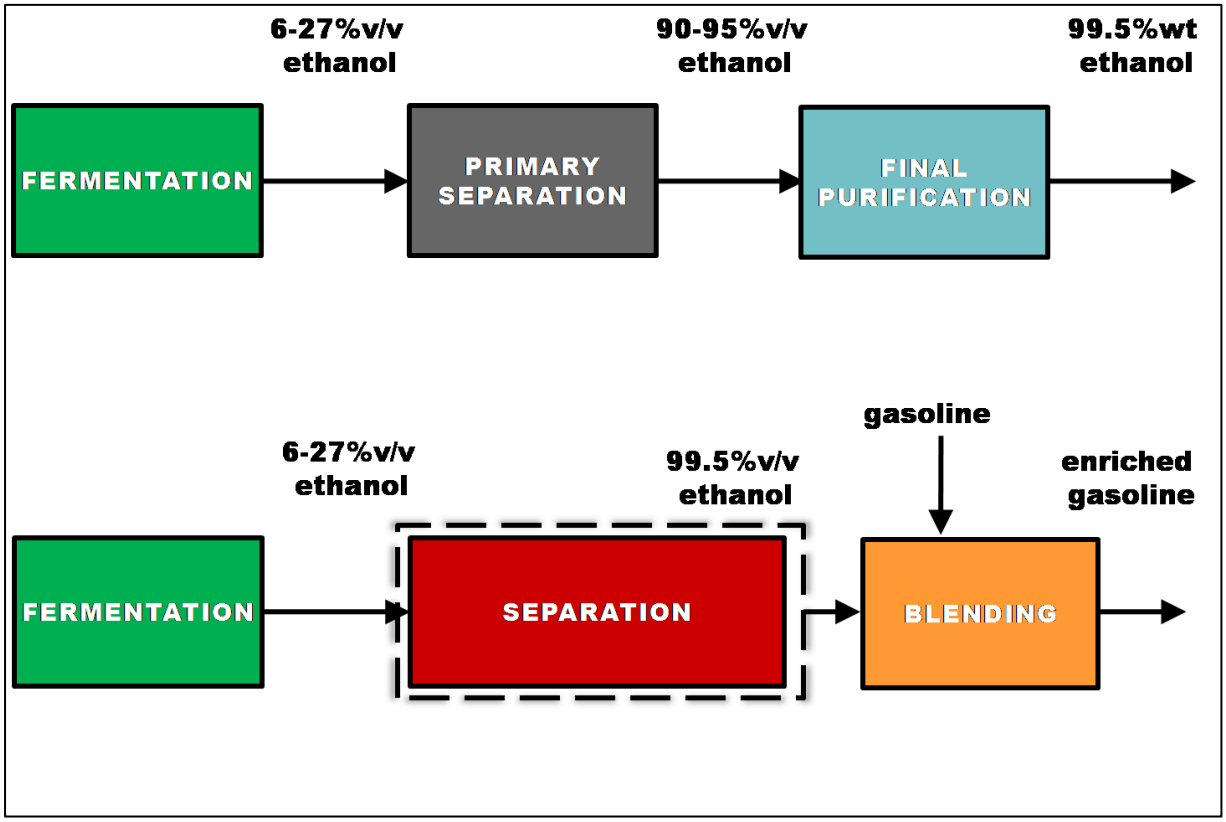


Figure 2.1: Flowsheet for ethanol purification and 2.1b: extended flowsheet for actual ethanol useage

However, if an ethanol-enriched fuel blend is the final product, then we are not restricted to flowsheets in which blending is the final stage and pure ethanol is produced as an intermediate. Blending could occur at an earlier stage in the process, potentially alleviating the energy requirements of separating pure components.

2.2.2 Revised overall flowsheet

Figure 2.2 shows a revised overall flowsheet for bioethanol production, taking into account the final useage of most bioethanol as a fuel additive. All existing processes for bio-ethanol purification are subsets of this flowsheet.

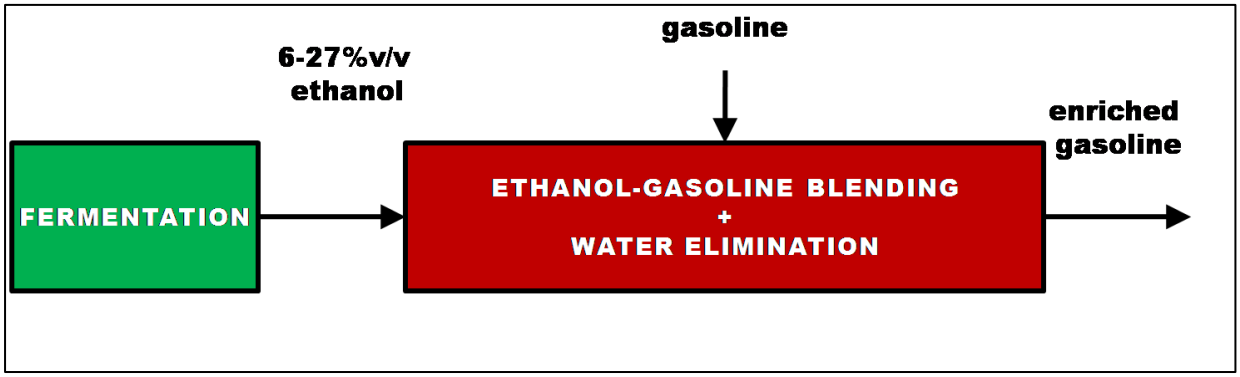


Figure 2.2: Revised overall flowsheet for bioethanol separation

This broad flowsheet permits a number of alternative approaches. For instance, one could blend fermentation products directly into petrol and then separate out a desirable fuel mixture. In fact, the same phase split which makes water a problematic impurity in petrol could be exploited to facilitate an energy-efficient separation; blending of water and petrol results in the formation of two separate liquid phases without the addition of any separation energy.

The revised overall flowsheet offers an enlarged optimisation space in which to search for improved processes. All processes discussed in this thesis are merely examples; doubtless there are numerous possibilities which have not occurred to me and it falls to future research to fully explore the bevy of possible processes.

2.3 Phase behaviour

Simulation of blending processes used the UNIQUAC thermodynamic model [20] to model phase equilibrium, using parameters fitted to experimental data provided from literature [21]. The fitted parameters are shown in Table 2.1 and Table 2.2.

Table 2.1: Structural parameters of Pure Components for UNIQUAC model

Component	***r***	***q***
Ethanol	2.11	1.97
Gasoline	4.55	2.55
Water	0.92	1.4

Table 2.2: Binary interaction parameters for UNIQUAC model

α_{ji}	***Ethanol***	***Gasoline***	***Water***
Ethanol	0	-199	157.12
Gasoline	619	0	950
Water	37.08	2300	0

These parameters are used for all modelling in this chapter, along with an assumption of ambient conditions of 25°C and 1atm pressure. A two-stage counter-current liquid-liquid extraction was simulated using a simple iterative scheme which reached convergence to 15 or more significant figures for all variables, with all material balances agreeing to 4 or more significant figures.

Figure 2.3 shows the liquid phase behaviour of a mixture of ethanol, water and petrol. The shaded region contains stable liquid mixtures while the unshaded region contains unstable liquid compositions, where a liquid-liquid phase-split will occur. The diagonal tie-lines within the unstable region denote how an unstable mixture will split and their end-points denote the compositions of the two resulting liquid phases. The dashed lines are mixing

vectors for blending with petrol, and unstable mixtures resulting from blending will split along tie-lines starting at points along these vectors.

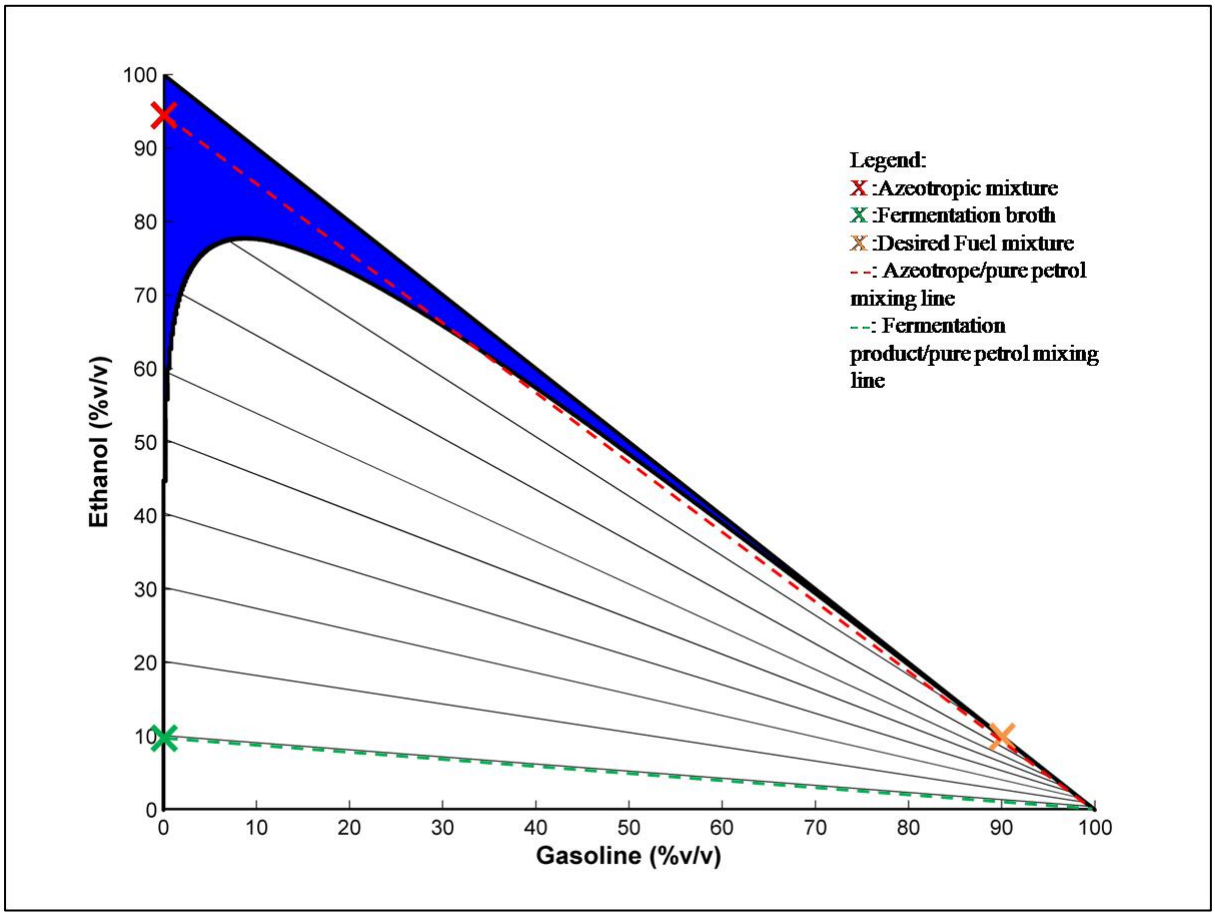


Figure 2.3: Liquid phase behaviour of Gasoline/Ethanol/Water mixture at 25°C and 1atm temperature, using the UNIQUAC model, fitted to experimental results from Rahman et al. [25]. This experimental data can be viewed in Figure 3.3. *Phase behaviour diagram provided by Aristoklis Hadjitheodorou, additional notations by Neil Stacey

Examination of this phase diagram reveals preliminary insights into the viability of this process. Firstly, blending fermentation products directly into petrol will not yield a high enough ethanol content to be worthwhile. However, blending an azeotropic mixture into petrol will result in the formation of a saturated hydrocarbon phase comprised predominantly of petrol but with some ethanol content. In other words, this phase-split yields a viable fuel mixture.

It must also be noted that the phase equilibrium behaviour of this mixture is highly dependent on a range of variables, not least of them temperature. Other factors are the precise makeup of the gasoline mixture, which is subject to considerable variance. Moreover, different brands of gasoline also include various proprietary fuel additives, further altering the phase equilibrium. Consequently, this phase equilibrium must considered to be a qualitative indication of the behaviour of this mixture, as opposed to a quantitative one.

2.3.1 Requirements for useable fuel

In order for a mixture to be usable as a fuel, it must form a single homogenous liquid phase. In other words, one requirement for a usable fuel is that the mixture lies outside the two-phase region at ambient conditions. Water in solution acts only as an inert diluent in a fuel mixture; it is only the liquid phase-split which affects engine function. Therefore, the boundary of the two-phase region is the threshold for a usable fuel, and this is the primary constraint on the water content of fuel. The same boundary is the limit of products obtainable by way of the naturally occurring phase separation.

This implies that a liquid phase separation will produce a hydrocarbon product which lies on the threshold of usability as a fuel. Any subsequent step to stabilize the fuel mixture will result in a mixture that is not susceptible to liquid phase separation at ambient conditions.

The final stabilisation step is discussed in detail in Chapter 3, but for now this conclusion is worth emphasizing; regardless of the specifics of the process leading up to the liquid phase separation, the hydrocarbon product of that separation will be a viable fuel with only minimal further processing.

2.4 Process flow-sheeting and modelling

With the bulk of the demand for ethanol already met by existing capacity, bioethanol producers have been reluctant to make the investments necessary to introduce new technology[22]. Because of this, a process which can be implemented by retrofitting existing plants is the ideal solution under current market conditions. Therefore, a simple approach is ideal, avoiding complex process equipment and significant investment.

Conventional processes make use of either one or two distillation columns to obtain an azeotropic mixture, and then use azeotropic distillation to achieve the final purification, as shown in Figure 2.3.

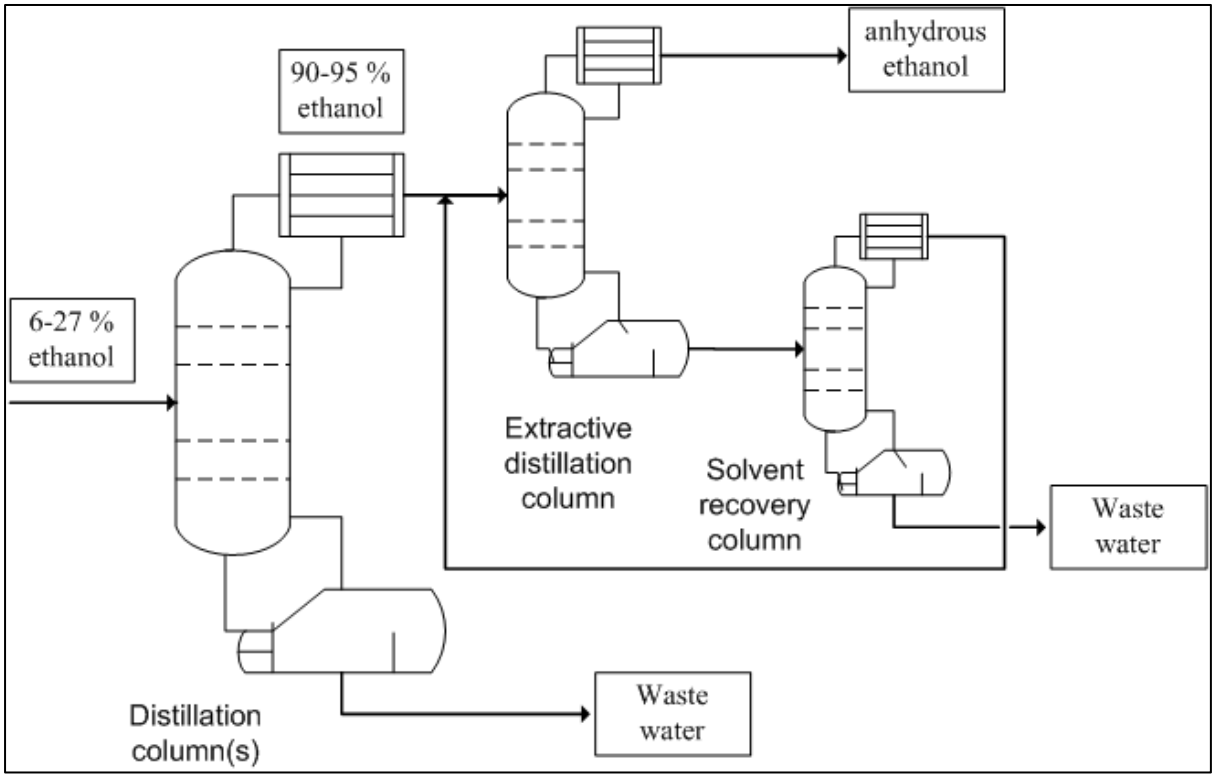


Figure 2.4: Conventional distillation Process Flowsheet. One primary disitillation column is depicted for convenience. In practice, multiple columns in sequence are often used.

The final purification from an azeotropic mixture is complicated by the azeotrope, which prevents conventional distillation from achieving further separation. As a result, an entrainer

is added for extractive distillation[23], [24] and must be recovered in an additional column. Even though only a fraction of the original water content remains to be eliminated, this last step contributes a significant portion of the separation energy requirements. Table 2.3 summarises the results of a literature review into the energy requirements of azeotropic distillation.

Table 2.3: Energy requirements of azeotropic distillation

Source	**Initial ethanol content**	**Energy to obtain azeotropic mixture**	**Energy requirement of azeotropic distillation**	**Percentage of separation energy**
Errico et al.[23]	14.6%	3.75MJ/*l* to 3.78MH/*l*	0.916MJ/*l* to 2.04MJ/*l*	19.6% to 35.1%
Vasquez et al.[24]	36.4%	2.86MJ/*l*	1.97MJ/*l*	40.8%
	26.5%	4.30MJ/*l*	1.96MJ/*l*	31.3%
	14.6%	3.82MJ/*l*	2.13MJ/*l*	35.8%
	6.20%	7.00MJ/*l*	2.01MJ/*l*	22.3%
Martinez et al.[25]	26.5%	6.93MJ/*l*	1.63MJ/*l*	19.7%
Garcia et al.[5]	94.8%	N/A	1.46MJ/*l*	17.3% to 33.8%*

Based on Table 2.3, replacing the final purification step with a simple liquid-liquid phase split will eliminate between 17.3% and 40.8% of the total separation energy, potentially saving between 0.916MJ and 2.04MJ per litre of ethanol produced. This assumes, however,

that it is possible to recover all of the ethanol in the fuel mixture. Any ethanol lost to a waste stream or recycled back to the distillation stage represents additional energy that is consumed without producing a product, adversely affecting the energy savings we are trying to achieve.

A single-stage phase split can be carried out in any vessel large enough for the task, but ethanol recovery from a single-stage setup may not be sufficient to improve the overall energy efficiency of the process. However, a two-stage counter-current liquid-liquid extraction still meets the requirement of suitability for retrofit of existing plants with only minimal expense.

The overall process shown in Figure 2.5 is an elegant refinement of existing processes. Equipment already in place is used for the bulk of the separation, but the final purification is replaced with a two-stage liquid-liquid extraction to transfer ethanol into gasoline in the overflow stream, while eliminating water in the underflow stream. The waste water stream will still contain ethanol and should therefore be recycled to the distillation circuit if possible, in order to improve overall ethanol recovery.

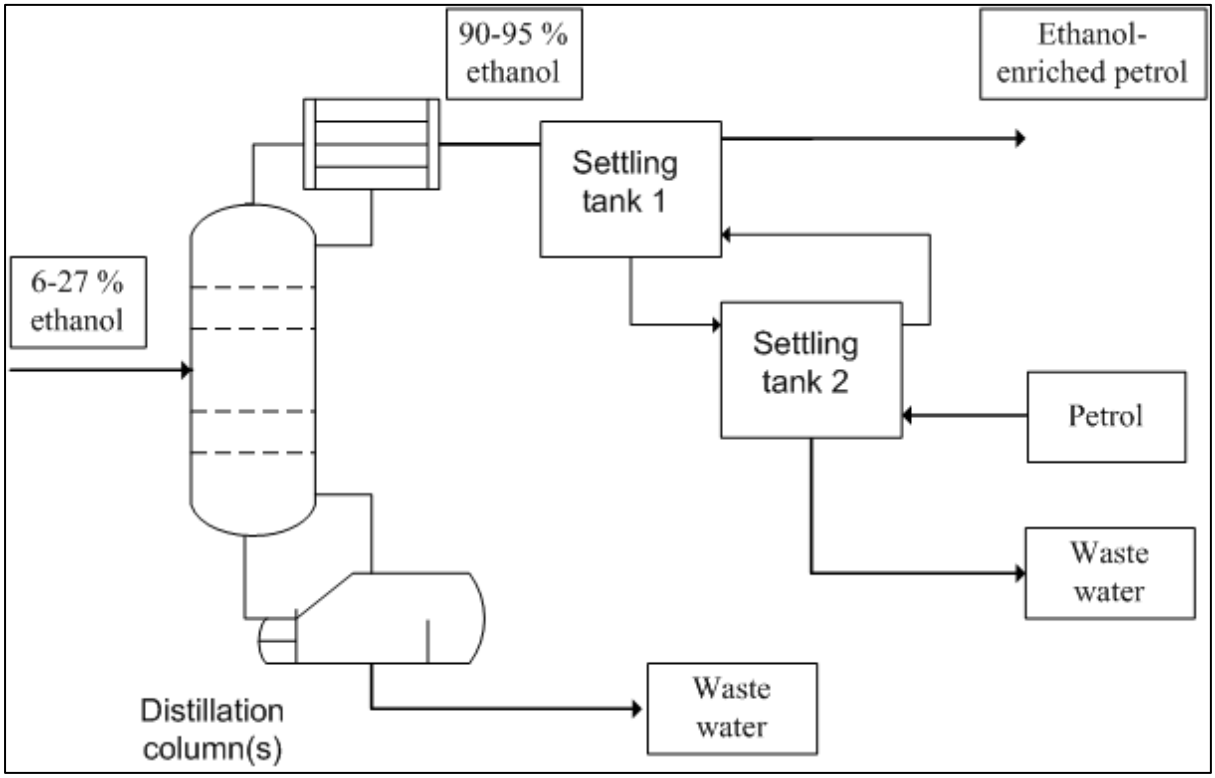


Figure 2.5: Proposed alternative process: conventional separation methods are used to produce an azeotropic mixture which is then blended in a two-stage liquid-liquid extraction process

This process will be easily implemented at existing plants with a minimum of equipment required. Azeotropic distillation generally requires two columns for the separation of the azeotropic mixture[5], [23–25] which means that in many instances there will be two vessels of suitable size already on site, along with all of the associated infrastructure. In any case, two process vessels for atmospheric conditions represent a minimal capital expenditure, with trivial operating expenses.

For our purposes at this stage, this process need not be modelled in its entirety; we are interested only in the ethanol/petrol blending portion of the process. Figure 2.6 shows a single blending process with a feed of 95% ethanol, while Figure 2.7 shows a two-stage blending process.

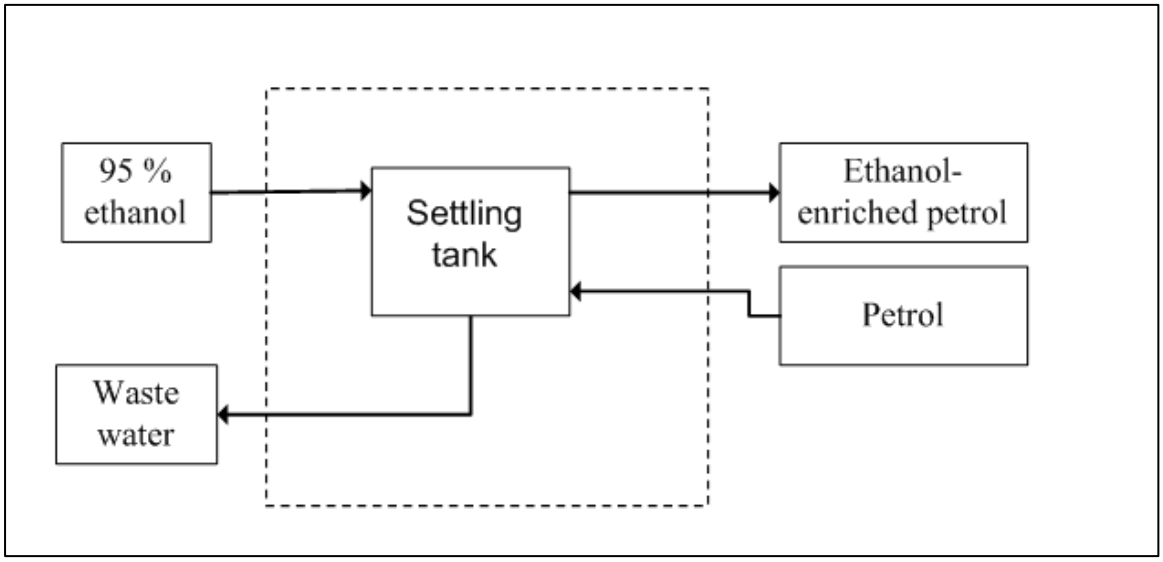


Figure 2.6: Single-stage petrol pre-blending flowsheet for simulation

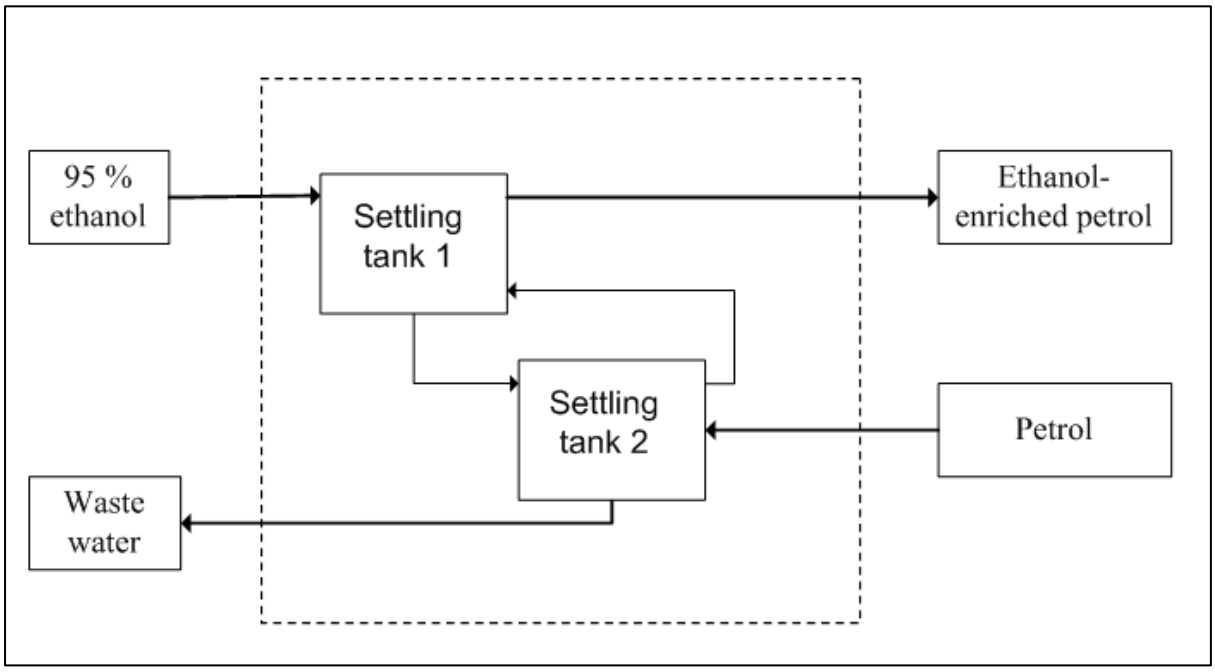


Figure 2.7: Two-stage petrol pre-blending flowsheet for simulation

2.5 Results and discussion

For a single-stage blending process with 95% ethanol feed, 10% ethanol content can be achieved by blending 7.1 litres of petrol for each litre of ethanol in the azeotropic mixture, as shown in Figure 2.8.

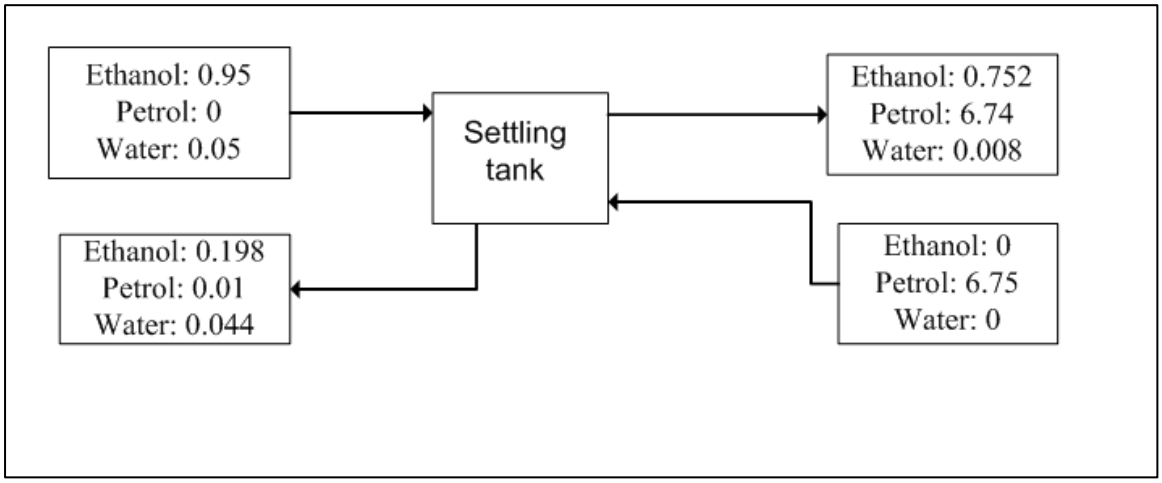


Figure 2.8: Flowsheet for a two-stage petrol blending process with blending ratio of 7.1. Flow-rates are given on a volumetric basis as a ratio to the initial flow-rate of the ethanol feed stream.

As shown above, only 79% of ethanol is recovered in the fuel mixture in this case. This recovery is intolerably low and in extreme circumstances could even be increasing the total energy consumption. If producing the azeotropic mixture requires 7.00MJ/*l* of ethanol as in the first Vasquez scenario in Table 2.3 and if only 79% of the ethanol is recovered then the energy requirement per litre of ethanol finally recovered is 8.86MJ/*l*. In the Garcia case in Table 2.3, final purification of the azeotropic mixture requires 1.46MJ/*l*. This means that the worst case for a single-stage liquid-liquid extraction in fact represents an increase in total energy consumption of 0.4MJ/*l*, a 4.5% increase in this scenario.

The best-case scenario for the single-stage liquid-liquid extraction is the first Vasquez case in Table 2.3, in which, by the same method of calculation as before, energy consumption is reduced by 35.2%.

The two-stage blending process is far more promising, as shown in the flowsheet in Figure.

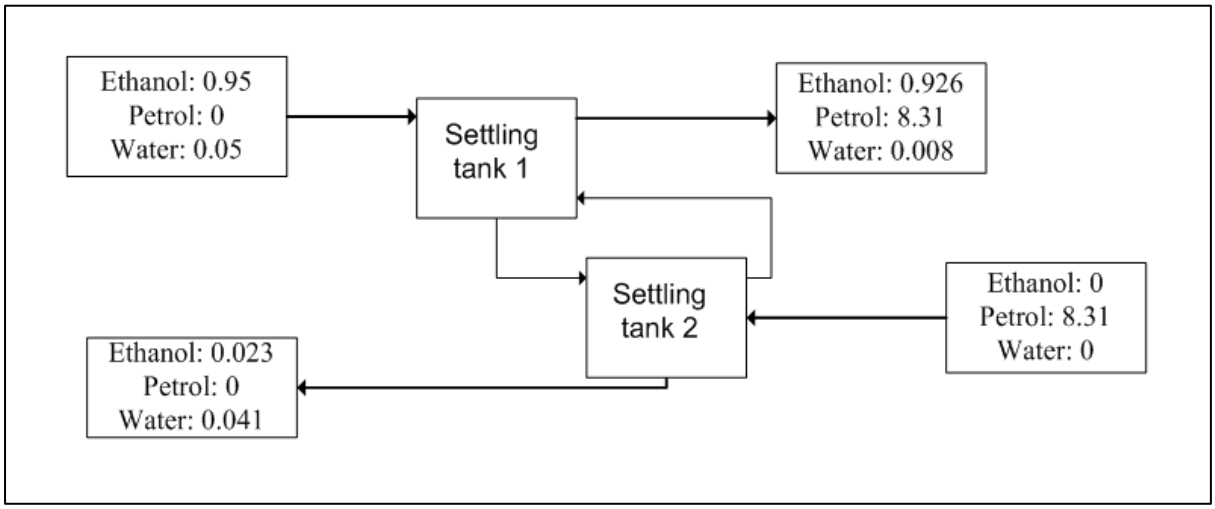


Figure 2.9: Flowsheet for a two-stage petrol blending process with blending ratio of 7.1. Flow-rates are given on a volumetric basis as a ratio to the initial flow-rate of the ethanol feed stream.

This process can also be visualised on a triangle diagram, as shown below in Figure 2.10.

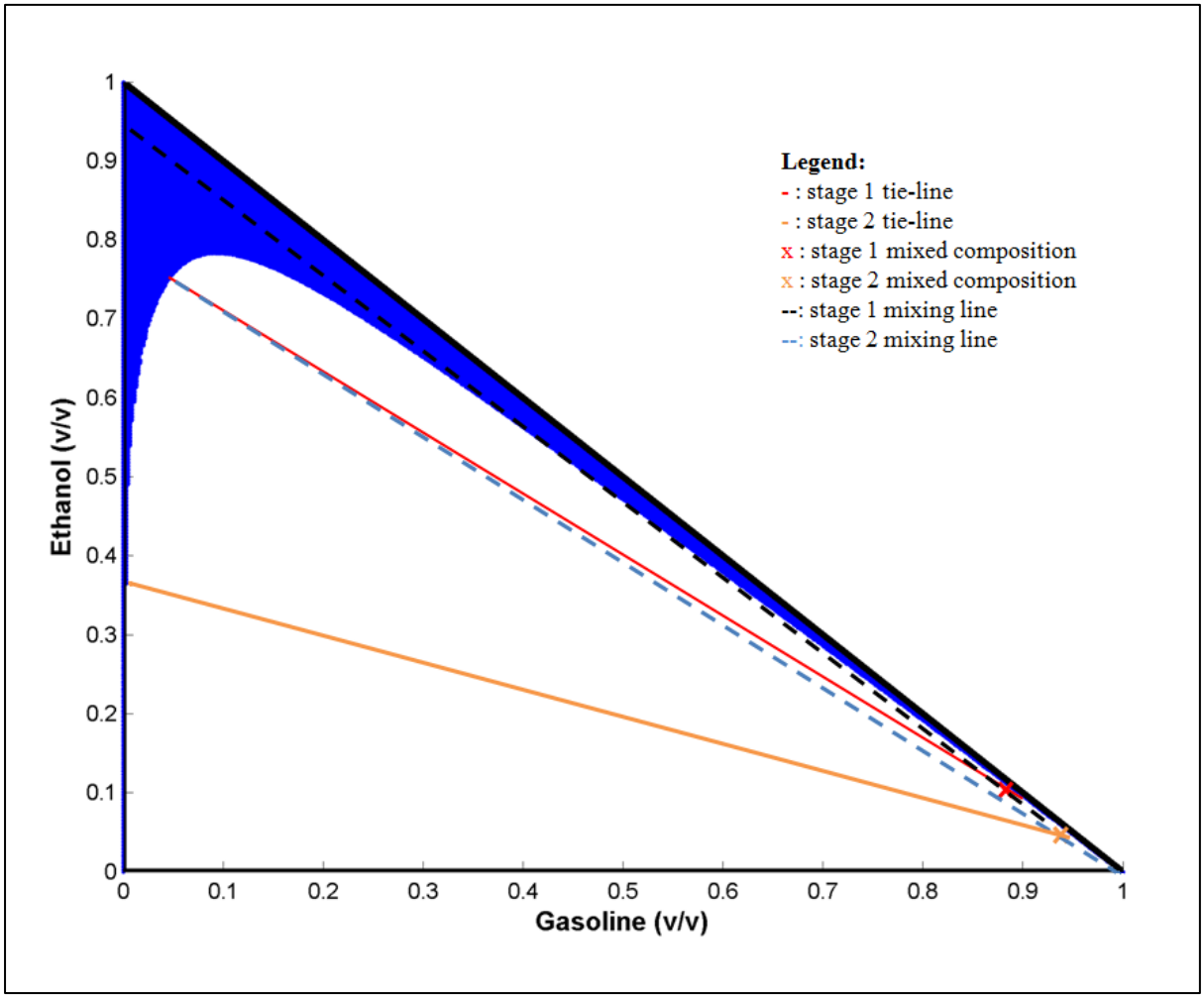


Figure 2.10: Two-stage petrol pre-blending separation process represented on triangular composition diagram. Feed compositions are pure petrol and an azeotropic ethanol blend, respectively.

Blending 8.75 litres of petrol for each litre of ethanol in the azeotropic mixture yields an enriched-petrol stream with an ethanol content of 10% while achieving an ethanol recovery of 97.5%.

Factoring in this small loss of ethanol, this amounts to an energy saving of between 17% and 40% when compared to typical processes using azeotropic distillation. The low flow-rate of the underflow waste stream also promises relatively simple waste handling, ideally by way of returning this stream to the distillation circuit.

This process can also be modified slightly to cater to different objectives in terms of ethanol composition. A two-stage blending process with a blending ratio of 48 as shown in Figure 2.11 was found to yield an ethanol content of 2%, and 99.9% ethanol recovery.

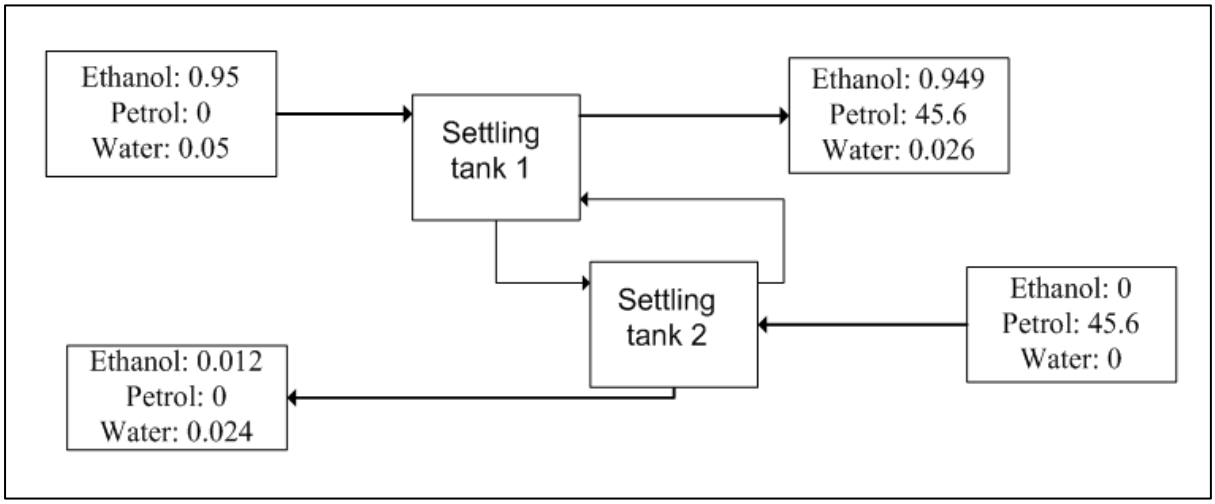


Figure 2.11: Flowsheet for a two-stage petrol blending process with blending ratio of 48. Flow-rates are given on a volumetric basis as a ratio to the initial flow-rate of the ethanol feed stream.

South African legislation due to come into effect in October 2015 mandates an ethanol content of 2% in all petrol, so this version of the process is highly promising for the South African market. The ethanol is almost completely recovered, resulting in an energy saving between 17.3% and 40.8% from a simple process with significantly lower capital costs than conventional separation methods.

This flowsheet is just one example of a process using the expanded optimization space afforded by discarding the erroneous assumption that complete purification is necessary in order to utilize bioethanol in a gasoline blend. Rigorous optimization and design using this shift of thinking could radically alter the energy consumption of bioethanol production. Alternative fermentation products such as butanol are also an option to be considered, and may offer more favorable liquid-liquid phase behavior.

2.6 Conclusions

It was shown in this chapter that the concept of direct blending is inherently sound. Even a very simple process modification, suitable for retrofitting, results in significant savings in separation energy which will bring with it reduced running costs.

The process proposed in this chapter consists of using conventional separation methods to obtain an azeotropic mixture of water and ethanol which is then blended directly into petrol in a two-stage counter-current liquid-liquid extraction. Only very basic process equipment is involved in this process modification; settling tanks can be safely assumed to be significantly less expensive than the distillation columns used in typical processes for the final purification of ethanol. This means that retrofitting existing processes to make use of this approach will involve minimal capital cost.

It is important to put this result into context. Globally, over 20 billion gallons of bioethanol are produced per year. Most of that bioethanol is purified for use in fuels, using the conventional distillation methods discussed in this chapter. Converting even a fraction of those existing processes to instead use the direct blending method described in this chapter would result in energy savings on the order of Terajoules per year, cutting global carbon dioxide emissions significantly while reducing the cost of renewable fuels. The content of this chapter sets out the groundwork for developing processes to achieve this goal.

Chapter 3 will investigate this process in more detail, exploring the effects of various process variables and developing more detailed designs tailored to specific contexts.

It must also be noted that this approach is equally applicable to the separation of other alcohols for fuel usage. Ongoing work is underway to develop a similar process for biobutanol separation, with the expectation of even larger energy savings owing to the fact

that butanol is a less polar molecule and will therefore tend to dissolve into the fuel phase more preferentially than ethanol does.

Chapter 3. Detailed investigation of process variables for direct blending of ethanol and petrol

The contents of this chapter and of chapter 2 are the subject of a provisional patent application filed by the University of the Witwatersrand with the South African Patent Office in April 2015

In Chapter 2 I demonstrated that the separation energy required for bio-ethanol recovery can be alleviated by discarding the assumption that pure ethanol must be obtained prior to blending with petrol. I concluded that the overall process shown in Figure 3.1 results in more efficient separation of bioethanol from fermentation products, with significant energy and cost savings.

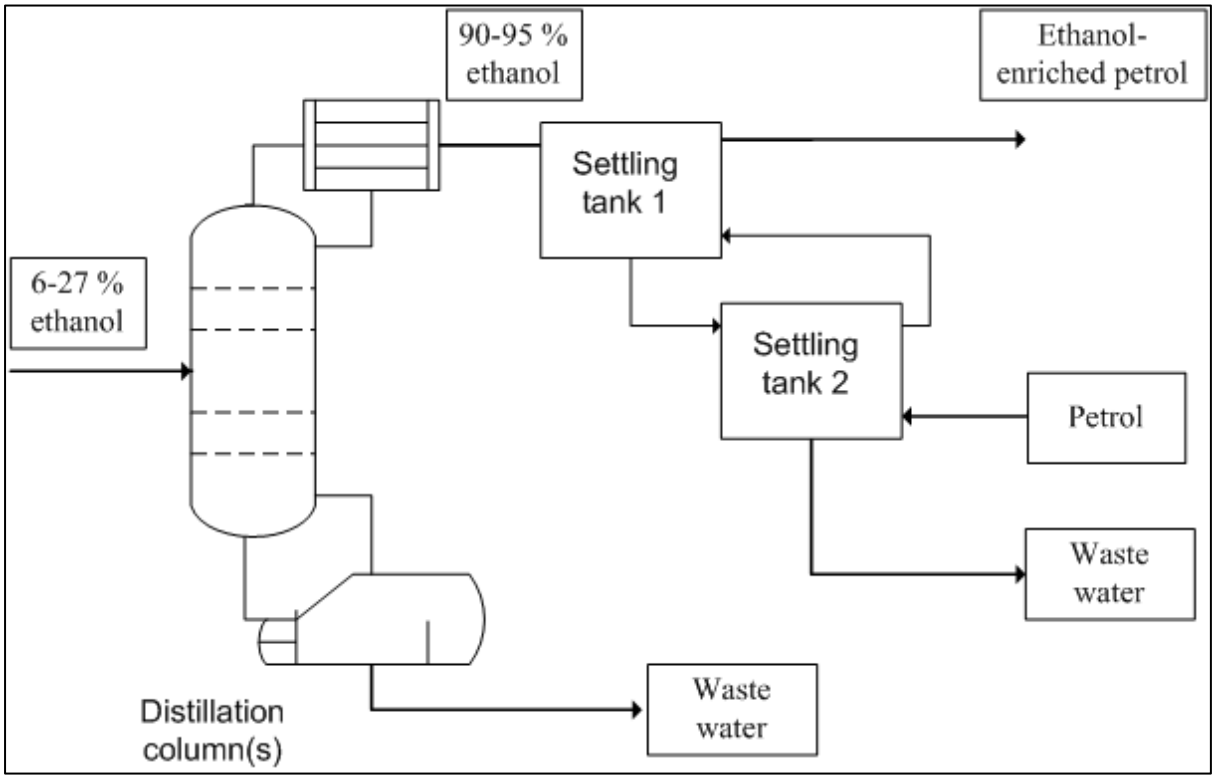


Figure 3.1: Overall process flowsheet for efficient bioethanol separation using ethanol pre-blending

In this chapter, more detailed engineering aspects of such a process are investigated. Our interest lies with the second portion of this process in which an azeotropic or near-azeotropic mixture is blended with petrol to produce a fuel mixture. Neglecting the initial separation steps results in the process flowsheet shown in Figure 3.2.

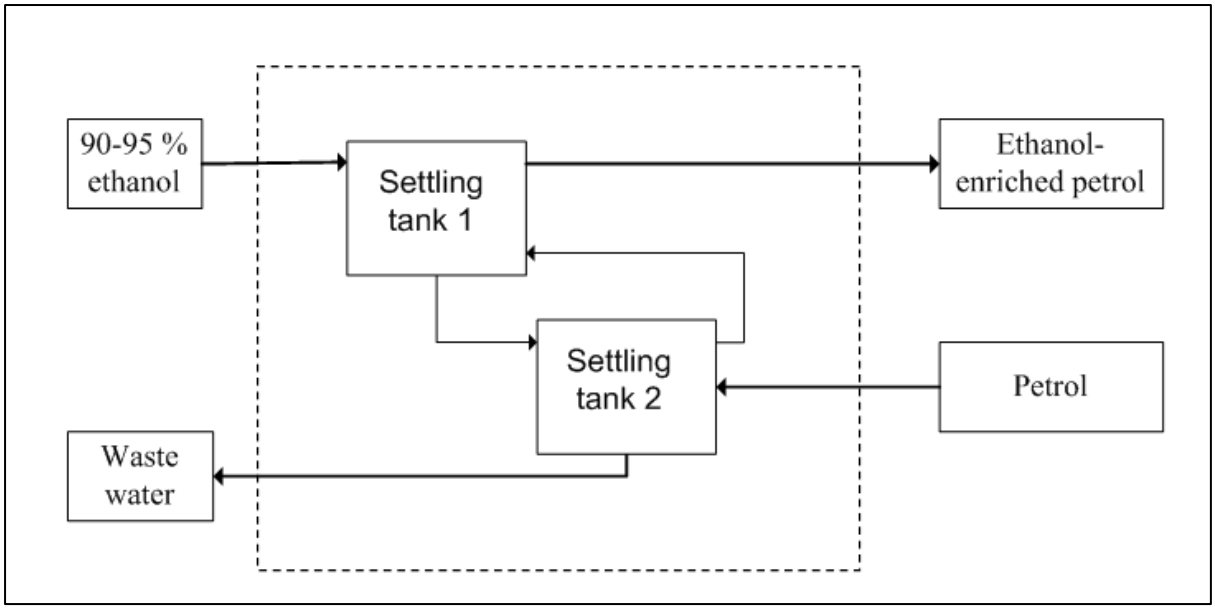


Figure 3.2: Process flowsheet for ethanol/petrol blending step

3.1 Stability requirements

As discussed in Chapter 2, a liquid-liquid extraction at atmospheric conditions will always produce a saturated fuel mixture, assuming sufficient settling time. However, an under-saturated mixture is required for quality fuel, and fuel standards of varying stringency exist in most parts of the world. In this thesis I will not attempt to adhere to or achieve any specific standard for fuel stability. Instead, I will outline the effects of process variables on stability and other aspects of performance.

Questions of fuel standard compliance must be left to ethanol producers, engaging with fuel producers and government representatives to outline the exact requirements according to the

circumstances. Fuel standards typically specify maximum allowable water content, so that is the most obvious measure of stability to use. However, the solubility of water in fuel increases along with ethanol content. This means that the more ethanol is present, the more water can be dissolved while still having a stable fuel mixture. Therefore, water content in isolation is a poor measure of fuel stability.

Moreover, the water content modelled here or elsewhere does not necessarily closely reflect the water content that will occur in practice. This is due in part to modelling errors but is also a result of the fact that petrol content is variable, as is the exact composition of trace impurities found in ethanol after processing. The water content predicted by the simulation of any process will be the result of the details of the simulation as much as it will be a reflection of the water content or indeed fuel stability afforded by the actual process. Consequently, water content is not necessarily the ideal method for representing stability.

For these reasons, quantitative measures of stability lie outside the remit of this thesis; stability will instead be discussed in a qualitative manner, hopefully including the broad insights that a process designer will need to consider in the preliminary stages of process development.

3.2 Modelling

In the previous chapter, it was possible to accurately predict phase equilibrium model using a rigorous model which had been fitted to experimental data from literature[25]. Unfortunately, the study by Rahman et al. [25] did not measure phase equilibrium at different pressures and temperatures, and these are both critical process variables with significant effects on liquid-liquid separation. Lacking data at a wide range of conditions it is impossible to verify the accuracy of our own modelling. Consequently, I elected to use the commercial simulation

package Aspen Plus for the phase equilibrium and process modelling in this chapter. The UNIQUAC model was selected, using inbuilt parameters.

The accuracy of this approach is somewhat debatable and the use of a fitted model is preferable where available but in the absence of data at a range of temperatures and pressures it becomes more sensible to use the in-built modelling of a commercial package, which can be assumed to be sufficiently accurate for determining qualitative trends at the very least.

Whereas the fitted model was able to make use of data for petrol specifically, data for petrol as a pseudo-component is not available in Aspen. I have elected to use Iso-octane as a stand-in. The study by Rahman et al. [25] also measured the liquid-liquid equilibrium for a mixture of Iso-octane, ethanol and water, and its behaviour closely resembles that of the petrol mixture examined in the same study. Figure 3.1 shows the respective liquid-liquid equilibrium phase diagrams for ethanol/water/isooctane and ethanol/water/petrol from the Rahman et al. [25] paper.

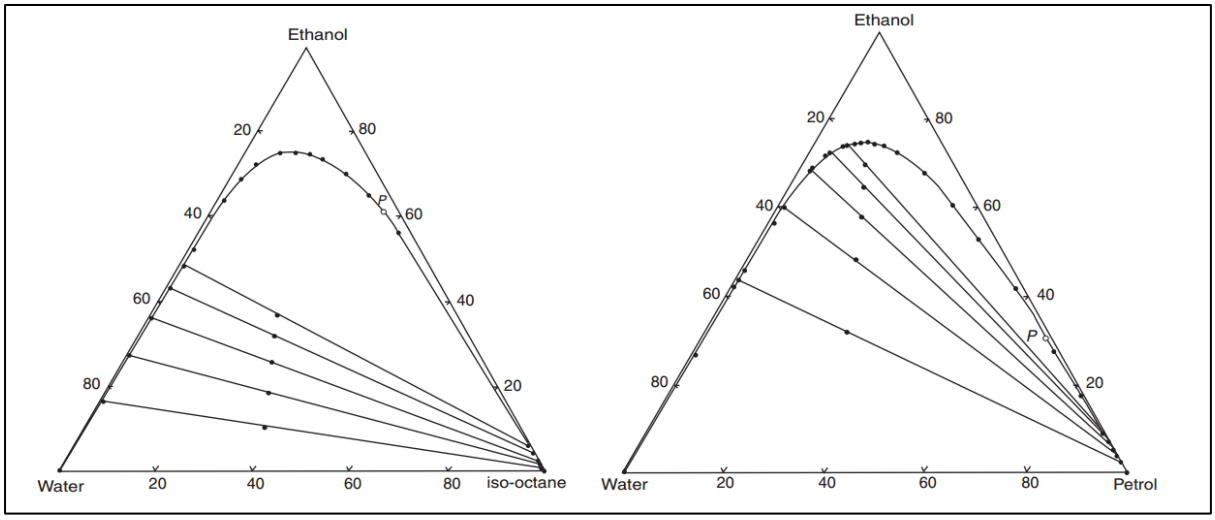


Figure 3.3: Phase equilibrium diagrams for water/ethanol/iso-octane and water/ethanol/petrol systems. Source: Rahman et al. (2007)

Figure 3.3 shows that these two mixtures have remarkably similar phase equilibrium behaviour. Therefore, process modelling using iso-octane as a stand-in can be considered to be adequate for our purposes. The two systems exhibit sufficiently similar behaviour to examine qualitative trends and determine broad design principles, although strict quantitative design will require more exact data.

Note that this would be the case even with experimental results using a petrol mixture; the actual content of petrol exhibits significant variance based on a multitude of factors. Consequently, quantitative design based on one particular petrol mixture won't be directly applicable to a process using a different source of petrol.

Further, a high degree of accuracy is not our area of particular interest in this investigation. Rather, I intend to gain insight into the effects of process variables on process performance. Even where the specific compositions differ, it can be assumed that these insights will translate qualitatively to the real world processes.

Chapter 2 used rigorous modelling to verify with a high degree of certainty that the process is effective; here in Chapter 3 I aim to use modelling of tolerably decreased accuracy to gain insights into the characteristics of the process in terms of its key variables.

Number of stages is a key parameter in separation performance so a variety of flowsheets with varying number of stages was simulated. Figure 3.4 shows the single-stage flow-sheet as simulated.

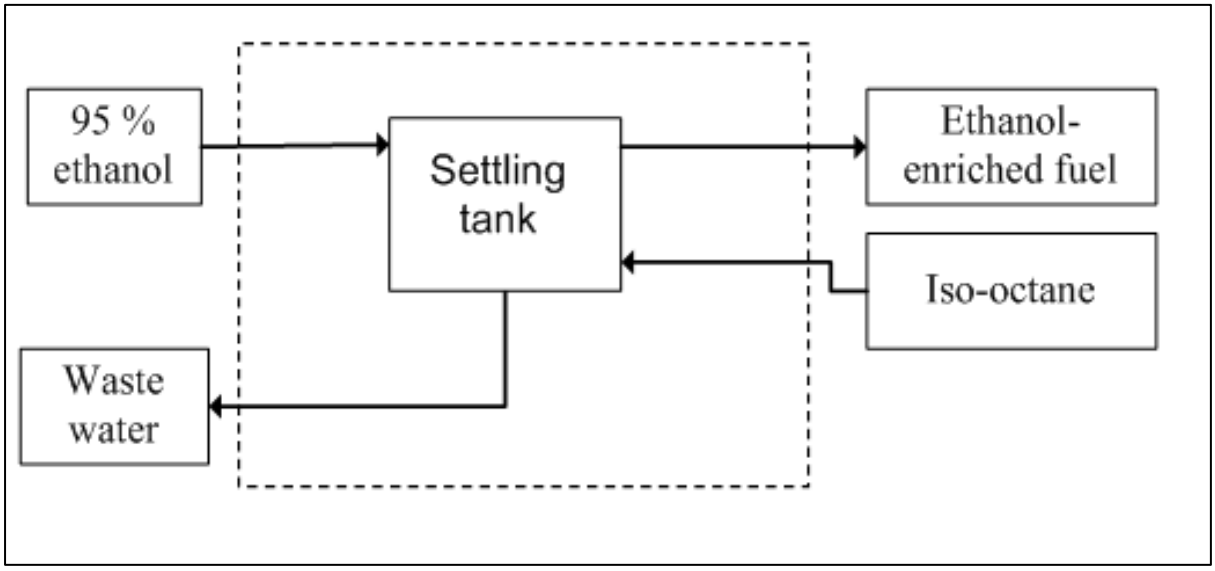


Figure 3.4: Single-stage process flowsheet for simulation

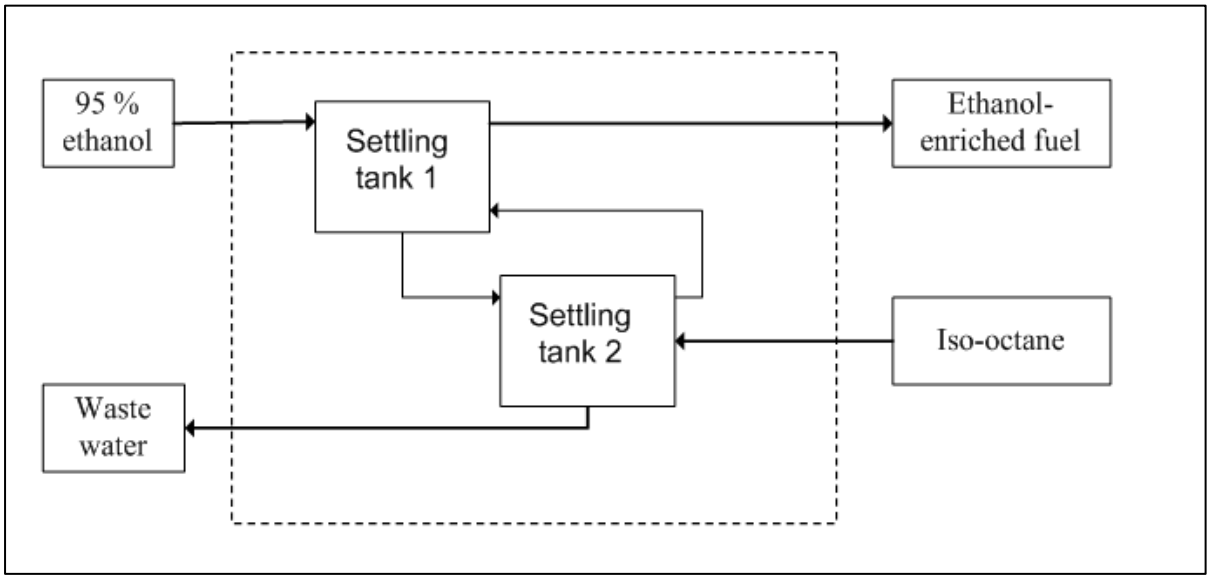


Figure 3.5: Two-stage process flowsheet for simulation

The results from chapter 2 indicate that a single-stage blending will not yield adequate recovery of ethanol and that a two-stage process is more desirable. A two-stage counter-current blending process flowsheet is shown in Figure 3.5.

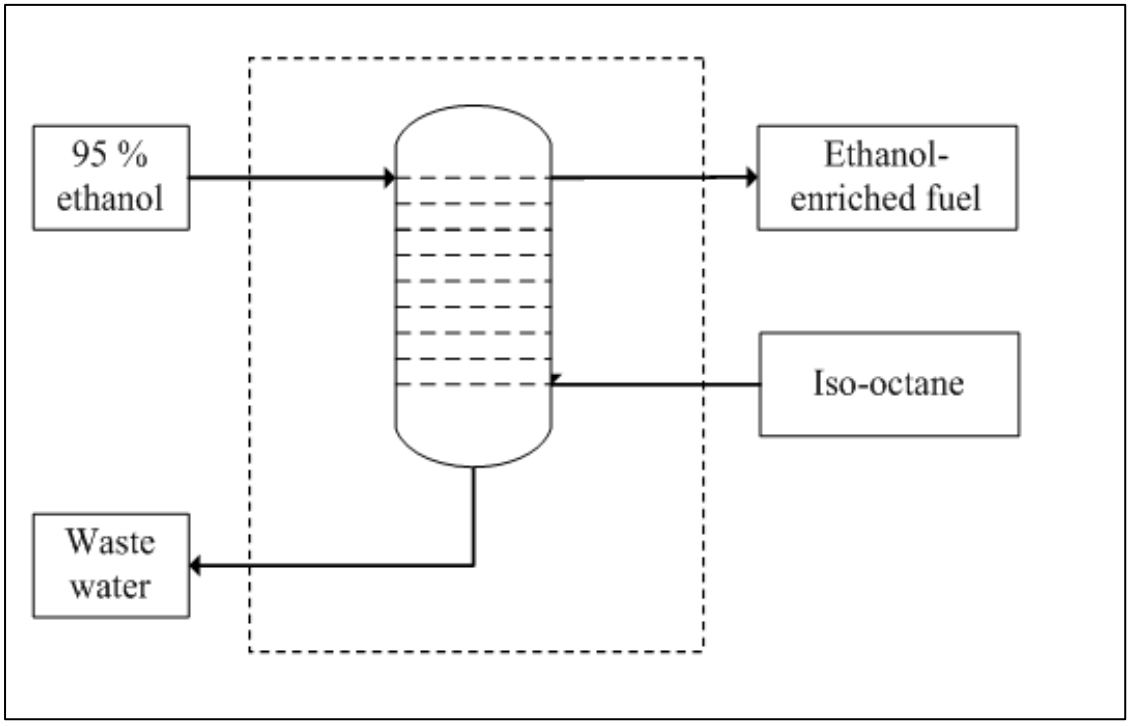


Figure 3.6: Multi-stage column process flowsheet for simulation

I also simulated a process using a 16-stage solvent extraction column. While a solvent extraction column will generally maximize recovery of ethanol, it must be noted that such columns are complex to operate and control, particularly when the two liquid phases are of similar densities. If a one- or two-stage process can achieve suitable separation performance then such a setup will be preferable.

For the purposes of all process modeling, ambient conditions are 25°C, 1 atmosphere pressure and all compositions are given on the basis of percentage volume at ambient conditions. Raw data for all simulations in this chapter can be found in Appendix A.

3.3 Process Variables

Within the constraints of the process flowsheet from Chapter 2, there are a number of variables which can be manipulated with significant effects on the overall performance of the separation circuit.

3.3.1 Blending ratio

I define blending ratio as the volume of petrol fed to the liquid-liquid extraction circuit divided by the volume of ethanol in the azeotropic mixture fed to the circuit. The blending ratio plays a crucial role in determining the ethanol content of the fuel mixture and also in determining the recovery of ethanol. Intuitively, higher blending ratios will result in recovery of more ethanol, but will reduce the final ethanol content.

Blending ratio is defined in terms of the ethanol flow-rate specifically, as opposed to the total flowrate of the feed mixture; this allows for the same terminology to be meaningfully applied to processes beginning with varying ethanol content. While blending ratio is to a large extent dictated by product specifications, it is still of interest to examine its effect on process behaviour since product specifications will vary under different circumstances.

3.3.2 Pressure

Pressure is a parameter with significant effects on many chemical processes, so its effects must be investigated. Manipulation of pressure is one of the options available for producing a more stable fuel mixture, but comes at the expense of capital and running costs.

3.3.3 Temperature

At lower temperatures, more of the water is eliminated in the liquid-liquid extraction, resulting in a more stable fuel mixture. However, this will also tend to reduce the recovery of ethanol, and very low temperatures processes are impractical and expensive.

3.3.4 Number of stages

Chapter 2 demonstrated that a two-stage liquid-liquid extraction is adequate for recovering 97.5% of ethanol while obtaining a 10% ethanol fuel blend, while showing also that a single settling tank does not give high enough recovery to be recommended for this process. While a

two-stage process can easily be carried out with simple, inexpensive equipment, the higher recovery obtained by a higher number of stages may well justify the additional expense and process complexity involved in using a solvent extraction column. Therefore, variables will be examined for a single-stage process, a two-stage process and for a multi-stage (16-stage) solvent extraction process.

3.4 Context

The details of bio-ethanol useage differ across national boundaries, often governed by legislative incentives and requirements. For the purpose of this thesis I will be considering two main contexts; the South African (local) context and the context of the United States of America, the world's largest producer of bio-ethanol.

3.4.1 The South African context

South African Government Notice R.719 specifies that the bio-fuels blending mandates laid out in Government Notice R.671 will take effect as of 1 October 2015. This means that from this date it will be mandatory for South African fuel producers to blend bio-ethanol into petrol to a content of 2% or higher, with tax incentives covering ethanol content up to 2%. Additional ethanol is permitted, but without further incentivisation. Biodiesel blending of 5% is also mandatory under these regulations.

This legislation is intended to kick-start growth in the bio-fuels sector, creating jobs in several sectors while also reducing national carbon emissions.

With financial incentives only covering ethanol content up to 2%, that is the ideal process target from a financial standpoint and an ideal starting point for introducing bio-ethanol processes. The ramping up of demand for bio-ethanol as the deadline approaches means that aside from existing bio-ethanol production capacity, there is also a demand for new capacity.

Consequently, retro-fitting of existing processes and development of new processes are both valuable in this context.

Since the 2% mixture required in this context can be obtained with a higher blending ratio than was used to obtain a 10% mixture in chapter 2, it follows that higher recoveries are possible when seeking a 2% mixture. It may be possible to readily obtain a 2% mixture by blending an initial ethanol mixture containing lower than the 95% composition studied in chapter 2. If this is the case, the costs of primary separation could be further reduced by relaxing the requirements for the distillation circuit.

3.4.2 The American context

The United States of America is the world's largest producer of bio-ethanol, which is widely blended into fuel across the country. The most common ethanol content is 10%, matching the composition of the product of the process described in Chapter 2. The process described in Chapter 2 is, therefore, a good starting point for developing processes for this market.

A saturated mixture high in ethanol will contain more water than one low in ethanol, and will therefore have higher corrosivity.

This means that when dealing with a 10% mixture as opposed to a 2% mixture, stability and water content become more of a concern. Therefore, the primary challenge in this context is to mitigate this issue, firstly by conducting the phase split as late in the supply chain as possible to reduce the amount of equipment exposed to water and secondly by attempting to optimise the process to minimize water content.

3.5 Effects of individual parameters: results and discussion

I will begin by presenting the effects of each variable in isolation, to offer an overview of the general trends. Subsequently, I will examine specific scenarios making use of multiple variables to improve the overall process performance.

3.5.1 Blending ratio and number of stages

Here I examine the effects of blending ratio at atmospheric conditions, using Aspen for process modelling. These results differ slightly from those predicted by the rigorous modelling in Chapter 2, but it is sensible to use the same modelling as for the other variables here in order to offer a valid basis of comparison.

Table 3.1: Effect of blending ratio on ethanol recovery and content

Blending ratio	1-stage recovery	1-stage Ethanol%	2-stage recovery	2-stage Ethanol%	16-stage recovery	16-stage Ethanol%
4	54.1	12.4	66.0	14.4	73.0	15.6
6	71.1	10.7	78.3	13.7	91.6	15.6
8	81.2	9.22	96.9	10.8	100	11.1
10	87.0	8.00	98.9	8.99	100	9.08
15	93.4	5.86	99.7	6.23	100	6.24
20	95.9	4.57	99.9	4.75	100	4.76
50	98.9	1.94	99.9	1.96	100	1.96

It must first be noted that the results in Table 3.1 are a fair match for those from Chapter 2 and for experimental results from Rahman et al. [25], indicating that this modelling approach offers a good approximation of actual phase behaviour. This corroborates the assumption that iso-octane serves as a reasonable stand-in for petrol for the purposes of preliminary design.

Table 3.1 demonstrates the expected result that higher blending ratios result in higher recovery of ethanol. For the 16-stage process, complete recovery of ethanol occurs for all blending ratios 8 and above, indicating that for that case there is no benefit increasing the blending ratio above 8, except perhaps for dealing with initial ethanol content lower than the 95% assumed here.

A two-stage process with blending ratio in the 8-10 range offers the desirable ethanol content along with almost complete recovery. The multistage process with blending ratios in this range also achieves the desired composition, but with complete recovery of ethanol. This is quite likely the most desirable starting point for designing a process for the American context.

It must be noted that the 2% ethanol blend required by South African law is easily obtained with a high recovery of ethanol. Even the single-stage process can achieve recovery of 98.9% for an ethanol content of 1.94%. The 2-stage process offers higher recoveries, approaching complete recovery for high blending ratios.

This has several implications for this process in the South African context. Firstly, a two-stage process will likely be adequate, giving designers the option of minimizing process complexity and capital cost while still achieving good process performance. This is particularly important if blending facilities are installed in a decentralized manner; a high number of small blending facilities would represent a large capital cost if those facilities are not kept simple and inexpensive.

Secondly, the multi-stage process so easily accomplishes what is necessary that it can be inferred that it may be possible to achieve a satisfactory performance when beginning with an ethanol mixture more dilute than the 95% studied above. This will be examined later in the chapter when context-specific examples are studied in detail.

3.5.2 Pressure

To get an idea of the effects of pressure, I will begin by looking at 2-stage processes at ambient temperature and at two blending ratios, 6 and 8.

Table 3.2: Effect of pressure on process performance

Pressure (atm)	Ethanol % at BR=6	Recovery at BR=6	Ethanol % at BR=8	Recovery at BR=8
0.8	12.83	88.42	10.79	96.93
1	12.85	88.58	10.79	96.97
1.5	12.85	88.58	10.80	96.98
2	12.83	88.38	10.80	96.98
3	12.82	88.36	10.80	96.98
5	12.82	88.36	10.80	96.98
10	12.83	88.40	10.80	96.98

It is clear that pressure has no particular effect on the phase equilibrium in these conditions, understandable with relatively incompressible liquids. At more extreme temperatures, either hotter or colder, pressure can be manipulated to prevent the formation of undesirable solid or vapour phases. In most cases, this process should be carried out at the pressure which is most convenient based on upstream and downstream pressures to avoid additional pumping costs. In most instances, ambient pressure will be ideal.

3.5.3 Temperature

Temperature can be expected to have a profound impact on phase equilibrium and consequently on process performance. The effects of temperature on a two-stage blending process at blending ratios of 6 and 8 are shown in Table 3.3

Table 3.3: Effect of temperature on liquid-liquid phase-split

Temperature (°C)	Ethanol % at BR=6	Recovery% at BR=6	Water% at BR=6	Ethanol % at BR=8	Recovery% at BR=8	Water % at BR=8
-25	7.05	44.1	0.0270	6.89	58.5	0.0265
-15	8.19	52.3	0.0423	7.93	68.5	0.0415
0	10.0	66.1	0.0775	9.42	83.1	0.0740
12	11.5	77.5	0.118	10.3	91.9	0.107
20	12.4	84.6	0.151	10.7	95.6	0.131
25	12.8	88.4	0.173	10.8	96.9	0.145
30	13.2	91.6	0.196	10.9	97.9	0.160
40	13.5	94.1	0.431	11.0	98.9	0.189
60	13.8	96.3	0.474	11.0	99.6	0.247

It is clear that temperature has a significant impact on phase equilibrium and on process performance. High-temperature phase-splits offer increased ethanol content and recovery but at the cost of reduced stability.

Lower temperature saturated mixtures have significantly lower water content than saturated mixtures at higher temperatures. This means that a mixture that is saturated at a high temperature will become unstable if the temperature is lowered, and that a mixture that is saturated at a low temperature will be under-saturated and highly stable at ambient conditions.

Low temperature phase-splits offer significantly more stable mixtures but this stability improvement is offset somewhat by the reduced ethanol content, which limits the possibility for stabilization through the blending of additional petrol. This, combined with the significant reduction in ethanol recovery and the general expense and impracticality of large-scale cryogenic processes suggests that these very low temperature processes are

economically unfeasible. However, it is worth investigating the possibility of achieving a stable 10% ethanol mixture at a low temperature using a multi-stage liquid-liquid extraction process to increase recovery.

Further, a temperature-swing phase split is worth examining, whereby an initial liquid-liquid extraction takes place at high temperature, resulting in a high recovery of ethanol in a mixture with high ethanol content. To improve stability, this mixture could subsequently be decanted at a lower temperature.

3.6 Improvements to basic process

Having established the general trends among the parameters for the process and having considered the specific contexts for its implementation, there are several modifications to the process that can be considered.

3.6.1 Temperature Swing process

It was seen earlier that higher temperature phase-splits result in higher ethanol content and recovery, but at the expense of stability. Running a phase-split at a higher temperature and following it with a decanting step at ambient temperature, however, will result in a second liquid-liquid phase-split producing a saturated hydrocarbon phase at ambient temperature.

In other words, a temperature swing process will result in a hydrocarbon product of the same stability as a phase-split at ambient temperature and hopefully with a higher recovery of ethanol. This approach can be extended by using multiple temperature intervals for decanting. This approach will also be quite practical in many instances, since fermentation products emerge from the process at elevated temperatures. Figure 3.7 below shows a flowsheet for a temperature swing process with a single decanting interval. Note, however, that this is just an

example flowsheet; the actual exit temperature of the blended mixture will depend on the blending ratio and the specifics of the distillation process.

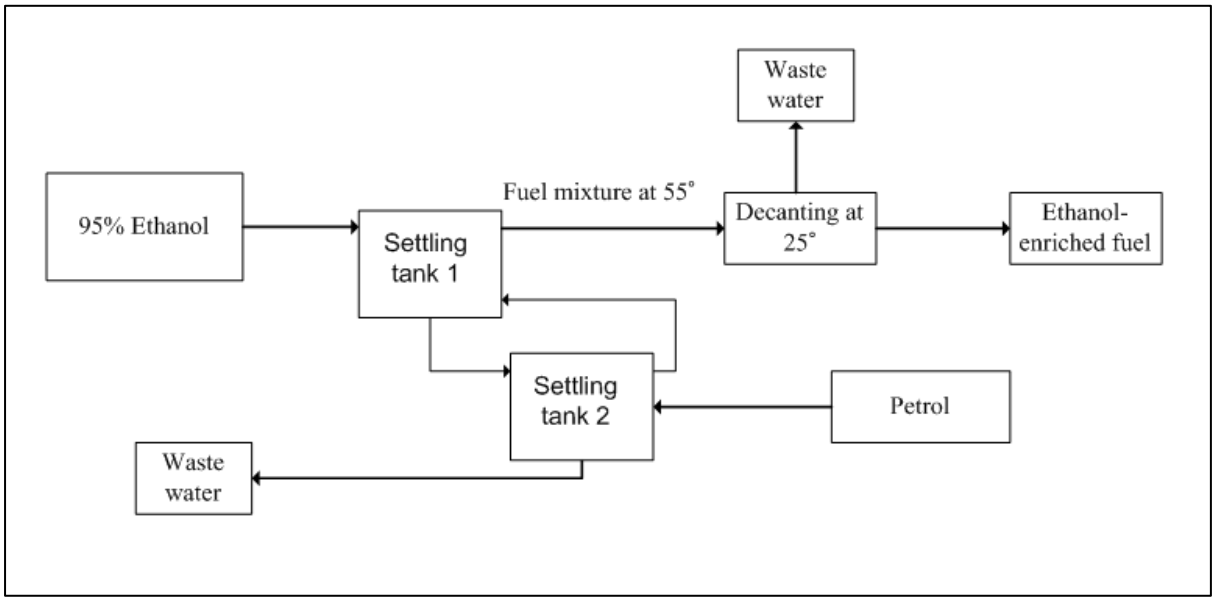


Figure 3.7: Temperature swing process flowsheet for petrol pre-blending with two temperature intervals

A temperature-swing process with three intervals can be visualised as shown in Figure 3.8 below. Note that multiple tanks are not absolutely necessary in practice. The temperature swing decanting could be done in a single vessel in a batch or semi-batch fashion.

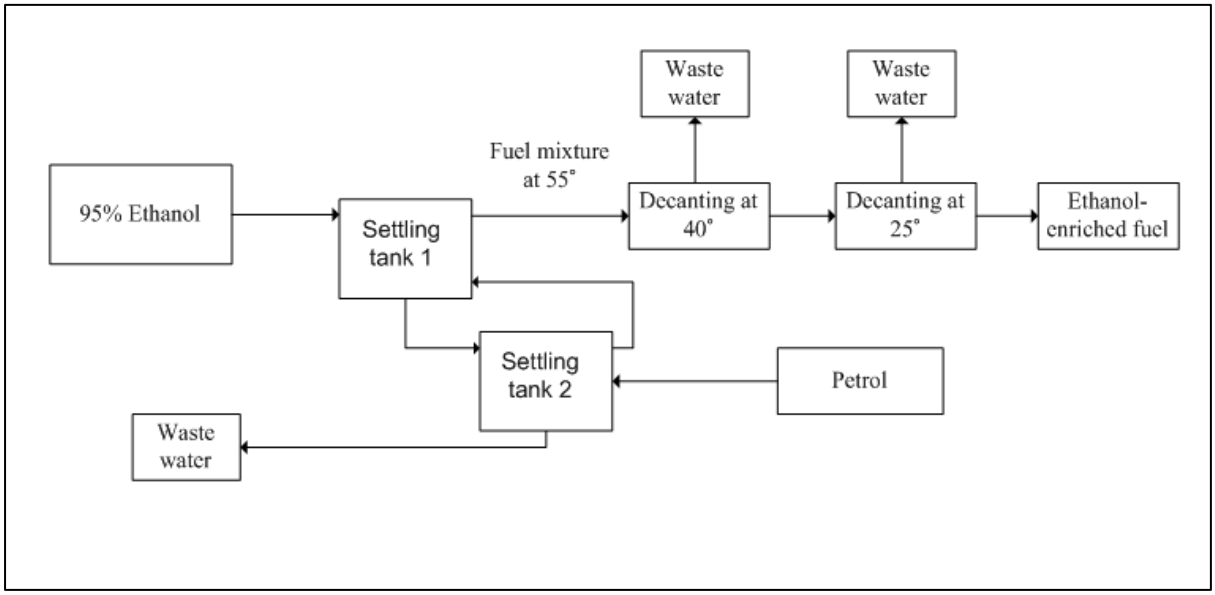


Figure 3.8: Temperature swing process flowsheet for petrol pre-blending with three temperature intervals

Table 3.4 shows the results of this approach, for both a two-step and a three-step decanting process.

Table 3.4: Performance of three-step, two-step and single-step decanting processes producing fuel mixture at ambient temperature

Temperature Intervals for decanting (C)	**Blending Ratio**	**Ethanol Content**	**Ethanol Recovery**
25	4	12.4	54.1
	8	9.22	81.2
	10	8.00	87.0
	15	5.86	93.4
	50	1.94	98.9
55,25	4	13.63	60.9
	8	9.76	86.53
	10	8.34	91.05
	15	5.99	95.63
	50	1.94	99.2
55,40,25	4	13.7	61.39
	8	9.82	87.11
	10	8.37	91.41
	15	6.00	95.8

	50	1.94	99.2

An initial phase separation at 55°C followed by decanting at ambient temperature results in increased ethanol content and improved recovery when compared to phase separation at ambient temperatures, particularly at low blending ratios. This result can be explained intuitively; as the temperature is lowered, water and gasoline become less and less miscible, so water is removed as temperature is dropped. Doing this at a series of staged temperatures instead of at a single low temperature minimizes the ethanol that is lost into the water phase as this occurs.

A 3-step decanting process with initial phase separation at 55°C and subsequent decanting at 40°C and 25°C results in further improvements. Consider the process with a blending ratio of 10: a single-step decanting results in 8% ethanol content with 87% recovery, while the 3-step decanting results in an ethanol content of 8.37% and 91.4% recovery.

The logical extreme of this approach is to decant in a batch process where the aqueous phase is removed as it forms while the temperature is gradually lowered. The final decanting step need not be at ambient conditions; it could be conducted at a lower temperature in order to achieve improved stability while offsetting the performance reductions of low temperature phase separation.

3.6.2 Lower ethanol content for South African context

The 2% ethanol mixture required by South African law can be easily reached with high recovery using just single or double stage liquid-liquid extraction. This simplifies the process equipment required, but also suggests that a more difficult extraction could be achieved using a multi-stage approach.

Starting with an ethanol composition lower than 95% would reduce the costs associated with the primary separation step and is therefore worth investigating in this case.

Table 3.5: Effect of lower initial ethanol content on 2-stage counter-current liquid-liquid extraction

Initial ethanol content	Temperature intervals (°C)	Blending ratio	Final ethanol content (%)	Ethanol recovery (%)
85	25	4	9.48	41.5
85	25	8	8.55	74.8
85	25	10	7.85	85.3
85	25	15	5.99	95.7
85	25	20	4.67	98.1
85	25	50	1.96	99.8
50	25	4	4.05	16.9
50	25	8	3.64	30.2
50	25	12	3.28	40.7
50	25	20	2.69	55.3
50	25	40	1.80	73.5
50	25	50	1.54	78.1
50	50,40,25	4	5.11	21.6
50	50,40,25	8	4.47	37.4
50	50,40,25	12	3.92	48.9
50	50,40,25	20	3.08	63.6
50	50,40,25	40	1.95	79.5
50	50,40,25	50	1.64	83.3

Table 3.5 shows that with an initial ethanol content of 85%, the process remains viable for the South African context, since near-total recovery of ethanol still occurs at a blending ratio of 50 while producing a fuel mixture with ethanol content close to the 2% required in SA. Purification to 85% can be presumed to be somewhat less costly than purifying to 95%, so this result suggests another avenue of possible cost-saving and optimization.

However, the lower ethanol content has a ruinous effect on the prospects of the process for the American context. With a starting ethanol content of 85%, a two-stage process with a blending ratio of 4 recovers only 41.5% of ethanol, and doesn't even achieve 10% ethanol content.

In other words, the more stringent requirements of the American context result in a process much more sensitive to starting ethanol content, whereas the South African context allows for a much more flexible process. In fact, beginning with an ethanol content of just 50% and using temperature swing decanting, a blending ratio of 40 results in a fuel mixture with ethanol content of 1.95%, and ethanol recovery of 79.5%.

Literature survey does not offer much by way of analysis of the energy requirements for distilling ethanol mixtures to this sort of composition, since it is not a step that is of particular interest in conventional processes to purify ethanol. However, it can be reasonably assumed that the energy requirements and capital cost investments required by such a process would be significantly below those involved in full purification, or even in purification to the azeotrope.

It is up to designers to evaluate on a case-by-case basis whether or not the benefits of reduced separations costs are worth the reduced ethanol recovery, but this preliminary analysis indicates that it is a possibility worth considering.

3.7 Conclusions

In this chapter, the effects of design parameters have been examined in detail, yielding insights into the specific design decisions likely to optimise performance in particular contexts, and into the general thinking involved in developing and implementing phase-separation processes for bioethanol recovery.

Temperature, blending ratio and number of phase equilibrium stages have been identified as the main parameters affecting performance of the phase separation process.

Higher temperatures result in higher ethanol content and recovery, but stability is linked to the temperature at which the final product is decanted. The temperature-swing decanting approach takes advantage of the improved ethanol recovery at higher temperatures without adversely affecting the stability of the final mixture. The step-wise decanting approach further improves process performance for the same reasons.

The blending ratio must be selected based on the desired ethanol content in the fuel product and is more or less determined as soon as a product specification is selected, excepting that there is some variation in the exact number insofar as other parameters affect the ethanol recovery and content to some degree.

The ideal number of stages, on the other hand, is highly contextual and will depend on economic considerations. The cost and process complexity involved in multi-stage processes are particularly undesirable if a high number of blending facilities are used at end-points on the fuel distribution network. A decentralised approach is ideal for limiting the financial impact of the corrosive effects of water, so this factor must be balanced against the economies of scale of central processing. In cases where a one- or two-stage process is able to achieve a desirable recovery and ethanol content, a decentralised approach becomes more viable.

In the South African context, the ideal approach is probably one where two-stage phase-separation is carried out at a number of locations near the end-points of a fuel distribution network. Reaching the azeotrope in the initial separation is not necessary if the required ethanol content is 2%, as in the South African context, and the most economical approach

will likely be to reduce the cost of that initial separation by using a mixture with purity somewhat below the azeotrope.

Figure 3.9 below shows a simple process flowsheet that produces a viable fuel mixture with almost complete ethanol recovery by blending an 85% ethanol/water mixture with petrol.

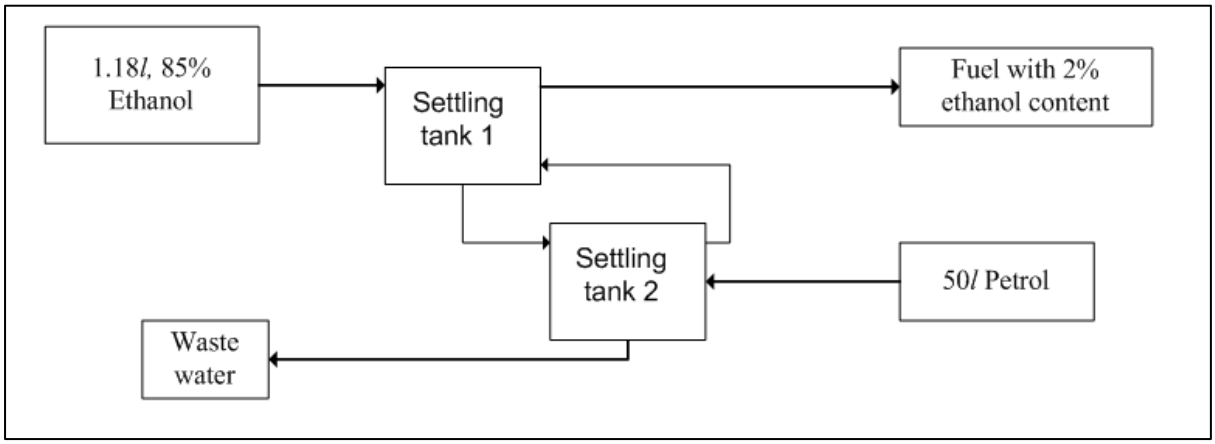


Figure 3.9: Two-stage petrol pre-blending process beginning with 85% ethanol mixture

This process achieves the desired ethanol content while recovering 99.9% of ethanol and requiring little additional process complexity. It also requires just 85% ethanol in the feed, so it offers a further reduction in energy usage when compared to the versions of this process making use of the azeotropic mixture.

Chapter 4. Multi-membrane Residue Curve Maps

The material in this chapter has previously been published[26] and is here reproduced in accordance with the permitted uses by authors of ACS Publications.

RCMs and M-RCMs have proven to be useful tools for gaining insight into distillation and membrane permeation respectively, so in this chapter an equivalent method is derived for Multi-Membrane operations.

4.1 Introduction

Residue Curve Maps (RCMs) were developed as a graphical synthesis tool for distillation, offering a straightforward visual representation of a ternary system's VLE behaviour. More recently, RCMs were applied to membrane separation, and Peters et al.[12] developed a graphical method for synthesising membrane processes using RCMs, with the intention of providing a synthesis tool for membrane processes. However, no method of this sort exists for synthesizing separation processes utilizing two different membranes in the same shell. The basic concepts of RCMs will not be explained in detail here, the reader is referred to the work of Doherty et al.[14] for a detailed treatment of the properties of such maps.

However, it is important to be familiar with the concepts of stable, unstable and saddle nodes. An unstable node is a point on the RCM from which residue curves originate, and a stable node is a point where residue curves terminate. Curves tend to approach a saddle node without reaching it, instead veering away toward the stable node. It can be said that residue curves, which are composition profiles, originate at the unstable node and proceed toward the saddle node before approaching the stable node, where they terminate.

Therefore, knowing the position and nature of a system's nodes allows one to gain insight into the manner in which the composition of a mixture will progress as material permeates from it. For idealised models such as constant relative volatility (for distillation) and constant relative permeability (for membrane separation), these nodes occur on the vertices of the mass balance triangle, in other words, at pure components.[13] For more complex permeation models, nodes can occur in other locations, and phenomena such as multiple stable nodes can occur.[27]

This chapter endeavours to develop a method for synthesizing separation processes utilising two membranes arranged in an asymmetric configuration in a single shell. The term 'asymmetric configuration', in this case, is used to indicate a setup whereby a single retentate stream is exposed to two different membranes. Javaid[28] defines a membrane as an interphase between two bulk phases. In the case of the asymmetric configuration, a single bulk retentate phase is separated from two bulk permeate phases by two membranes each acting as an interphase, so two interphases are applied to a single retentate phase. The use of the term 'asymmetric configuration' is to distinguish this setup from an 'internally staged' setup, in which the retentate is exposed to only one interphase, but the resulting permeate phase is itself exposed to a second interphase. This concept is distinct from that of an 'asymmetric membrane', which refers to a single membrane formed of multiple layers of different material and refers to the nature of an actual membrane. The term 'asymmetric configuration' refers not to an actual membrane, but rather to a structure involving multiple membranes.

Of particular interest is the possibility of achieving problematic separations using membranes of fairly low selectivity, particularly porous membranes, since these tend to be far less costly than selective membranes and have far higher permeability than non-porous membranes[9], resulting in lower membrane areas required for separation, and lower cost relative to

membrane area. For polymers, an inverse linear relationship between permeability and selectivity has been identified, showing a clear trade-off between these membrane characteristics [29], [30]. Polymer membranes in particular are a field in which rapid advancement is being made, and offer good performance characteristics along with versatility and robustness [10], [31]. Therefore, devising equipment to be able to use such membranes to achieve a wide variety of separations is preferable to fabricating new membrane materials for specific separations. In order to adequately take advantage of available membrane materials, a synthesis methodology for identifying how best to apply a particular set of available membranes is needed. This chapter endeavours to provide a method for synthesising two-membrane permeators and identifying scenarios where such setups are advantageous when compared to more conventional approaches.

A two-membrane permeator in the asymmetric configuration has been previously shown to be advantageous for the separation of binary mixtures by Stern et al. [32]. This chapter aims to investigate the possibility of similar advantages being found for the separation of ternary mixtures. Note also that for a binary mixture, using simple flux modelling, there are only two positions for stationary points, so the only significant topographical change that is possible is switching the stable and unstable nodes. This means that the RCM of a two-membrane permeator cannot exhibit topographical properties which are significantly different from those of its constituent membranes. In a ternary system, however, three stationary points exist, so a wider variety of topographical properties becomes possible.

The use of two-membrane permeators for the separation of ternary systems has been previously examined by Sengupta and Sirkar [33], who simulated and tested a two-membrane permeator using cellulose acetate fibres and silicone rubber capillaries to separate a mixture of helium, carbon dioxide and nitrogen. In that paper, they compared the performance of a two-membrane permeator to that of the a setup using the same two membranes in

conventional permeators in two different series configurations, and examined the performance of these configurations in terms of the purity of the slowest permeating component in the retentate stream, and that of the fastest-permeating component in the permeate stream. They found that the performance of the two-membrane permeator always fell between those of the two possible series configurations. In this chapter, RCMs are used to examine such systems in a more generalised manner, and topographical phenomena and their effects on performance are investigated.

In order for it to be possible to modify the topography of a multi-membrane residue curve map, the membranes considered must have differing orders of relative permeabilites for the components in the mixture. Javaid [28] points out five significant mechanisms of transport within porous membranes, and notes that a number of factors contribute to determining which of these mechanisms dominates the separation. Koros and Fleming [8] point out that diffusivity selectivity favours the smallest molecule, while solubility selectivity favours the most condensable molecule and Knudsen diffusion is proportional to the inverse square of the molecular weight of the molecule. Since these different mechanisms will favour different components, variation of the order of relative permeability is likely to be a fairly common occurrence, so the results found in this chapter should be widely applicable.

Previously, Huang et al[27] have used a combination of reaction, vapour-liquid equilibrium and single-membrane permeation to obtain new RCM topographies. It must also be noted that in that work, stable and unstable nodes can occur at points not lying on vertices of the mass balance triangle, due to the influence of reaction on the residue curve maps. This also results in multiple stable or unstable nodes under certain conditions.

In this chapter, the often problematic purification of “intermediate” components is investigated. By this it is meant that the component in question is neither the fastest-

permeating nor the slowest-permeating component. In the scenario considered, a ternary mixture is considered, for which two membranes are available which invert the fastest- and slowest-permeating components, but share an intermediate component. In such a scenario, obtaining the shared intermediate in high purity would typically be problematic, and require multiple unit operations.

4.2 Derivation of Residue Curve Equation and choice of flux model

Consider a chamber which contains an initial charge of material, from which material pemeates simultaneously through two non-identical membranes in a batch experiment.

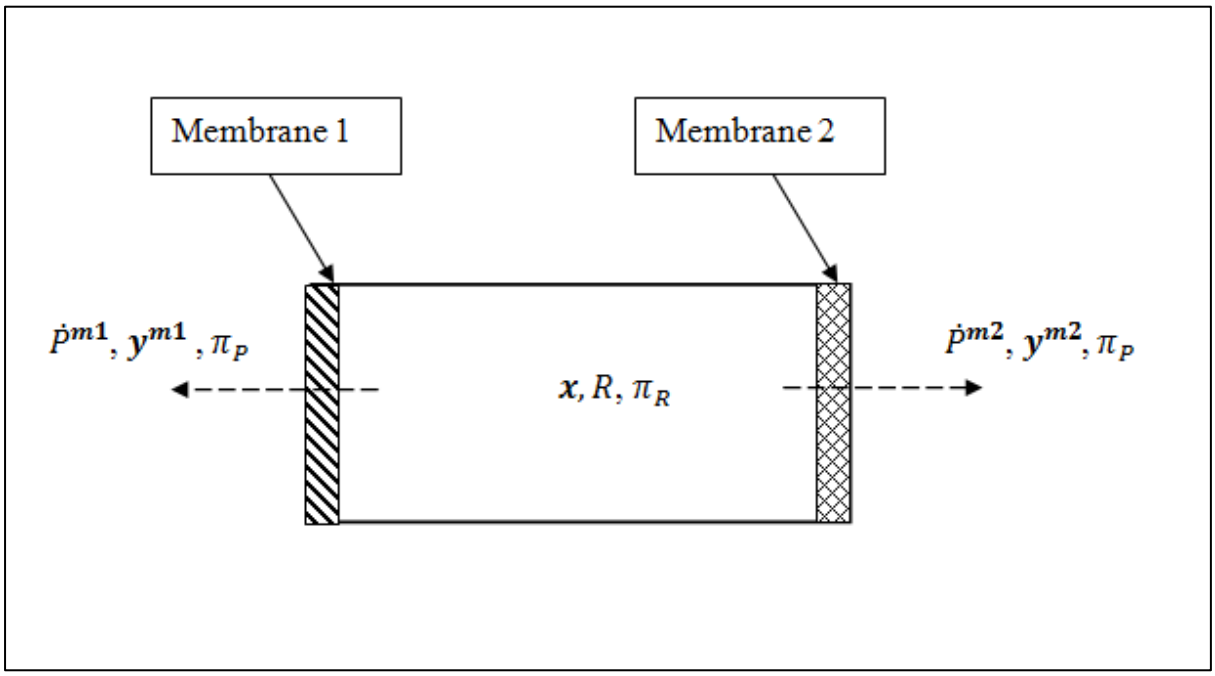


Figure 4.1: sketch of a batch, two-membrane permeator in an asymmetric configuration

In Figure 4.1:

$\dot{P}^{m1}$ refers to the rate of permeation through membrane 1 per unit area $\left[\frac{mol}{s.m^2}\right]$

$\dot{P}^{m2}$ refers to the rate of permeation through membrane 2 per unit area $\left[\frac{mol}{s.m^2}\right]$

$\boldsymbol{y^{m1}}$ and $\boldsymbol{y^{m2}}$ are vector quantities referring to the fractional composition of material permeating through membranes 1 and 2 respectively.

R refers to the quantity of retentate remaining in the chamber, and $\boldsymbol{x}$ refers to the composition of the retentate.

π_P is the pressure in the permeate phase and π_R is the pressure in the retentate phase. $[Pa]$

Now, mass balance indicates that:

$$\frac{d}{dt}(R) + \dot{P}^{m1} + \dot{P}^{m2} = 0 \qquad (4.1)$$

And, component mass balance indicates that:

$$\frac{d}{dt}(R.\boldsymbol{x}) + \dot{P}^{m1}.\boldsymbol{y^{m1}} + \dot{P}^{m1}.\boldsymbol{y^{m2}} = 0 \qquad (4.2)$$

Applying the chain rule yields:

$$R.\frac{d}{dt}(\boldsymbol{x}) + \boldsymbol{x}\frac{d}{dt}(R) + \dot{P}^{m1}.\boldsymbol{y^{m1}} + \dot{P}^{m2}.\boldsymbol{y^{m2}} = 0 \qquad (4.3)$$

But, with (1):

$$\frac{d}{dt}(R) = -\dot{P}^{m1} - \dot{P}^{m2} \qquad (4.4)$$

And, introducing a split ratio, s, such that

$$s = \frac{\dot{P}^{m2}}{\dot{P}^{m1}} \qquad (4.5)$$

It follows that

$$\dot{P}^{\boldsymbol{m1}} = -\frac{1}{1+s}.\frac{d}{dt}(R) \tag{4.6}$$

$$\dot{P}^{\boldsymbol{m2}} = -\frac{s}{1+s}.\frac{d}{dt}(R) \tag{4.7}$$

Substituting these into (1.3) yields:

$$R.\frac{d}{dt}(\boldsymbol{x}) + \boldsymbol{x}\frac{d}{dt}(R) - \frac{1}{1+s}.\frac{d}{dt}(R).\boldsymbol{y}^{\boldsymbol{m1}} - \frac{s}{1+s}.\frac{d}{dt}(R).\boldsymbol{y}^{\boldsymbol{m2}} = 0 \tag{4.8}$$

Gathering terms and dividing through by $\frac{d}{dt}(R)$ yields:

$$\boldsymbol{x} - \frac{1}{1+s}.\boldsymbol{y}^{\boldsymbol{m1}} - \frac{s}{1+s}.\boldsymbol{y}^{\boldsymbol{m2}} = -\left. R.\frac{d}{dt}\boldsymbol{x} \right/ \frac{d}{dt}(R) \tag{4.9}$$

This reduces to

$$\boldsymbol{x} - \frac{1}{1+s}.\boldsymbol{y}^{\boldsymbol{m1}} - \frac{s}{1+s}.\boldsymbol{y}^{\boldsymbol{m2}} = -R.\frac{d}{dR}\boldsymbol{x} \tag{4.10}$$

If we define

$$d\tau = -\frac{dR}{R}$$

Then

$$\frac{d}{d\tau}\boldsymbol{x} = \boldsymbol{x} - \frac{1}{1+s}.\boldsymbol{y}^{\boldsymbol{m1}} - \frac{s}{1+s}.\boldsymbol{y}^{\boldsymbol{m2}} \tag{4.11}$$

4.3 Permeation modeling

Now, the relationship between $\boldsymbol{x}$ and $\boldsymbol{y}^{\boldsymbol{mi}}$ depends upon the properties of the actual membrane used, and may be affected by other parameters such as temperature and pressure.

Likewise, the split ratio, s, will depend on the permeabilities of the two membranes and the ratio of membrane areas, as well as the pressures in the respective permeate phases. Furthermore, since permeation rate is dependent on retentate composition, the split ratio will vary with composition rather than remaining constant. Other factors contributing to permeation rate, on the other hand, can be kept constant, and must be set before integration can be performed. So, in order to plot residue curves, a suitable model for membrane flux must be selected, and the necessary constants must be set.

4.4 Simple permeation model

A simple model for permeation as given by [34] is used for the first two examples in this chapter, where the rate of permeation of a particular component per unit area is given by:

$$J_i = \frac{x_i.p.\pi_R.\alpha_i - y_i.\pi_P.p.\alpha_i}{\delta} \qquad (4.12)$$

Where J_i is the rate of permeation of component i per unit area $\left[\frac{mol}{s.m^2}\right]$

p is the permeability of the reference component $\left[\frac{mol.m}{s.m^2.Pa}\right]$

π_n is the pressure in phase n $[Pa]$

x_i is the mole fraction of component i in the retentate phase

y_i is the mole fraction of component i in the permeate phase

δ is effective membrane thickness $[m]$

α_i is the relative permeability of component i, which is the ratio of the permeability of component i to that of the reference component, $\frac{p_i}{p}$

Now, if one applies the simplifying assumption of vacuum permeate, then $\pi_P = 0$ and equation 1.12 reduces to

$$J_i = \frac{x_i.p.\alpha_i.\pi_R}{\delta} \tag{4.13}$$

Now, by definition,

$$y_i = \frac{J_i}{J} \tag{4.14}$$

the total permeation, J, is the sum of all J_i, so:

$$y_i = \frac{\frac{x_i.p.\alpha_i.\pi_R}{\delta}}{\sum_j^n \frac{x_j.p.\alpha_j.\pi_R}{\delta}} \tag{4.15}$$

Eliminating common factors, this further reduces to

$$y_i = \frac{\alpha_i.x_i}{\sum_j^n \alpha_j.x_j} \tag{4.16}$$

Additionally, it must be noted that the split ratio is not constant, since permeation rate is a function of retentate composition, so the relative permeation rates through the two membranes will vary with changing composition. Therefore, with a flux model selected, one must determine split ratio as a function of retentate composition. Taking the sum of the rates for each component as given by equation 1.13, the total permeation rate through a membrane is given by:

$$J = \sum_j^n \frac{x_j.p.\alpha_j.\pi_R}{\delta} \tag{4.17}$$

Since the split ratio, s, is the ratio of the permeation rates of the two membranes:

$$s = \left. A^{\mathbf{m2}} . \sum \frac{p^{\mathbf{m2}} (x_j . \alpha_j . \pi_R)^{\mathbf{m2}}}{\delta_2} \right/ A^{\mathbf{m1}} . \sum \frac{p^{\mathbf{m1}} (x_j . \alpha_j . \pi_R)^{m1}}{\delta_1} \tag{4.18}$$

By gathering constants, this reduces to

$$s = \left[\frac{A^{\mathbf{m2}} . \delta_1 . p^{\mathbf{m2}}}{A^{\mathbf{m1}} . \delta_2 . p^{\mathbf{m1}}}\right] . \frac{\sum (x_i . \alpha_i)^{\mathbf{m2}}}{\sum (x_i . \alpha_i)^{\mathbf{m1}}} \tag{4.19}$$

All of the terms enclosed within square brackets in equation 1.19 are constant. If these are gathered into a single term, this equation is simplified greatly. This single constant term will be referred to as 'relative ease of permeability' since it quantifies the relative ease with which the reference component passes through the two membranes, and it shall be denoted as E. Applying the additional simplification of vacuum permeate, as before, the following equation for split ratio arises:

$$s = E . \frac{\sum (x_i . \alpha_i)^{\mathbf{m2}}}{\sum (x_i . \alpha_i)^{\mathbf{m1}}} \tag{4.20}$$

Using E as a variable rather than the membrane area ratio is convenient because it allows one to produce RCMs without making any statements about the properties of a membrane aside from modeling permeating composition. For simple membranes, relative permeabilities are not strongly dependent on the manner of fabrication of the membrane, but membrane thickness and overall permeability can vary. Thus, synthesizing permeators using E means that the synthesis is not dependent on physical properties of the membrane, and various fabrication options will remain open, barring physical constraints on what area ratios are achievable.

To obtain a particular value of E, one must first measure the physical parameters of the two membranes as bundled together in equation 4.19, aside from the area ratios. Once the ratios

of the other parameters are known, E can be set accordingly by selecting an appropriate area ratio.

4.5 Location of Stationary points

Stationary points are found when the differential equation is equal to zero. Noting equation 4.11, this will occur at pure component compositions. If the retentate is a pure component, then the permeating material must likewise be pure. In other words, at pure components, the permeating composition is identical to the retentate composition and therefore, the retentate composition does not change. If one refers to equation 4.11, this can be confirmed mathematically, since at a pure component composition, $\boldsymbol{y^{m2}}=\boldsymbol{y^{m1}}=\boldsymbol{x}$, therefore $\frac{d}{d\tau}\boldsymbol{x}=0$.

Therefore, under the assumption of vacuum permeate and no back-permeation, there are always stationary points on each of the vertices of the mass balance triangle. For the simple permeation model used in this chapter, no other stationary points occur. However, for complex permeation modelling, additional stationary points do exist, and this phenomenon is covered in Chapter 5.

4.6 Manipulation of RCM topography and classification of nodes

4.6.1 Vector notation for relative permeability

A vector notation is used to denote the relative permeabilities of various membranes and takes the following form for a single membrane:

$$[\alpha_A, \alpha_B, \alpha_C]$$

where α_i is the relative permeability of component i, noting that α_B is always 1, since B is used as the reference component.

For a two-membrane system, the vector notation takes the following form:

$$[\alpha_A^1, \alpha_B^1, \alpha_C^1 ; \alpha_A^2, \alpha_B^2, \alpha_C^2]$$

where α_i^j is the relative permeability of component i through membrane j. Once again α_B^1 and α_B^2 are always 1, since B is used as the reference component.

4.6.2 Plotting of residue curve maps

Consider two membranes, with constant relative permeabilites of [0.7, 1, 4] and [2, 1, 0.4], these membranes being referred to hereafter as membrane 1 and membrane 2 respectively. Individually, these two membranes would yield the M-RCMs shown in Figure 4.2 and Figure 4.3.

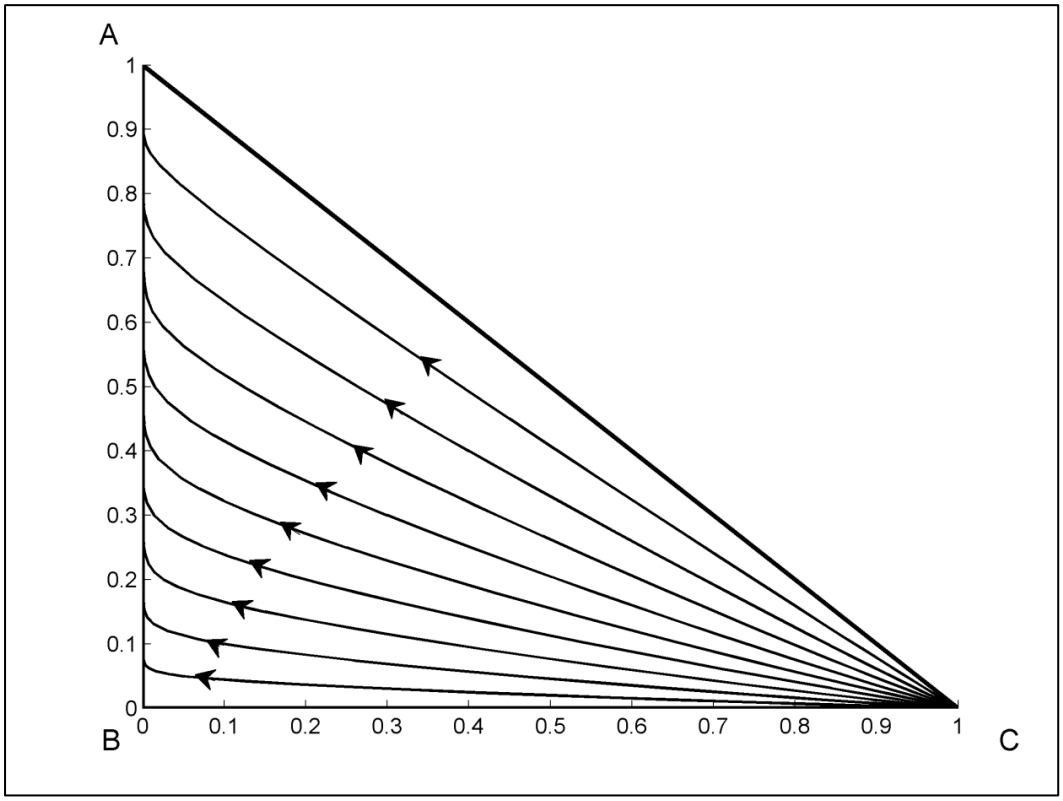


Figure 4.2: Simple M-RCM with α= [0.7, 1, 4]

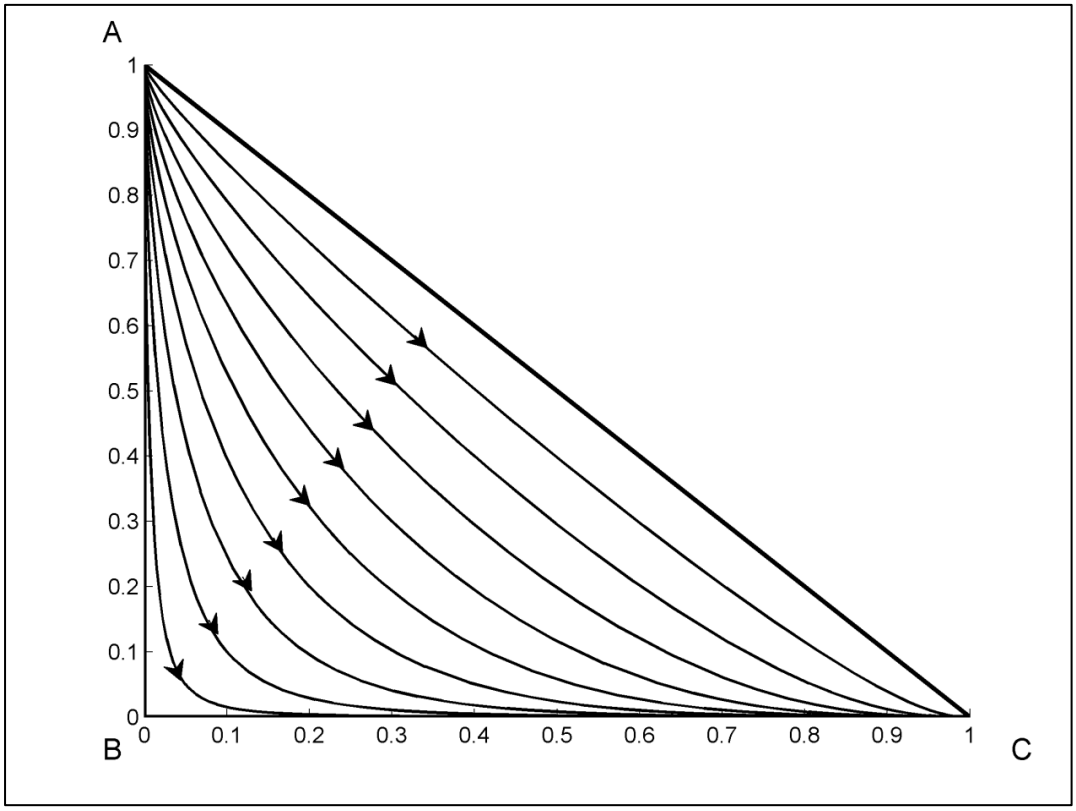


Figure 4.3: Simple M-RCM with α= [2, 1, 0.4]

In the case of membrane 1, the stable node lies at pure component A, and the unstable node at pure component C, while a saddle node occurs at pure component B. In the case of membrane 2, the saddle node is, likewise, at pure component B, but the stable and unstable nodes are switched. Looking at these M-RCMs, it is apparent that using either of these membranes individually, components A or C can be obtained as pure products without difficulty. However, obtaining component B in high purity is problematic since neither membrane results in curves that approach that node.

Neither of these membranes are individually suitable for obtaining pure component B and, if single-membrane permeators are used, a series of two units is needed to reach high purity of component B. Further, residue curves which reach pure B will occur only if a binary mixture containing B is used as a feed. Therefore, the first stage in such a sequence must proceed to sufficient extent as to approach a boundary of the mass balance triangle. The subsequent

stage could then obtain B in high purity. By requiring high extents of permeation in both stages, such a sequence would produce a low yield of component B and would require a large membrane area. Alternatively, one could combine these two membranes in a multi-membrane permeation setup. Figure 4.4 shows residue curves from each of these two single-membrane permeators overlaid on the same plot.

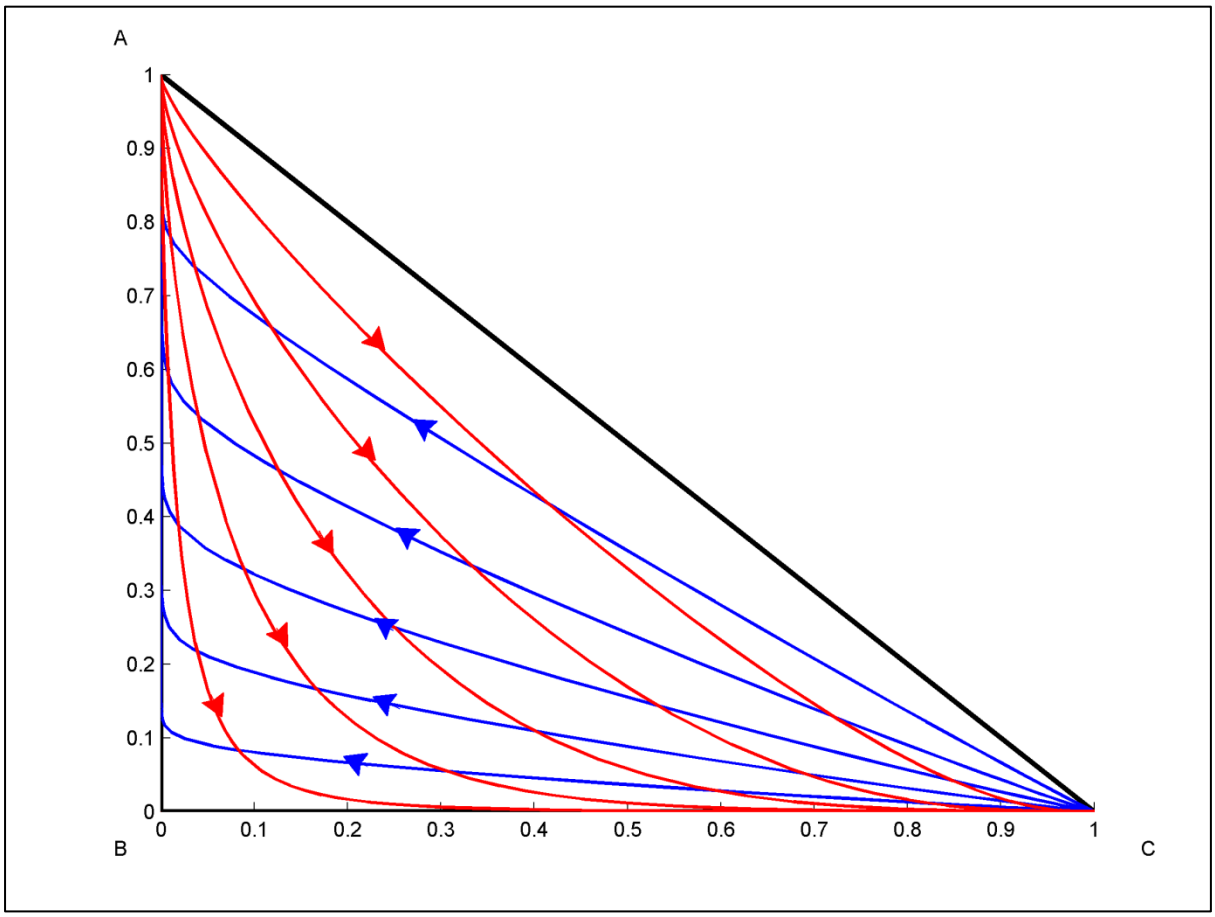


Figure 4.4: Membrane Residue Curves for two different membranes shown on same axes. Curves for α= [0.7, 1, 4] shown in blue, curves for α= [2, 1, 0.4] shown in red

Looking at the vectors of the different curves in Figure 4.4, one might intuitively expect that with certain area ratios, the combinations of those vectors could result in curves that trend toward pure component B. With a relative ease of permeation (E) of 1, the two-membrane M-RCM shown in Figure 4.5 is obtained.

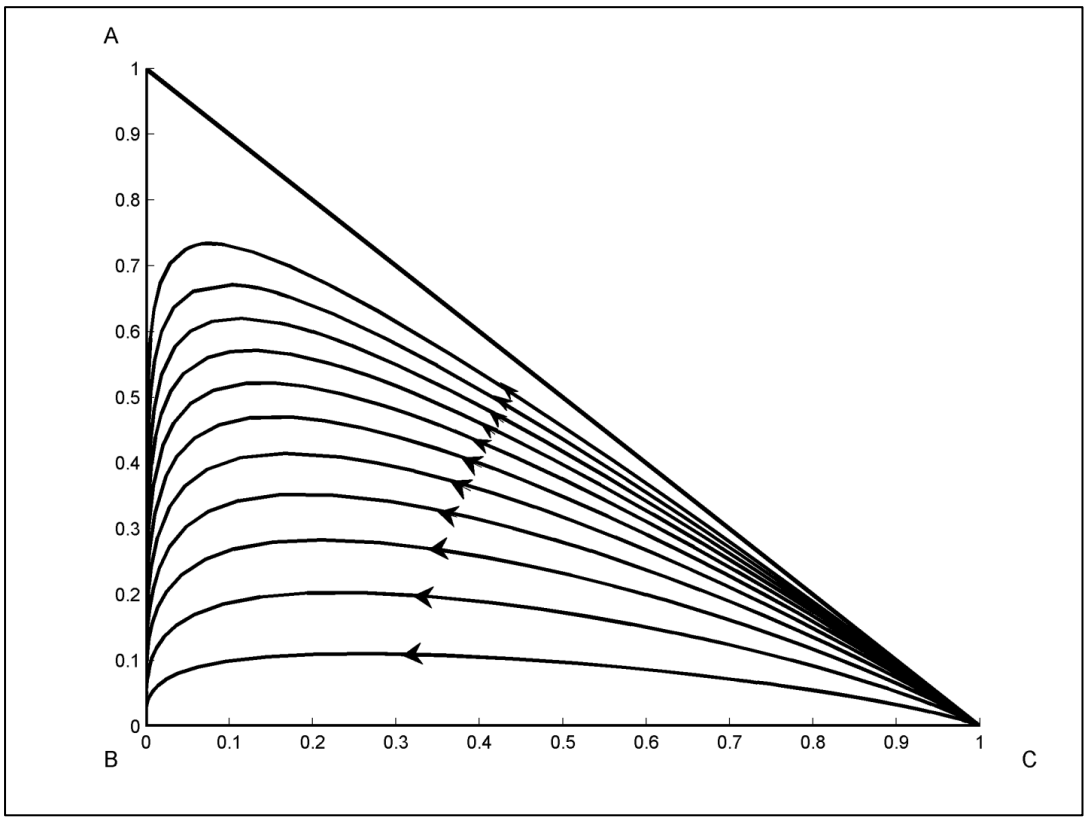


Figure 4.5: Two-membrane M-RCM with α= [0.7, 1, 4; 2, 1, 0.4] and E=1

Pure Component B is now the stable node of this system, meaning that high purity component B can be readily obtained as a retentate product. This example serves to illustrate a graphical process synthesis technique which offers a ready comparison of the suitability of separation processes of these types and also illustrates a scenario in which an asymmetric permeation unit would be preferable to traditional membrane units, which is discussed in more detail in Section 4.9. Note that, in such a system, this phenomenon will not be observed for all values of E. Since changes in the nature of the nodes have significant implications for performance, it is important for a designer to be able to identify the conditions under which these phenomena occur.

4.7 Effect of varying area ratio on topography

When setting up a two-membrane permeator, the value of E is governed by the effective membrane thickness and the area ratio. Effectively, this means that E can be varied by manipulating the area ratio. Figure 4.6 below shows the effect of varying values of E on such a setup.

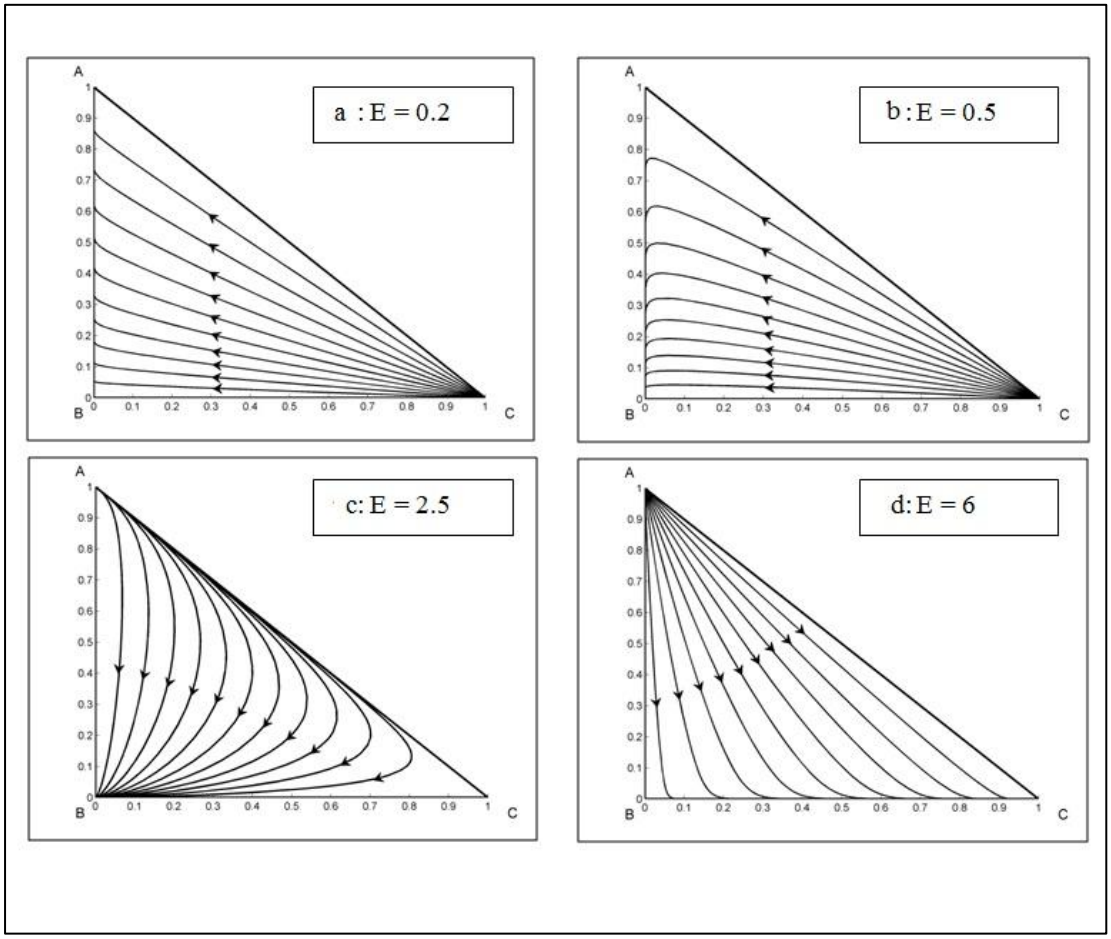


Figure 4.6: a-d Asymmetric Permeation M-RCMs with α= [0.7, 1, 4; 2, 1, 0.4] and E varied between 0.2 and 6

Examination of this collection of M-RCMs reveals several insights. Firstly, one can note that the nature of the stationary points is altered by variation of the value of E. The useful property of this system, that an otherwise difficult to obtain intermediate component can become the stable node, is present only for a certain range of values of E. This means that, in

order to take advantage of this phenomenon, a designer is restricted to a particular range of area ratios. Further, within this range of values, it is possible to switch the unstable node between components A and C, while B remains the stable node. This reveals further flexibility available to the designer attempting to beneficially modify the topography of such a map.

These effects can be explained in an intuitive way, by discussing the physical forces which are at work. The key is to note that the permeation rate through either membrane varies with respect to the retentate composition, and that the effect of either membrane on the overall separation is proportional to the permeation rate through that membrane. Since, for any one membrane, the stable node is the slowest permeating component, proximity to the stable node reduces the permeation rate through that membrane, allowing the other membrane to dominate the separation, particularly in cases like this, where the stable node of each membrane is also the unstable node of the other. This means that as either membrane's stable node is approached by a residue curve, the separation mechanics act to push the curve away from that node. As a result, residue curves cannot approach the stable nodes of either membrane, and the overall stable node must lie elsewhere. Of course, extreme values of E allow one membrane to dominate the separation, resulting in maps closely resembling those of the individual membranes.

4.8 Classification of nodes and use of eigenvalue plots for synthesis

The topographical behavior discussed conceptually in section 4.7 can also be explained mathematically by identifying nodes and classifying them according to Lyaponouv's theorem of stability. Nodes, or stationary points, are found at points where the differential equation used for plotting residue curves is equal to zero. For the simple flux model used above, these

always occur on the vertices of the mass balance triangle, because when the retentate is a pure component, then the permeating compositions are likewise pure in that component.

This means that $\boldsymbol{x} = \boldsymbol{y^{m1}} = \boldsymbol{y^{m2}}$. Since $\frac{1}{1+s} + \frac{s}{1+s} = 1$, the right hand side of equation 1.11 reduces to zero. With the stationary points thus located, it remains to classify the nodes. According to Lyaponouv's theorem of stability, this can be done by evaluating the eigenvalues of the Jacobian of the residue curve equation. Thus, evaluating the eigenvalues at the vertices of the mass balance triangle allows one to determine the nature of the nodes occurring at those points. Two negative, real eigenvalues indicates an unstable node, two positive, real eigenvalues indicates a stable node and two real eigenvalues, one positive and one negative, indicates a saddle node. Complex eigenvalues are not addressed in this chapter, and nodes with complex eigenvalues are not found within the mass balance triangle.

By plotting curves of the eigenvalue pairs of the three nodes against values of E, it is possible to graphically represent the variations in topographical behaviour. Such a plot is shown in Figure 4.7, for a pair of membranes with $\boldsymbol{\alpha}$= [0.7, 1, 4; 2, 1, 0.4]. In the plot shown in Figure 4.7, the x-axis shows values of E/E+1, rather than values of E, so as to represent all values of E from zero to infinity with a range of numbers from zero to one. Also, it was found that such a plot more evenly distributes the points of interest across the x-axis, allowing for a clearer picture.

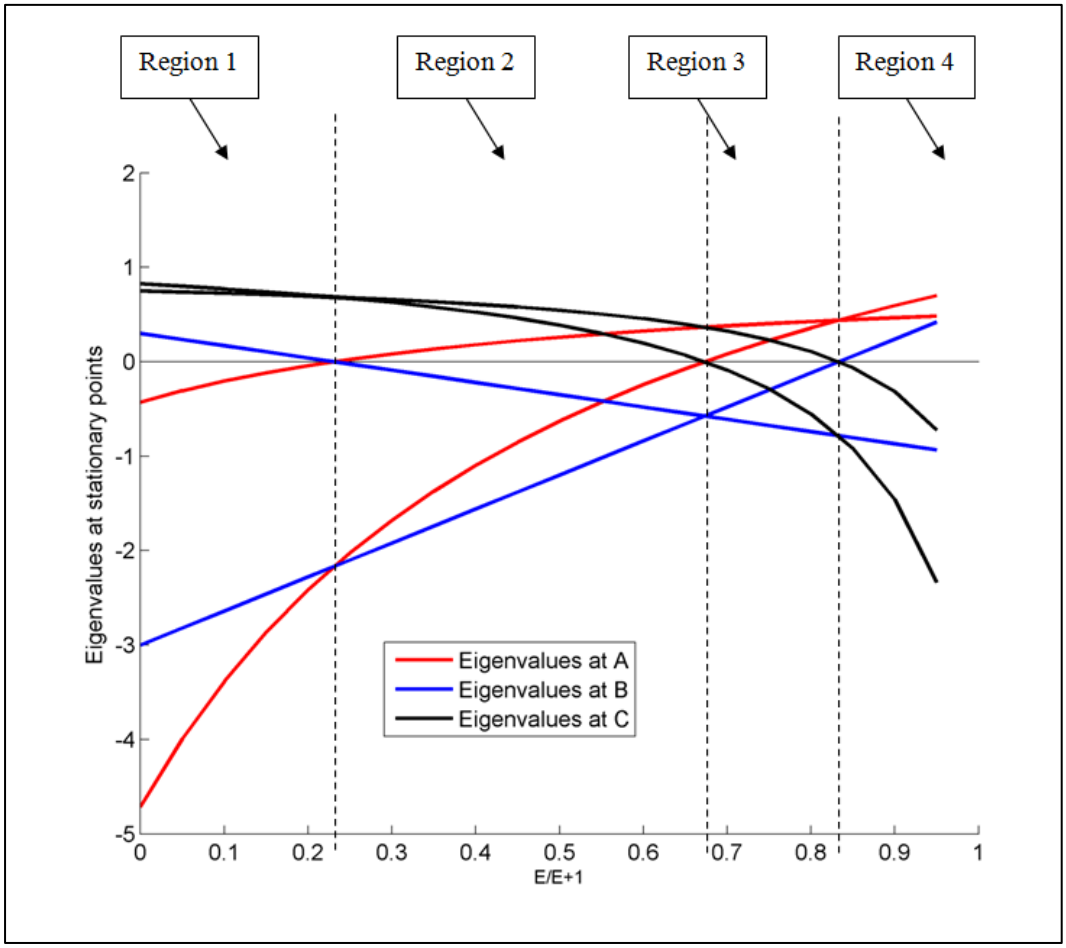


Figure 4.7: Eigenvalues at stationary points plotted against E/E+1

In Figure 4.7, four regions are apparent, with disparate topographical properties. These properties are summarised in Table 4.1. Changes in the nature of the nodes occur at the points where curves intersect with the x-axis, when an eigenvalue changes sign. Note that on this plot, two curves always intersect the x-axis simultaneously. This is because such a system always has one saddle node, one stable node and one unstable node. Therefore, the nodes change nature simultaneously. Potentially, four curves could intersect simultaneously, if all three nodes change properties at the same point.

Table 4.1: Properties of nodes in different operating regions

	Region 1	Region 2	Region 3	Region 4
Node at A	Stable	Saddle	Unstable	Unstable
Node at B	Saddle	Stable	Stable	Saddle
Node at C	Unstable	Unstable	Saddle	Stable

Having identified the topographical properties of different regions, it becomes possible to determine how a particular separation could best be achieved. For example, if one wishes the retentate to be enriched in a particular component then, ideally, one would operate in a region in which that component is a stable node.

If one wishes for a component to be depleted in the retentate, then one would operate in a region in which that component is an unstable node. The reverse relationships hold true for the concentration of components in the permeate streams. It was stated earlier that the goal in this example is to obtain component B in high purity, and it can be seen in Table 4.1 that in regions 1 and 2 component B is the stable, favouring its enrichment in the retentate stream.

Note that the methods developed so far can find ranges of values for which desirable topographical behaviour is possible. As yet, no method has been developed for finding an optimal value for E within such a range. Initial observations indicate that the best results occur when the value of E/E+1 falls in the region of midway between the endpoints of the chosen range, but this is a very rough generalisation. Once a range has been found, further optimisation will be required to maximise performance.

4.9 Comparison of continuous processes

Considering the same hypothetical pair of membranes used for section 3 above, a continuous process can be simulated. In the continuous permeator pictured in Figure 4.8, a single retentate stream enters a permeator vessel, and is exposed to both membranes, producing two permeate streams.

Considering a small segment of a continuous permeator, in which a small change in retentate flow-rate, dR, occurs as a result of permeation from the retentate stream into the two permeate streams, and once again using a split ratio, s, mass balance dictates the following:

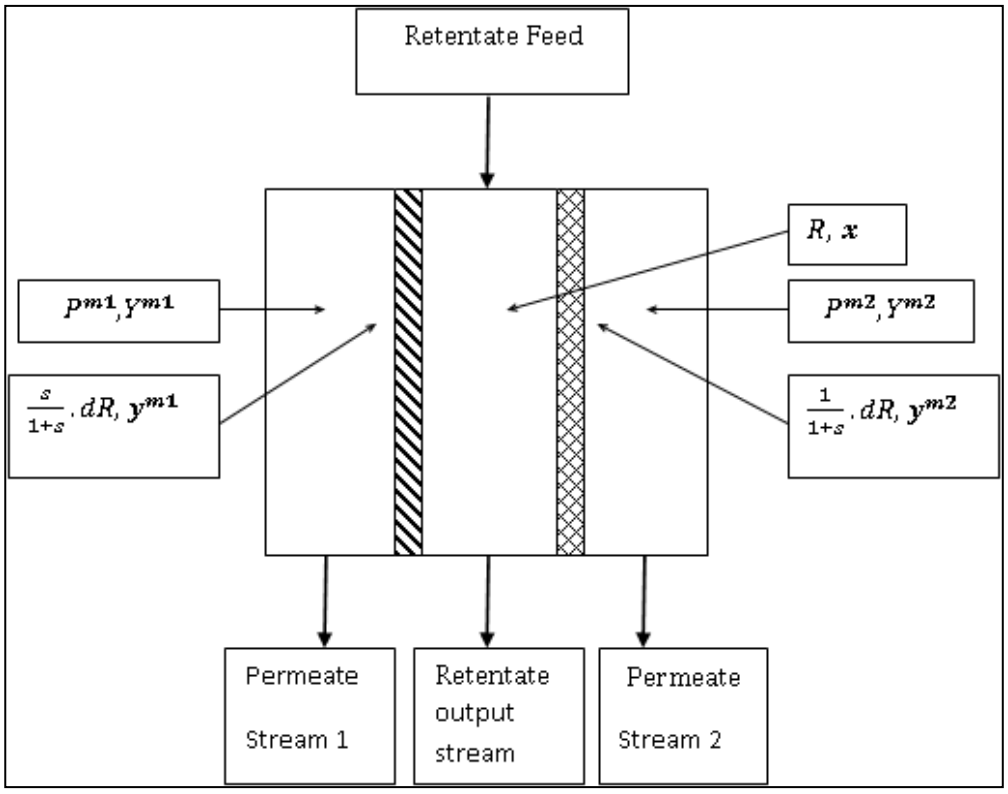


Figure 4.8: sketch of continuous permeation setup of two-membrane permeator in asymmetric configuration

$$dP^{m1} = -\frac{1}{1+s}.dR \qquad (4.22)$$

$$dP^{\boldsymbol{m2}} = -\frac{s}{1+s}.dR \tag{4.23}$$

$$dY_i^{\boldsymbol{m1}} = \frac{(P^{\boldsymbol{m1}}.Y_i^{\boldsymbol{m1}} - \frac{1}{1+s}.dR.\boldsymbol{y}^{\boldsymbol{m1}})}{(P^{\boldsymbol{m1}} - \frac{1}{1+s}.dR)} - Y_i^{\boldsymbol{m1}} \tag{4.24}$$

$$dY_i^{\boldsymbol{m2}} = \frac{(P^{\boldsymbol{m2}}.Y_i^{\boldsymbol{m2}} - \frac{s}{1+s}.dR.\boldsymbol{y}^{\boldsymbol{m2}})}{(P^{\boldsymbol{m2}} - \frac{s}{1+s}.dR)} - Y_i^{\boldsymbol{m2}} \tag{4.25}$$

$$d\boldsymbol{x}_i = (\boldsymbol{x}_i.R + \frac{1}{1+s}.dR.\boldsymbol{y}^{\boldsymbol{m1}} + \frac{s}{1+s}.dR.\boldsymbol{y}^{\boldsymbol{m2}}) \Big/ (R + dR) - \boldsymbol{x}_i \tag{4.26}$$

Where $\dot{P}^{\boldsymbol{m1}}$ refers to the rate of permeation through membrane 1, $\dot{P}^{\boldsymbol{m2}}$ refers to the rate of permeation through membrane 2, $\boldsymbol{y}^{\boldsymbol{m1}}$ and $\boldsymbol{y}^{\boldsymbol{m2}}$ are vector quantities referring to the composition of material permeating through membranes 1 and 2 respectively. R refers to the quantity of retentate remaining in the chamber, and $\boldsymbol{x}$ refers to the composition of the retentate. $Y^{\boldsymbol{m1}}$ and $Y^{\boldsymbol{m2}}$ refer to the bulk compositions in permeate phases 1 and 2 respectively.

Note also that dR will be a negative quantity if one considers the direction of retentate flow to be the positive direction, since, neglecting back-permeation, the retentate flow-rate will be decreasing as it proceeds down the length of the membrane.

For comparison, a series configuration of membranes will be used in the setup shown in Figure 4.9.

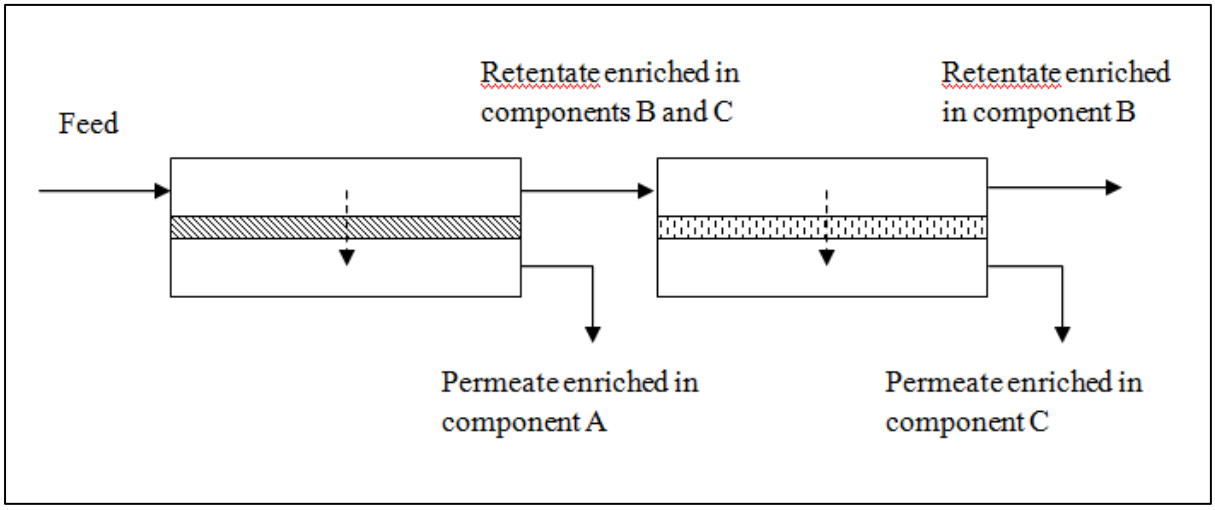


Figure 4.9: Series configuration of two single-membrane permeators in series

Note that the ordering of the membrane units can be switched around and in fact, both possible configurations are considered.

The flux modeling discussed in Section 4.2 is used, along with the assumption of vacuum permeate for simplicity since, under this assumption, the composition of the permeating material is a function only of the retentate composition and not the composition of the permeate phase, allowing one to simulate the progression of retentate composition without considering the conditions of the permeate. A conventional single-membrane permeator can be modeled in a similar manner.

A series configuration would typically be used to obtain a shared intermediate component, so, in order to provide a basis for comparison by which the performance of the two-membrane permeator can be assessed, a series configuration of the two membranes in question can be similarly simulated. In this section, performance comparisons will be made between a two-membrane permeator and the two possible configurations using the two membranes in series.

In Section 4.8, it was shown that for membranes with relative permeability vectors of [0.7, 1, 4] and [2, 1, 0.4], the intermediate component is the stable node of the RCM when relative ease of permeability (E) falls in the range 0.23 to 5, therefore a value of 0.8 was chosen for E

in the simulation of the two-membrane permeator, as it yielded the best results within this range. The series configurations are simulated such that the retentate stream is transferred from the first unit to the second when membrane cut is 0.5.

In Figure 4.10, the product purity in the three possible setups is plotted against membrane cut, which refers to the ratio of the quantity of material which has permeated from the retentate phase to the quantity originally present in the retentate phase. A feed composition of [0.2 0.6 0.2] is used. Also, for the series configurations, a stage cut of 0.5 is used, where stage cut is the fraction of the original retentate flow-rate which has permeated.

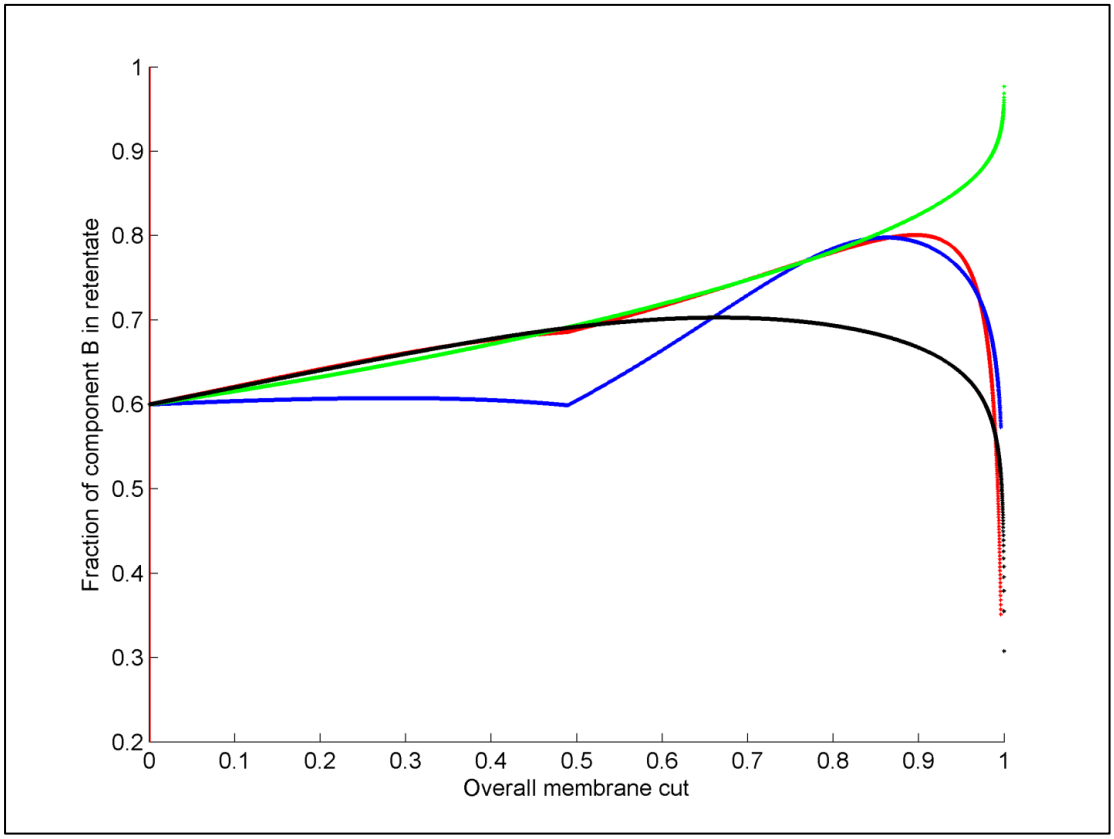


Figure 4.10: Purity of intermediate component in retentate, with feed of mole fractions [0.2, 0.6, 0.2] and membranes with relative permeability vectors of [0.7, 1, 4] and [2, 1, 0.4]. series configuration with membrane one followed by membrane two is shown in red, series configuration with membrane two followed by membrane one is shown in blue. Two-membrane membrane configuration with E=0.8 is shown in green. Two-membrane membrane configuration with E=0.1 is shown in black

As can be seen in Figure 4.10 the two-membrane permeator with E=0.8 offers considerably higher product purities for high membrane cuts, approaching one hundred percent purity as membrane cut approaches one, as one would expect with the stable node of the system. A similar simulation was also run, but using a value of E falling outside of the range for which component C becomes the stable node (E=0.1). However, Figure 4.10 also shows that when operating conditions are such that the intermediate component is a saddle point, then the two-membrane permeator is ineffective for purification of the intermediate component, demonstrating that the advantages of this sort of setup are contingent on the area ratio used.

4.9.1 Separate permeate streams

Withdrawing a single permeate stream results in physical equipment equivalent to a conventional single-membrane permeator, offering a useful basis for comparison in terms of separation performance. However, this is by no means a binding constraint. Withdrawing two separate permeate streams is simple to do and therefore worth investigating.

The membranes we have examined above are individually well suited to the purification of components A and C, as those components are either the slowest- or fastest-permeating components of each membrane. The use of a multi-membrane permeator makes it possible to selectively purify component B in the retentate stream but it is still useful to examine how effective this setup is at purifying components A and C in the two permeate streams.

The compositions of all three streams can be plotted on axes the same as those used for MM-RCMs, tracking the compositional changes along the length of a multi-membrane permeator unit. The retentate composition curve will simply follow a residue curve trajectory on the MM-RCM from its initial composition and approaching the local stable node as the last of the material is permeated. Figure 4.10 shows the composition profiles for a co-current multi-membrane permeator. The complete profiles are those of a total permeator, which is to say a unit that runs to conclusion with all material permeated through the two membranes.

In a single-membrane setup, a total permeator has no separation effect because mass balance dictates that if all material is permeated then the permeate composition must be identical to the original feed composition. In a two-membrane setup, however, a total permeator is able to achieve separation by splitting material between two permeate streams.

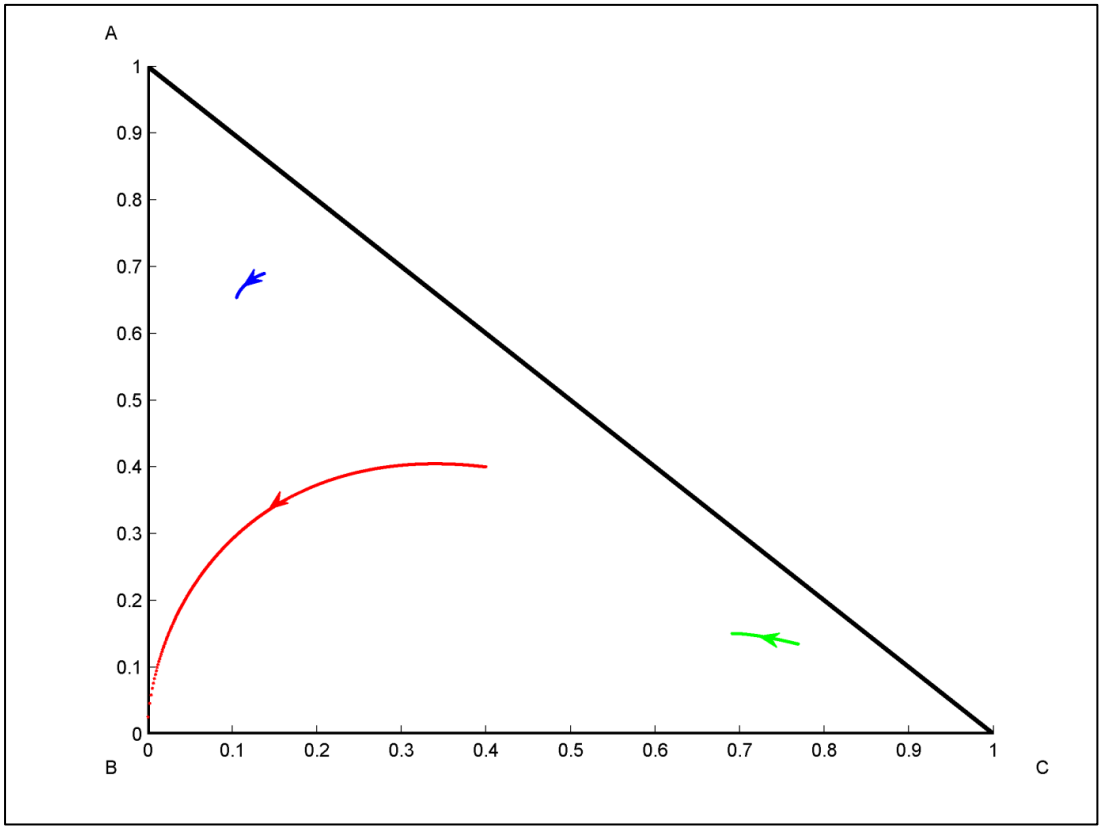


Figure 4.11: Composition profiles for retentate and separate permeate streams for two-membrane total permeator with membranes of relative permeability vectors of [0.7, 1, 4] and [2, 1, 0.4] and molar feed composition [0.4, 0.2, 0.4] and E=1.5. Retentate composition profile is shown in red, while permeate through membrane 1 is shown in green and permeate through membrane two is shown in blue.

For a co-current unit all compositions progress together down the length of the permeator. At any point along the length of the permeator, mass balance dictates that the sum of each component flow-rate in the permeate streams is equal to the amount of that component that has left the retentate up to that point.

Consequently, terminating the permeator unit at any point along the retentate composition curve results in permeate composition curves that are just the corresponding portions of the full permeate composition curves. The composition curves in Figure 4.11 therefore embody

the composition profiles of all co-current columns with these permeabilities and this feed composition, regardless of the membrane cut.

For a counter-current unit, however, this is not true. Terminating at different points along the permeator will result in totally different permeate composition curves. The composition curves for a total permeator do not therefore embody all of the permeate composition curves for a counter-current unit, as they do for a co-current unit.

However, we know that under conditions of permeate vacuum, co- and counter-current units will achieve identical separations for any particular membrane cut. This is because in vacuum conditions, the permeate composition does not affect permeation and consequently, outlet permeate composition for a particular membrane cut is identical for the two flow regimes, though the permeate composition profiles will differ.

Hence, the permeate composition curves for a total permeator not only embody all permeate composition curves for co-current units of any membrane cut but also represent the loci of outlet permeate compositions for counter-current units of any membrane cut.

Figure 4.11 therefore gives us insight into the permeate product streams from both co- and counter-current units. Note that this would not hold true for non-vacuum permeate conditions, where the permeate compositions directly affect permeation.

Figure 4.11 shows that this multi-membrane setup is not only well-suited to producing high-purity component B in the retentate stream but also offers a good degree of separability between the two permeate streams.

This same unit can be operated as a total permeator ie a unit in which all material is permeated. This results in only two product streams in the form of the two permeate streams, with approximately equal flow-rates in this case and with outlet compositions of [0.15, 0.16,

0.69] and [0.65, 0.24, 0.11] for membrane 1 and membrane 2 respectively. We can once again compare this separation to that which is achieved by a single-membrane unit, which will also produce two separate product streams, the retentate and the permeate. Membrane 1 by itself and with a membrane cut of 0.5 produces a permeate stream of composition [0.21, 0.14, 0.66] and a retentate stream of composition [0.59, 0.26, 0.15]. Membrane 2 by itself and with a membrane cut of 0.5 produces a permeate stream of composition [0.60, 0.20, 0.20] and a retentate stream of composition [0.20 0.20, 0.60].

This demonstrates that besides being more effective in purifying component B in the retentate stream, the two-membrane setup also offers superior performance than either of these membranes for the task of purifying components A and C across two product streams.

We can explore this possibility further by examining the same setup but at other values of E.

Figure 4.12 shows the composition profiles for the same membrane setup as Figure 4.11, but with E=9, allowing membrane 2 to dominate the separation to some degree.

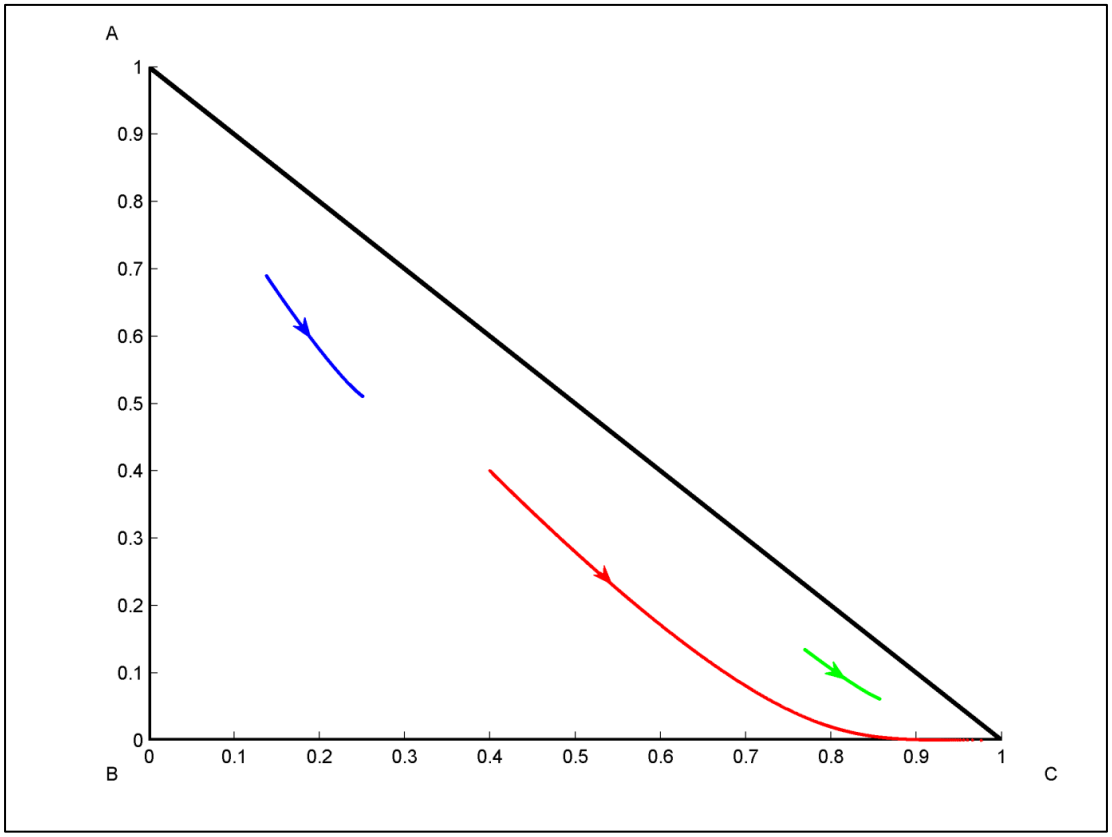


Figure 4.12: Composition profiles for retentate and separate permeate streams for two-membrane total permeator with membranes of relative permeability vectors of [0.7, 1, 4] and [2, 1, 0.4] and molar feed composition [0.4, 0.2, 0.4] and E=9. Retentate composition profile is shown in red, while permeate through membrane 1 is shown in green and permeate through membrane two is shown in blue.

The first point of interest to note in Figure 4.12 is the progression of the composition of the permeate stream through membrane 1. The composition profile begins at the permeating composition corresponding to the initial retentate composition and then proceeds toward higher purity of component C. In a single-membrane setup, the permeate composition profile would begin at the same point and then proceed toward the initial retentate composition.

Hence, that initial composition represents the highest obtainable purity of component C in a single-membrane setup. Note also that a single-membrane setup can achieve that purity only in trace amounts with the purity decreasing as membrane cut is increased. The two-membrane

setup pictured above achieves higher purities as overall membrane cut increases, circumventing a fundamental limitation of single-membrane permeation and achieving higher permeate purity than would be achievable in any single-membrane unit.

It must be noted, however, that with E=9, membrane 2 dominates this separation and the flowrate of membrane 2's permeate stream in the total permeator, V^{m1}, is only a fraction of the original feed flow rate. It follows that, while this separation setup can achieve purities outside of what is otherwise achievable in a single unit, it is constrained in terms of the flow-rate of membrane one's permeate stream. However, examining the performance of the total permeator unit for a feed rate of 1 mol/s reveals that V^{m2} = 0.7555mol/s and V^{m1}=0.2445 mol/s. With an E of 9 one might intuitively expect the final flow-rates to more strongly favour membrane 2 but the retentate composition progressing toward pure component C increasingly favours permeation through membrane 1, which is more selective for component C. The split ratio is initially high because of the high value of E, but decreases as the retentate composition progresses.

This results in surprisingly good recovery of component C along with its high purity, a result which highlights another potential application of multi-membrane permeation.

The increased purity arises because the permeating compositions ($\mathbf{y^{mi}}$) are related to the retentate and therefore tend to track the progression of **x**. Consequently, establishing pure component C as a stable node permits higher purities of C in the permeate by bringing the retentate composition toward pure C as permeating progresses, increasing the driving force for the permeation of component C. In a single-membrane unit selectively permeating component C the opposite occurs and the retentate profile moves away from component C, resulting in reduced driving force.

This demonstrates that MM-RCM topographical behaviour can be used to manipulate the driving forces for permeation into the respective permeate streams.

V^{m2} remains the larger permeate stream in terms of flow-rate, however, so it is of interest to consider how successful this setup is at enriching component A in that stream. A straightforward basis for comparison is a single-membrane setup using membrane 1 and with a membrane cut of 0.7555, with the same initial feed of [0.4, 0.2, 0.4]. This is easily simulated and results in a single permeate stream with composition [0.51, 0.22, 0.27]. The permeate product through membrane 2 in the two-membrane total permeator has a composition of [0.51,0.24,0.25] and the same flow-rate.

While the purity of component A is the same, the two-membrane setup achieves a higher purity of component C, with a permeate composition of [0.068, 0.086, 0.85] as compared to [0.049, 0.14, 0.81] in the retentate from the single-membrane setup.

This result suggests an interesting trend when E is set such that one membrane becomes predominant. The membrane with higher flux achieves diminished separability while the membrane with lower flux achieves increased separability. This result makes intuitive sense; permeation through a membrane will tend to progress in such a way as to reduce the driving force for separation in terms of the composition of the retentate. Allowing one membrane to dominate therefore permits separation to proceed in such a way as to reduce its effectiveness while potentially increasing the effectiveness of the other membrane.

The comparisons thus far have demonstrated that the two-membrane setup can outperform conventional single-membrane permeators when producing two separate product streams. However, the truly unique property of a two-membrane permeator is its capacity to produce three product streams as opposed to the two streams to which a single-membrane unit is limited. Figure 4.9 already demonstrated that a two-membrane unit can achieve better

separation than two single-membrane units in series when producing just one permeate stream. If, instead, two permeate streams are produced and the additional separation between those two streams is considered then the overall separation capacity of such a unit is far greater than that of the single-membrane setup.

Let us once again consider the two-membrane setup analyzed in Figure 4.10. If, instead of total permeation, this setup is operated with an overall membrane cut of two-thirds, the result is three separate product streams with approximately equal flow-rates and compositions of [0.40, 0.27, 0.32], [0.14, 0.11, 0.74] and [0.68, 0.19, 0.12] for the retentate stream and the permeate streams of membranes 1 and 2 respectively.

We can once again analyze two possible arrangements of single-membrane permeators in series, each with a membrane cut of one-third of the original feed.

The series setup with membrane 1 first achieves three product streams with compositions of [0.49, 0.23, 0.27], [0.17, 0.12, 0.72] and [0.71, 0.17, 0.14] for the retentate stream and the permeate streams of membranes 1 and 2 respectively.

The series setup with membrane two first achieves three product streams with compositions of [0.42, 0.22, 0.35], [0.14, 0.11, 0.75] and [0.69, 0.18, 0.13] for the retentate stream and the permeate streams of membranes 1 and 2 respectively.

The two-membrane setup compares favourably overall to both of these setups, enriching component B better than either. It also enriches component C in the second retentate stream better than either series setup. However, it is interesting to note that both series setups are more effective at enriching component A in the permeate than the two-membrane setup.

This fact serves as a reminder that any particular separation method is rarely strictly superior to another. Details such as the exact separation requirements and feed composition will often determine the optimal separation unit for a given task.

4.10 Conclusions

This chapter has derived a residue curve equation for plotting MM-RCMs and has shown how their topography can be manipulated in order to achieve desirable behaviour. Further, it has shown that desirable topographical behaviour corresponds to improved equipment performance and that two-membrane permeators can achieve problematic separations using membranes which are individually unsuited to the task.

The fabrication of multi-membrane units with a combined permeate stream will have the same number of inlets and outlets as a typical single-membrane permeator, so the performance benefits demonstrated in this chapter may come without significant additional costs. However, process control and operating strategies may become more problematic, so these have to be factored in. Moreover, two different membranes will not undergo fouling at the same rate, so the effective area ratio of a multi-membrane unit might change over the course of its operating lifetime. A multi-membrane unit will also require replacement when just one of the two membranes has become fouled, so the replacement costs may also increase.

This chapter has also demonstrated that producing two separate permeate streams can be advantageous and that with carefully selected topographical behaviour, two-membrane permeators can achieve permeate compositions of higher purity than can be achieved in a single-membrane unit.

The synthesis method presented in this chapter will serve to assist in identifying cases where multi-membrane permeators are preferable and in designing multi-membrane permeator units.

Achieving full separation into pure components generally requires membrane cascades, so this single unit analysis does not offer an entirely complete picture of separation using these units. However, it has demonstrated that two-membrane permeators offer improved performance along with the design flexibility required to achieve specific separation goals.

It is conceivable that membrane cascades using two-membrane permeators along with conventional single units could offer significant performance improvements. It is also conceivable that an optimal cascade for a particular separation might involve multiple two-membrane permeators with different area ratios in accordance with each unit's specific role in the cascade. The additional degree of freedom offered by the ability to manipulate area ratio allows for tremendous flexibility in the design and synthesis of separation schemes including multi-membrane permeators. The methods developed in this chapter enable a designer to predict and manipulate the separation behaviour of a particular unit to suit their specific needs.

The MM-RCM methodology also serves as an intuitive teaching tool for instructing design engineers in the fundamentals of multi-membrane permeation processes. No chemical process can be widely adopted without first being widely understood by engineers within the industry and MM-RCMs are sufficiently intuitive and easy to understand to be taught on an undergraduate level. One obstacle to understanding is the mathematical complexities that underpin eigenvalue analysis and this will be addressed in Chapter 5, where I examine an alternative method of characterizing nodes in M-RCMs and MM-RCMs.

MM-RCM behaviour with complex permeation modelling is also examined in Chapter 5 and the MM-RCM synthesis technique is expanded to include such cases. Additionally, the use of node classification is extended to a four-component mixture, using a real-world example to demonstrate the applicability of these synthesis methods.

Chapter 5. Quaternary mixtures and complex permeation

Much of the material in this chapter has previously been published[26] and is here reproduced in accordance with the permitted uses by authors of ACS Publications.

Chapter 4 demonstrated the usefulness of MM-RCMs and node classification using the simple case of a ternary mixture and a simple permeation model. To further illustrate the application of the MM-RCM and node classification methods, this chapter extends the method to more sophisticated examples. Firstly, an MM-RCM is drawn for a ternary system with complex permeation, using the residue curve equation derived in chapter 3. Then, the node classification method is used for a real-world system of four components.

5.1 Complex permeation modelling

Huang et al[27] have previously considered the effects of complex permeation on the performance of membrane permeators. In that paper, the precise mechanisms of permeation are not considered and the effects of complex permeation are instead examined in a general way by using binary mass transfer coefficients. The same approach is used in this chapter, making use of the following model for complex permeation of a component:

$$J_i = \frac{\pi_R.p.x_i.(\alpha_i+\sum(x_j.\gamma_{i,j}))}{\delta} \qquad (5.1)$$

Where J_i is the rate of permeation of component i per unit area $\left[\frac{mol}{s.m^2}\right]$

p is the permeability of the reference component $\left[\frac{mol.m}{s.m^2.Pa}\right]$

π_n is the pressure in phase n $[Pa]$

x_i is the mole fraction of component i in the retentate phase

y_i is the mole fraction of component i in the permeate phase

δ is effective membrane thickness [m]

α_i is the relative permeability of component i, which is the ratio of the permeability of component i to that of the reference component, $\frac{p_i}{p}$

γ_{ij} is a binary interaction parameter quantifying the dependency of the permeability of component i on the concentration of component j. $\gamma_{i,j}$ can be either a positive or negative number, since one component's presence can inhibit or enhance the permeation of another.

As before, the split ratio must be calculated as a function of composition by dividing the total permeation through membrane 2 by the total permeation through membrane 1. It can be seen in the above equation that $x_j.\gamma_{i,j}$ will have the same units as α_i. Since x_j and α_i are both dimensionless, it follows that $\gamma_{i,j}$ will be dimensionless.

Using this model for complex permeation, phenomena such as multiple stable nodes and binary nodes are observed, just as predicted by Huang et al[27].

5.2 Additional stationary points

When complex permeation modeling is used, additional stationary points can occur. Huang et al[27] have previously observed this phenomenon occurring, identifying what they termed "binary arheotropes" occurring when binary mass transfer coefficients were included in the permeation modeling. Section 5.4 of this chapter examines the effects of two-membrane

permeation on the location and behavior of additional nodes arising from complex permeation.

5.3 Complex behaviour

Consider two membranes, membrane 1 and membrane 2 respectively, with relative permeabilites of [10, 1, 0.1] and [0.1, 1, 0.3]. If membrane 1 exhibits complex behaviour such as would arise from a binary mass transfer coefficient of $\gamma_{C,B}$ = 3, while membrane 2 exhibits no complex behaviour, then the single-membrane M-RCMs shown in Figures 5.1 and 5.2 arise.

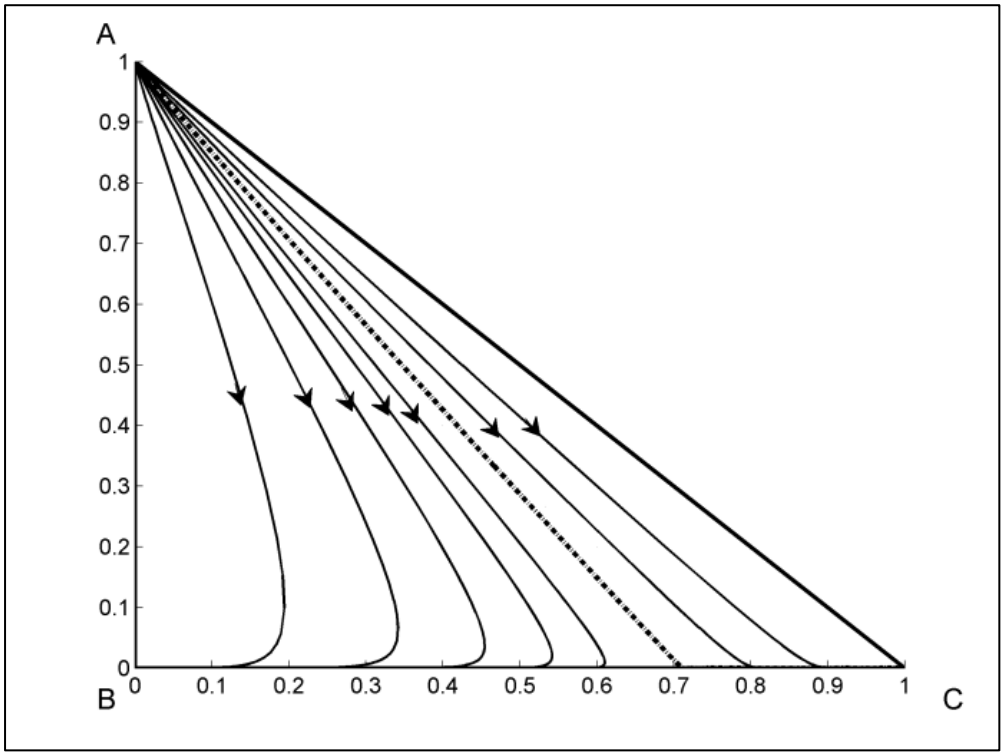


Figure 5.1: Single-membrane M-RCM with complex permeation. α = [10, 1, 0.1], γ_(C,B) = 3

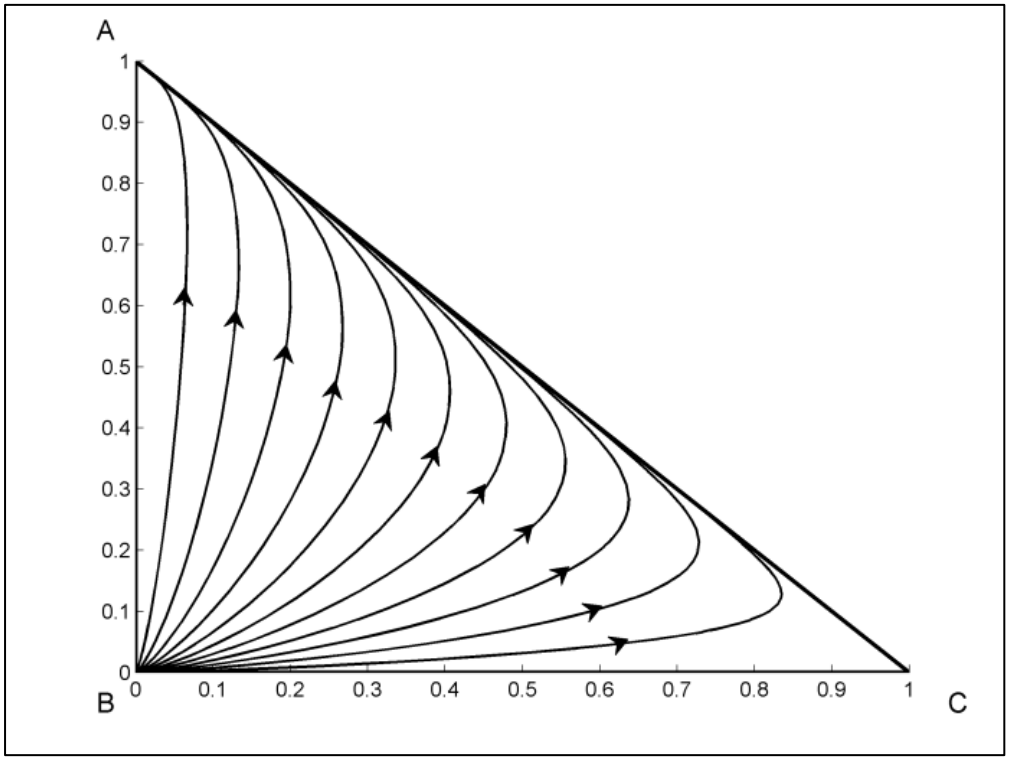


Figure 5.2: Single-membrane M-RCM with α = [0, 1, 0.3]

Figure 5.1 shows that membrane 1 has stable nodes at pure components B and C, and a saddle node occurring at a composition of roughly (0 0.7 0.3). The existence of this additional saddle point and the presence of multiple stable nodes results in a boundary dividing the composition space into two regions, the boundary between which is shown by a dotted curve on Figure 5.1. The region lying to the left of the boundary will be referred to as region 1, and the region to the right of the boundary will be referred to as region 2.

In region 1, curves originate at the unstable node at pure component A and terminate at the stable node at pure component B. In the second region, pure component C is the stable node. This means that if the feed lies in region 1, pure component C can't be obtained as a retentate product from a single-membrane permeator, in spite of it being the slowest-permeating component individually. Therefore, for a broad range of feed compositions, membrane 1 is unsuitable for purification of component C.

Membrane Two has a stable node at pure component A and an unstable node at pure component B, with a saddle node at C. Therefore, this membrane is unsuitable for purification of component C for all feed compositions.

For a large range of feed compositions, neither of these membranes are individually suitable for the purification of component C. A two-membrane permeator may offer a superior solution.

Now, simply locating and classifying all of the nodes will not provide sufficient insight for the synthesis of a separation using membranes exhibiting complex behavior, because the precise path of the boundary between regions 1 and 2 must be known in order to determine which region the feed lies in. As a result, MM-RCMs are required in order to synthesize two-membrane permeators for systems with complex permeation.

Figures 5.3 and 5.4 show the MM-RCMs for these two membranes paired, with values of of E = 1, and E=5 respectively.

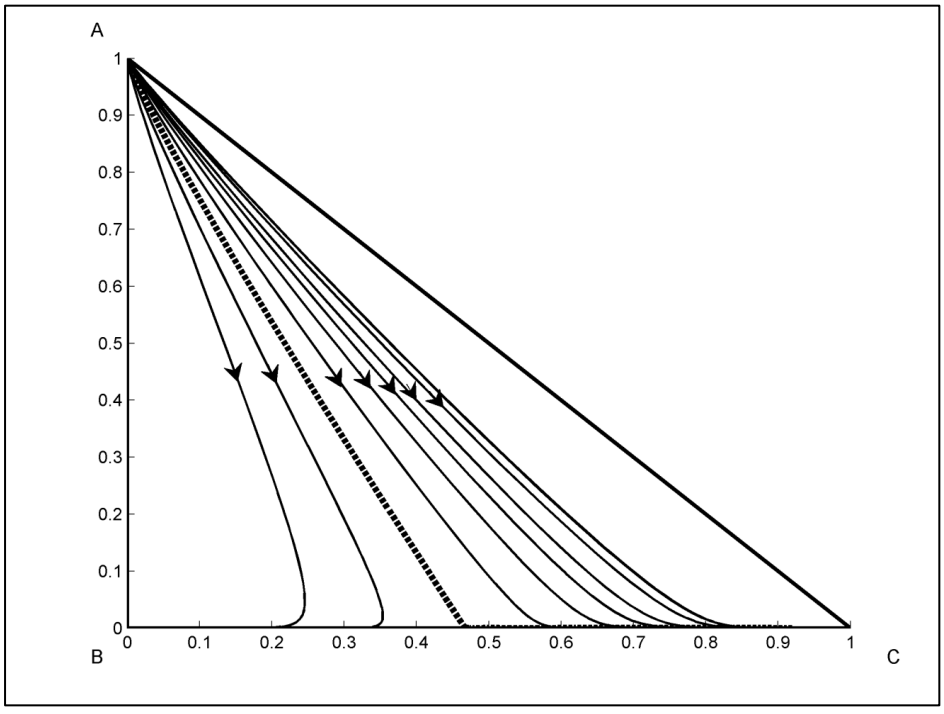


Figure 5.3: Two-membrane M-RCM; Membrane One: α = [10, 1, 0.1] and γC,B = 3; Membrane Two: α = [0.1, 1, 0. 3], E=1

In Figure 5.3, the boundary between region 1 and region 2 has shifted considerably to the left, enlarging the region of feeds from which pure component C can be purified.

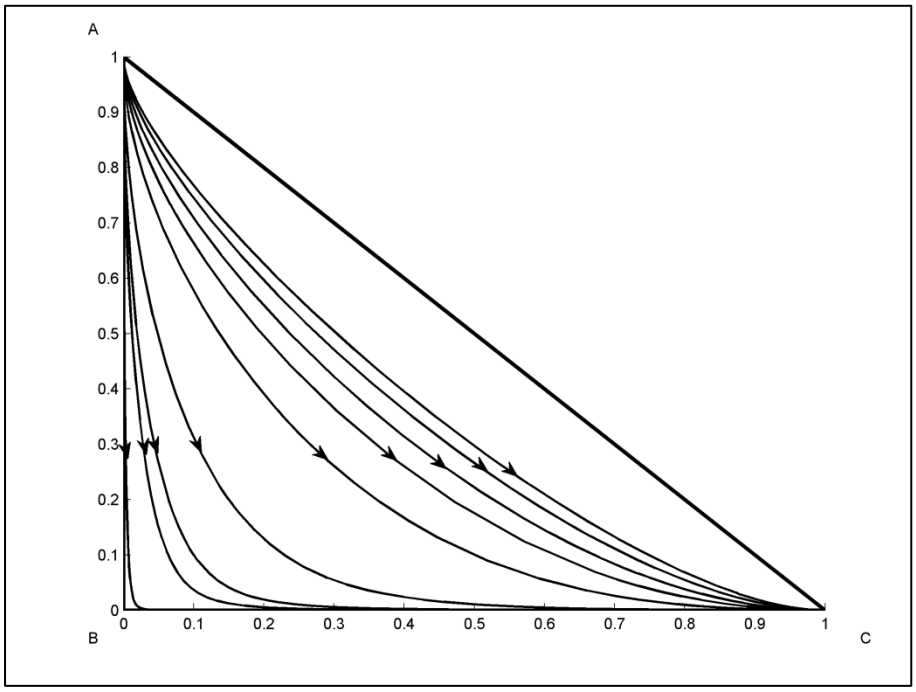


Figure 5.4: Two-membrane MM-RCM; Membrane One: α = [10, 1, 0.1] and γC,B = 3; Membrane Two: α = [0.1, 1, 0. 3], E=5

In Figure 5.4, A is the unstable node, C is the stable node and the additional stationary point has disappeared. This means that pure component C can be obtained from any initial feed composition.

It is particularly interesting to note that the separation space is no longer divided into two regions. This means that the main drawback of Membrane 1's complex permeation behaviour has been eliminated. However, the combined system still has the desired properties of component A as an unstable node and component C as a stable node.

This illustrates once again how it is possible to use multi-membrane units to favourably combine the properties of different membranes in order to achieve separations for which those individual membranes are unsuitable.

5.3.1 Combination of two membranes with complex permeation

Let us consider the same two membranes used in the previous example, excepting that we add complex behaviour to membrane 2, such that $\gamma_{A,C} = 1$. The M-RCM for membrane 1 is the same as shown earlier in Figure 5.1, but the M-RCM for membrane 2 is significantly altered, as shown in Figure 5.5.

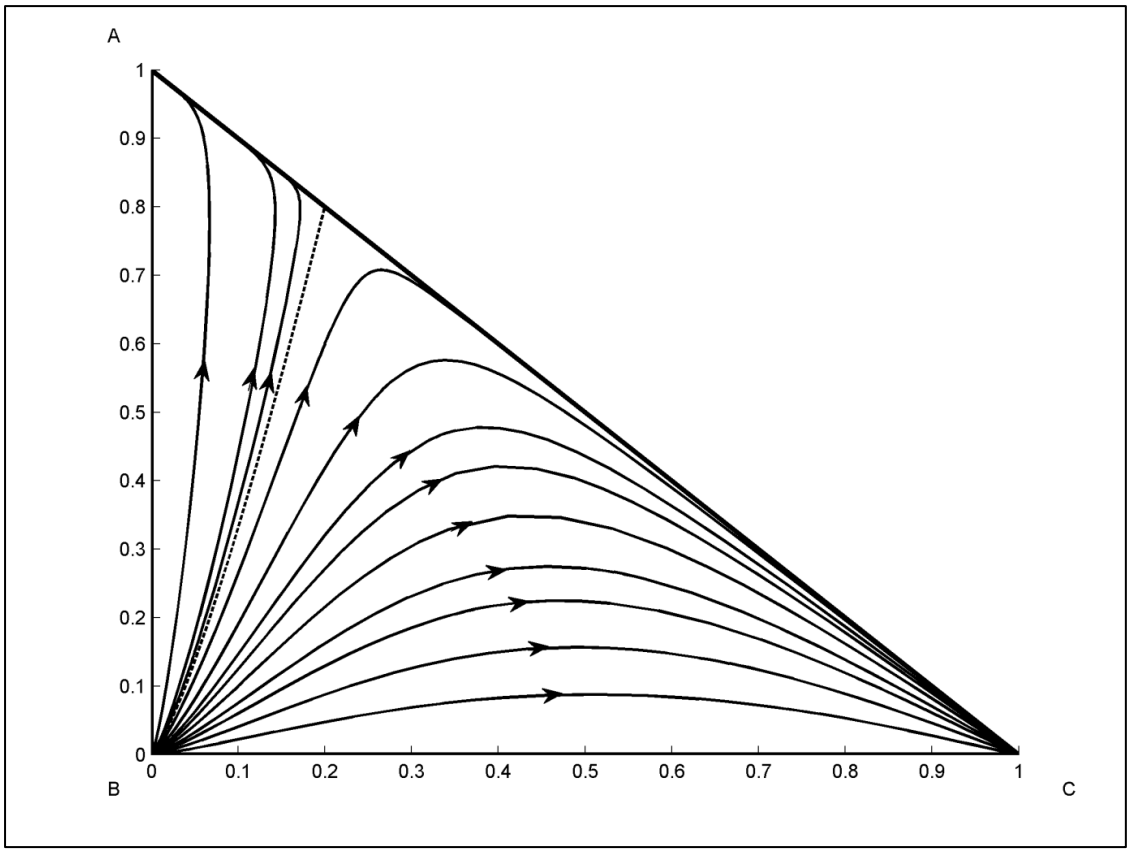


Figure 5.5: M-RCM with complex behaviour. α = [0.1, 1, 0. 3] and γA,C = 1

As before, combining these two membranes results in altered topography. Figure 5.6 shows the combination of these two complex permeation membranes with an E of 2.

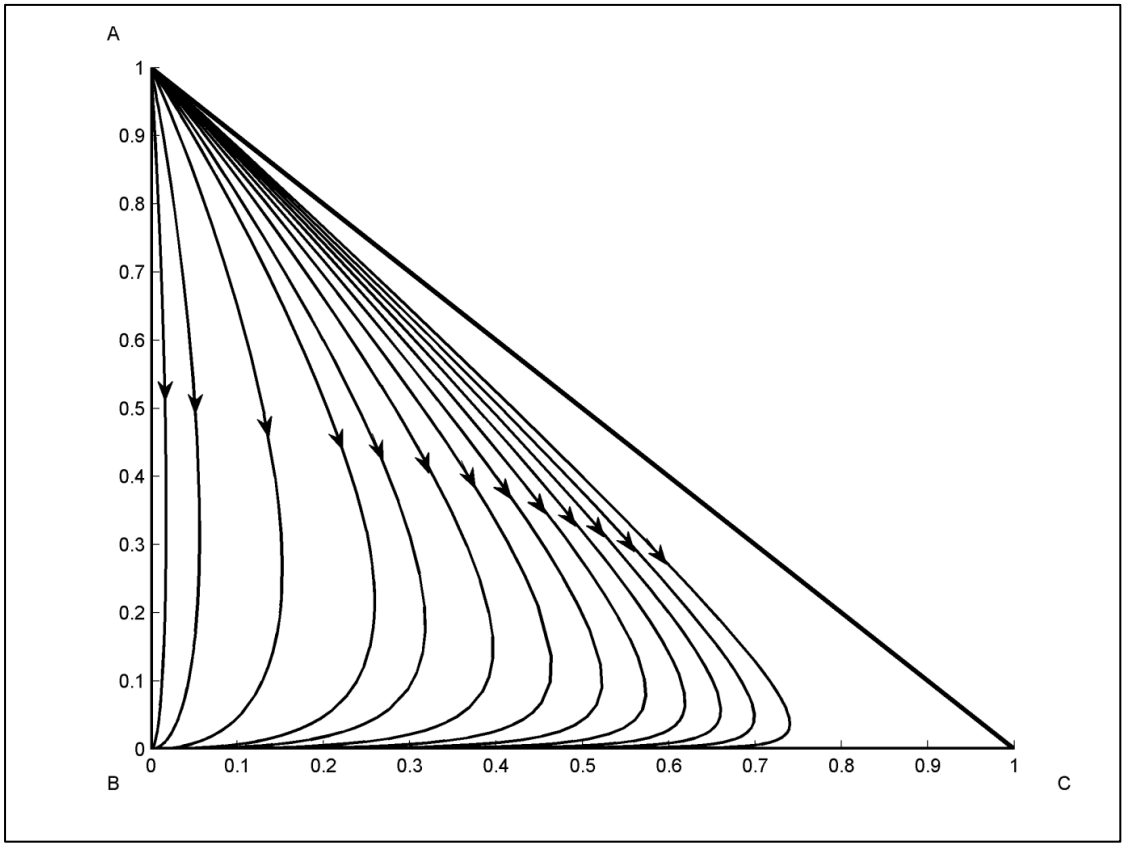


Figure 5.6: Two-membrane M-RCM; Membrane One: α = [10, 1, 0.1] and γC,B = 3; α = [0.1, 1, 0. 3] and γA,C = 1, E=2

The combination of these two membranes yields an MM-RCM without binary arheotropes, despite the fact that both membranes separately exhibit such behaviour. This is an interesting result, which once again demonstrates that multimembrane permeation can, with judicious selection of area ratios, alleviate problems of complex permeation behaviour which can interfere with membrane separation.

5.4 Quaternary mixtures

Mixtures with four or more components become problematic to visualise using two-dimensional residue curve maps. The node classification method, however, is suitable

regardless of the number of components present, provided that complex permeation does not occur.

The mixture of Nitrogen, Argon, Xenon and Krypton occurs as nuclear off-gas and is commonly separated using membranes[35]. Ohno and colleagues ([36], [37]) have previously studied the separation of this mixture using multi-membrane permeators, and offer the following permeabilities of these components through membranes of silicone rubber, cellulose acetate and 4-methylpentene:

Table 5.1: relative permeabilities for polyethylene, 4-methylpentene and cellulose acetate

Membrane material	*Relative permeability vector [N_2 Ar Kr Xe]*
Silicone rubber (sheet)	*[1 1.6 3.04 6.7]*
4-methylepentene (sheet)	*[1 4.0 4.4 4.9]*
Cellulose acetate (sheet)	*[1 0.80 0.63 0.37]*

Now, the order of permeabilities for both silicone rubber and 4-methylpentene are the reverse of that of Cellulose Acetate. Therefore, one might pair cellulose acetate with either Silicone Rubber or 4-methylpentene in a two-membrane permeator, resulting in two possible membrane pairings. The results of node classification for both of these pairings are shown in Table 5.2 and Table 5.3.

Table 5.2: Node classification for Silicone rubber and Cellulose Acetate

Region	***1***	***2***	***3***	***4***	***5***	***6***	***7***
Range of E	*0→3.0*	*3.0→5.5*	*5.5→8.5*	*8.5→9.1*	*9.1→12*	*12→14*	*14→∞*

Stable node	*A*	*B*	*B*	*C*	*C*	*C*	*D*
Saddle	*B*	*A*	*C*	*B*	*B*	*D*	*C*
Saddle	*C*	*C*	*A*	*A*	*D*	*B*	*B*
Unstable node	*D*	*D*	*D*	*D*	*A*	*A*	*A*

Table 5.3: Node classification for 4-methylpentene and Cellulose Acetate

Region	*1*	***2***	***3***	***4***	***5***	***6***	***7***
Range of E	*0→1.9*	*1.9→2.1*	*2.1→2.4*	*2.4→6.2*	*6.2→9.2*	*9.2→15*	*15→∞*
Stable node	*A*	*A*	*A*	*A*	*D*	*D*	*D*
Saddle	*B*	*B*	*D*	*D*	*A*	*C*	*C*
Saddle	*C*	*D*	*B*	*C*	*C*	*A*	*B*
Unstable node	*D*	*C*	*C*	*B*	*B*	*B*	*A*

Comparison of Table 5.2 and Table 5.3 reveals an interesting development in that, while Silicone Rubber and 4-methylpentene show the same order of permeability, they exhibit different node behaviour when paired with cellulose acetate. Table 5.2 shows that for the pairing of Silicone Rubber and Cellulose Acetate, any of the four components can be made the Stable node of the two-membrane system, while only Nitrogen or Xenon can be made the Unstable node. Table 5.3 shows that any of the four components can be made the unstable

node for the pairing of 4-methylpentene and Cellulose Acetate, while only Nitrogen or Xenon can be made the Stable node.

This implies that a pairing of Silicone Rubber and Cellulose Acetate would be suitable for preferentially retaining either of the intermediate components (Krypton or Argon) in the retentate, while a pairing of 4-methylpentene and Cellulose Acetate would be suitable for preferentially eliminating either of the intermediate components from the retentate.

The differences in behaviour of these two pairings in spite of the fact that 4-methylpentene and Silicone Rubber possess relative permeabilities in the same order underlines the usefulness of node classification in synthesising systems such as this as well as the importance of correctly selecting the relative surface areas of two membranes in order to obtain desirable membrane behaviour.

5.5 Shortcut node classification: flux criterion

The node classification method depends upon evaluating the stability of nodes for a number of values of E in order to locate the ranges which offer desirable topographical behaviour. As discussed in Chapter 4, this is typically done by the method of calculating the eigenvalues and evaluating their signs.

This becomes geometrically more computationally intensive as the number of components and membranes increases. Not only does the computational difficulty of finding an eigenvalue increase, so too does the number of eigenvalues that must be found.

To readily apply this method to systems with large numbers of membranes and/or components, a more rapid method of classifying nodes would be useful.

I propose that in cases where complex permeation does not occur, nodes can be evaluated by calculating the total material flux through the membranes at that composition. This hypothesis can easily be examined mathematically for systems with simple permeation and a low number of membranes and chemical species. This can be done by restating this criterion as well as the conventional eigenvalue method in terms of the vector of relative permeabilities, $\boldsymbol{\alpha}$, and confirming that the methods are equivalent for vectors of any values.

Since α_i is a unitless ratio of the relative permeability of component i and x_i is a composition fraction, the product of those two quantities gives us a unitless number independent of the physical specifications of the membrane. That quantity indicates the flux of that component as a ratio to the quantity of the reference component that would permeate if the retentate were a pure stream of the reference component. This quantity will hereafter be referred to as relative flux. Total flux can be expressed in the same way, as shown in equation 5.2.

$$J^r{}_{tot} = \sum x_i \,.\, \alpha_i \qquad (5.2)$$

At pure component i, $x_i = 1$, and the other compositions are all zero and all fluxes aside from that of component i are zero. Therefore, equation B-1 reduces to:

$$J^r{}_{tot} = \alpha_i \qquad (5.3)$$

We can therefore summarize the total fluxes at the node compositions as follows:

$$J^r{}_{tot(x_1=1)} = \alpha_1;\ J^r{}_{tot(x_2=1)} = \alpha_2;\ J^r{}_{tot(x_1=3)} = \alpha_3 \qquad (5.4)$$

We can therefore tabulate the order of the fluxes at each node, and therefore the predicted node properties, in terms of a set of inequalities of the values of $\boldsymbol{\alpha}$**.**

Table 5.4: Relationship between total flux and relative permeability vector

Order of fluxes	*Node-type at pure component 1*	*Node-type at pure component 2*	*Node-type at pure component 3*
$\alpha_1 > \alpha_2 > \alpha_3$	*Unstable*	*Saddle*	*Stable*
$\alpha_1 > \alpha_3 > \alpha_2$	*Unstable*	*Stable*	*Saddle*
$\alpha_2 > \alpha_1 > \alpha_3$	*Saddle*	*Unstable*	*Stable*
$\alpha_2 > \alpha_3 > \alpha_1$	*Stable*	*Unstable*	*Saddle*
$\alpha_3 > \alpha_1 > \alpha_2$	*Saddle*	*Stable*	*Unstable*
$\alpha_3 > \alpha_2 > \alpha_1$	*Stable*	*Saddle*	*Unstable*

Now we examine the conventional approach in the same way, by determining the eigenvalues of the residue curve equation in terms of $\boldsymbol{\alpha}$**.** For a single-membrane system of three components, the residue curve equation is:

$$\frac{d}{d\tau}\boldsymbol{x} = \boldsymbol{x} - \boldsymbol{y} \qquad (5.5)$$

Since the elements of $\boldsymbol{x}$ and those of $\boldsymbol{y}$ always sum to 1, the fraction any one component can always be inferred from the fractions of the other two. Therefore, this residue curve equation can be considered to be a system of two equations, with two variables, those equations being:

$$\frac{d}{d\tau}x_1 = x_1 - \frac{\alpha_1.x_1}{S} \qquad (5.6)$$

$$\frac{d}{d\tau}x_2 = x_2 - \frac{\alpha_2.x_2}{S} \qquad (5.7)$$

Where:

$$S = \alpha_1.x_1 + \alpha_2.x_2 + \alpha_3.(1 - x_1 - x_2) \qquad (5.8)$$

The Jacobian matrix of this system is given by:

$$JM = \begin{bmatrix} 1 - \frac{\alpha_1.s - \alpha_1.x_1.(\alpha_1 - \alpha_3)}{s^2} & \frac{\alpha_1.x_1.(\alpha_2 - \alpha_3)}{s^2} \\ \frac{\alpha_2.x_2.(\alpha_1 - \alpha_3)}{s^2} & 1 - \frac{\alpha_2.s - \alpha_2.x_2.(\alpha_2 - \alpha_3)}{s^2} \end{bmatrix} \quad (5.9)$$

The eigenvalues of this system of equations will define the nature of the nodes of the residue curve map. The eigenvalues are given by the solutions to the characteristic equation:

$$determinant\ (JM - \lambda I) = 0 \quad (5.10)$$

In practice, this amounts to subtracting λ from the diagonals in equation 5.9, and finding the values of λ for which the determinant of the resulting matrix is zero. This results in the following equation for λ**:**

$$\left(1 + \frac{\alpha_1.x_1.(\alpha_1 - \alpha_3)}{s^2} - \frac{\alpha_1}{s} - \lambda\right).\left(1 + \frac{\alpha_2.x_2.(\alpha_2 - \alpha_3)}{s^2} - \frac{\alpha_2}{s} - \lambda\right) - \frac{\alpha_1.x_1.(\alpha_2 - \alpha_3)}{s^2}.\frac{\alpha_2.x_2.(\alpha_1 - \alpha_3)}{s^2} = 0 \quad (5.11)$$

Now, since nodes occur at each pure component, we wish to evaluate this equation at pure component values. Conveniently, the equation simplifies when we do this. Let us evaluate λ at $x_1 = 1$, where $x_2 = 0$ and S reduces to α_1.

Equation 5.11 reduces to:

$$\left(1 - \frac{\alpha_3}{\alpha_1} - \lambda\right).(1 - \frac{\alpha_2}{\alpha_1} - \lambda) = 0 \quad (5.12)$$

This equation has two solutions for λ:

$$\lambda = 1 - \frac{\alpha_3}{\alpha_1} \text{ or } \lambda = 1 - \frac{\alpha_2}{\alpha_1} \quad (5.13)$$

From equation 5.13, the eigenvalues at this node can be evaluated purely in terms of the values of $\boldsymbol{\alpha}$, noting that we assume all elements of $\boldsymbol{\alpha}$ to be positive real numbers. If $\alpha_1 > \alpha_2$

and $\alpha_1 > \alpha_3$, then both solutions for λ will be positive and the node at pure component 1 will be unstable. If $\alpha_1 > \alpha_2$ and $\alpha_1 < \alpha_3$, then one solution will be positive and the other negative, resulting in a saddle node. This is true also if $\alpha_1 < \alpha_2$ and $\alpha_1 > \alpha_3$. If $\alpha_1 < \alpha_2$ and $\alpha_1 < \alpha_3$, then both solutions will be negative and the node at pure component will be a stable node.

The nodes at pure components 2 and 3 can be similarly evaluated, resulting in the following table relating $\boldsymbol{\alpha}$ to node properties.

Table 5.5: relationship between eigenvalue properties and relative permeability vector

Order of fluxes	*Node-type at pure component 1*	*Node-type at pure component 2*	*Node-type at pure component 3*
$\alpha_1 > \alpha_2 > \alpha_3$	*Unstable*	*Saddle*	*Stable*
$\alpha_1 > \alpha_3 > \alpha_2$	*Unstable*	*Stable*	*Saddle*
$\alpha_2 > \alpha_1 > \alpha_3$	*Saddle*	*Unstable*	*Stable*
$\alpha_2 > \alpha_3 > \alpha_1$	*Stable*	*Unstable*	*Saddle*
$\alpha_3 > \alpha_1 > \alpha_2$	*Saddle*	*Stable*	*Unstable*
$\alpha_3 > \alpha_2 > \alpha_1$	*Stable*	*Saddle*	*Unstable*

Since this table is identical to the one resulting from the flux criterion, we can conclude that for a single-membrane ternary system with simple permeation, the flux criterion predicts the same node properties as the eigenvalue criterion for any and all possible values of $\boldsymbol{\alpha}$, which covers all possible systems with simple permeation. Therefore, we can conclude that the flux criterion is suitable for predicting node properties in any such system.

Extending the same proof to higher order systems results in Jacobian matrices that are too cumbersome for easy manipulation and certainly too cumbersome for clear presentation.

In principle, however, the properties of a node in any number of dimensions are just an aggregate of its properties in each of those individual dimensions. A stable node can be properly defined as a node that is stable in all dimensions of interest, while an unstable node can likewise be defined as a node that is unstable in all dimensions of interest. A saddle node, on the other hand, is a node that is stable in some dimensions of interest and unstable in others.

This logic extends beyond the explicit dimensions of components that are actually present to implicit dimensions of components that we consider to be of interest. Consider a ternary system with nodes at the pure components. At each of those nodes, only one component is actually present.

However, we examine the properties of that node in terms of components that are not physically present and the properties of that node therefore depend upon our selection of components of interest.

The topology of a Residue Curve Map in any number of dimensions is affected by the node properties in all dimensions of interest, but the permeation of a real mixture is governed only by the node properties with regards to the components that are actually present.

For any system there are an infinite number of implicit dimensions, including any possible chemical species that could hypothetically be present. This includes chemical species that don’t necessarily exist but to which we can nevertheless assign permeation properties. Node properties are subject to change when we consider additional species to be of interest, even if those species are not in fact present. Consider the example from Chapter 4 of a mixture of

Nitrogen, Argon, Krypton, and Xenon exposed to a membrane of Silicone Rubber. For this system, pure Xenon is the unstable node, as it is the fastest permeating component.

If, however, we consider an additional dimension in the form of Hydrogen then pure Xenon will become a saddle node. It will remain an unstable node in each other individual dimension; in the Xenon-Nitrogen, Xenon-Argon, and Xenon-Krypton dimensions pure Xenon is unstable but in the Xenon-Hydrogen dimension it is stable and consequently, for this four-dimensional system it is a saddle node.

I noted earlier that both criteria for classifying nodes distinguish between different types of saddle node, depending on how many eignenvalues are positive and how many are negative, or on exactly where the node falls in the flux order. The above line of reasoning offers a useful interpretation of that observation. Eliminating certain components can effectively change a saddle node into either a stable or unstable node by moving the system into the explicit dimensions in which it has the desired properties.

This is a useful insight when sequencing multiple units because it informs a designer of how the effective node properties will change when particular components are eliminated or introduced.

This same line of logic also leads one to expect that if a criterion for node classification is separately valid in all dimensions of interest then it should be valid for the system as a whole. This is not, however, a statement that is easily accepted without thorough mathematical proof. In the absence of compelling proof for this statement or a proof for the flux criterion that extends to any number of dimensions and membranes, empirical corroboration is of tremendous value in offering greater confidence in the broad validity of total membrane flux as a means of classifying nodes.

Here I will offer empirical corroboration for this criterion as applied to two-membrane systems with simple permeation and four chemical species.

In Chapter 4 I used a graphical method to find the values of E at which node properties switch over. The same type of plot can be used with any number of components and/or membranes, noting that each additional component adds an additional node and thus adds two more eigenvalues that need to be plotted. Other than that, the methodology is unchanged.

A similar plot can be used to compare total flux at nodes. If lines are plotted with values of E / E +1 on the x-axis and the differences between fluxes at nodes on the y-axis, then those lines will cross the origin at points where those nodes exchange places if they are ordered in terms of total flux. In other words, if my surmise that total flux is indicative of node properties is correct, then the values of E at which those lines intersect the origin should match those for which the eigenvalues intersect the origin as in the previous method.

By overlaying these lines on the same set of axes for a number of different pairs of membrane properties, this flux criterion can be tested in a graphical way.

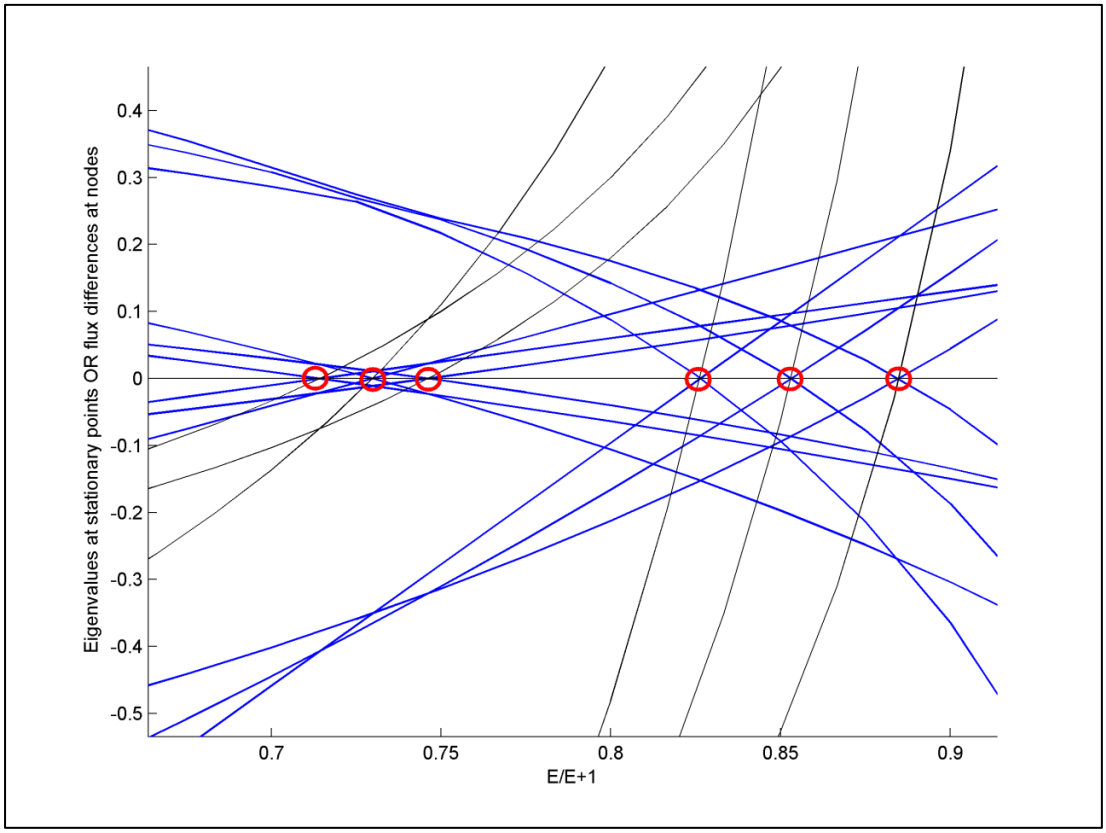


Figure 5.7: Eigenvalue method and Flux criterion plotted on same axes: Membrane One: α = [1, 1.5, 2, 4]; Membrane Two: α = [1,0.8,0.63,0.37]

For the example shown in Figure 5.7, it can be seen that eigenvalues and flux differences cross the origin at the same points and that the two methods therefore predict the same flux behaviour for all values of E.

Table 5.6: Comparison of node properties predicted by different methods for two membranes with α = [1, 1.5, 2, 4] and α = [1,0.8,0.63,0.37] respectively

Region	***1***	***2***	***3***	***4***	***5***	***6***	***7***
Range of E	*0→2.5*	*2.5→2.7*	*2.7→2.9*	*2.9→4.8*	*4.8→5.8*	*5.8→7.7*	*7.7→∞*
Order of fluxes	*1,2,3,4*	*2,1,3,4*	*2,3,1,4*	*3,2,1,4*	*3,2,4,1*	*3,4,2,1*	*4,3,2,1*
Eigenvalues at A	*---*	*--+*	*-++*	*-++*	*+++*	*+++*	*+++*
Eigenvalues at B	*--+*	*---*	*---*	*--+*	*--+*	*-++*	*-++*

Eigenvalues at C	*-++*	*-++*	*--+*	*---*	*---*	*---*	*--+*
Eigenvalues at D	*+++*	*+++*	*+++*	*+++*	*-++*	*--+*	*---*

For this example, there are 7 distinct regions separated by the switching of eigenvalue properties and flux order. There is something interesting to take note of here. We do not distinguish between the two saddle points. However, both methods of evaluating nodes show a distinction between them. The node with the second-fastest total flux has two positive eigenvalues and one negative, while the node with the third-fastest flux has two negative eigenvalues and one positive.

In this case, the permeability orders are completely inverted and 7 switches are required to transition from the ordering of membrane one to that of membrane two. When the permeability orders are less different, then the number of regions will be reduced, as in Figure 5.8 below.

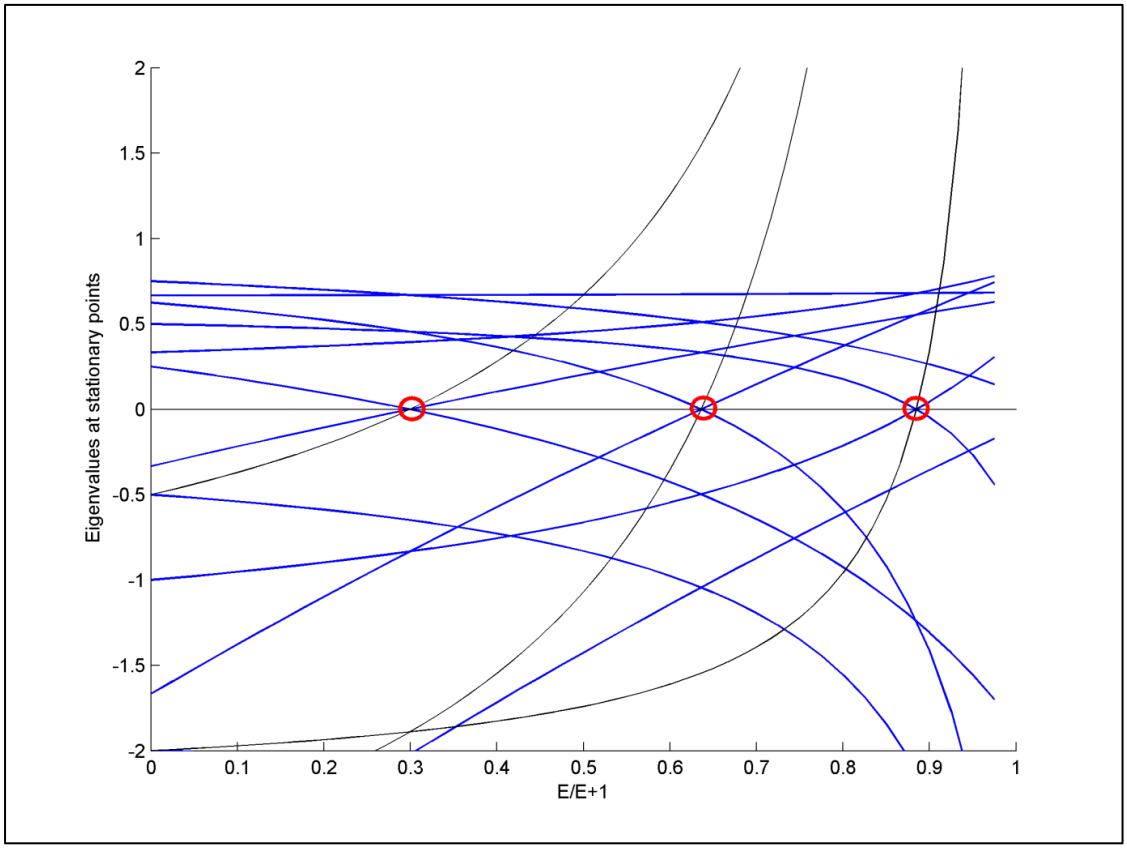


Figure 5.8: Eigenvalue method and Flux criterion plotted on same axes: Membrane One: α = [6, 1.5, 2, 4]; Membrane Two: α = [2, 1.8, 0.63, 0.37]

Table 5.7: Comparison of node properties predicted by different methods for two membranes with α = [6, 1.5, 2, 4] and α = [2, 1.8, 0.63, 0.37]] respectively

Region	***1***	***2***	***3***	***4***
Range of E	*0→2.9*	*2.9→2.8*	*7.7→∞*	*7.7→∞*
Order of fluxes	*2,3,4,1*	*3,2,4,1*	*3,4,2,1*	*4,3,2,1*
Eigenvalues at A	*+++*	*+++*	*+++*	*+++*
Eigenvalues at B	*---*	*--+*	*-++*	*-++*
Eigenvalues at C	*--+*	*---*	*---*	*--+*
Eigenvalues at D	*-++*	*-++*	*--+*	*---*

The two methods of node classification once again predict the same node behaviour for all values of E. Three switches must take place for the system to transition from the properties of membrane one to those of membrane two. Once again, one of those switches swaps the order of the two saddle nodes, a change which will not have a noticeable effect on the overall topography of the MM-RCM in question.

5.5.1 Implications of shortcut node classification

Moving on under the assumption that the flux criterion is suitable for node classification in all cases of membrane or multi-membrane permeation with simple permeation and a retentate vacuum, node classification becomes much simpler and more rapid; nodes can be classified for all values of E using simple algebraic methods.

For any particular value of E, nodes can be evaluated by simply comparing total flux at each node. For simple permeation, the nodes occur at pure components, greatly simplifying the flux equations. Flux through a membrane at pure component i is given by equation 5.1.

$$J = \frac{A.x_i.p.\alpha_i.\pi_R}{\delta} \tag{5.1}$$

Total flux through two membranes at pure component i, then, is given by equation 5.2.

$$J_{tot} = \frac{A_1 x_i.p.\alpha_i^1.\pi_R}{\delta_1} + \frac{A_2 x_i.p.\alpha_i^2.\pi_R}{\delta_2} \tag{5.2}$$

As in Chapter 4, the constant terms can be bundled together, allowing us to express equation 5.2 in terms of E, the relative permeability constant defined in Chapter 4. Since the

$$J_{tot,i} = P.(x_i.\alpha_i^1 + E.x_i.\alpha_i^2) \tag{5.3}$$

Where $P = \frac{A_2.\pi_R}{\delta_1}$ and $E = \frac{A_1.\pi_R}{\delta_1} / \frac{A_2.\pi_R}{\delta_2}$ as in Chapter 4. Now, we can locate all values of E at which nodes switch properties by simply finding all of the zeros of the differences between the fluxes at different nodes, given by equation 5.4.

$$P.(x_i.\alpha_i^1 + E.x_i.\alpha_i^2) - P.(x_j.\alpha_j^1 + E.x_j.\alpha_j^2) = 0 \quad (5.4)$$

Equation 5.4 can be simplified by eliminating the constant P and rearranging to make E the subject of the equation, resulting in equation 5.5, which I shall hereafter refer to as the node property threshold equation.

$$E = \frac{x_j.\alpha_j^1 - x_i.\alpha_i^1}{x_i.\alpha_i^2 - x_j.\alpha_j^2} \quad (5.5)$$

The values of E at which two nodes exchange properties are all the positive, real solutions to node property threshold equation. I will hereafter refer to those values as node property thresholds, since they are the values of E at which node properties change. Each threshold corresponds to a pair of nodes which are exchanging properties. Finding all of these values will separate the E space into regions with distinct node properties. The properties within all of those regions can be evaluated by once again evaluating the total fluxes to determine the order of total flux magnitudes at each node.

Alternatively, if the node properties in one region are known, then the properties in the subsequent region can be determined by simply switching the properties of the two nodes that exchange at that threshold. Procedurally, one can begin by looking at the node properties at $E = 0$. Those properties will hold for the range from $E = 0$ to the lowest positive, real solution for equation 5.5. To assess the properties for the next region, exchange the properties of the nodes of the lowest node property threshold. Repeat this for successively larger

thresholds until reaching the highest threshold, at which point the node properties will be those of membrane two.

This procedure is computationally trivial but yields the same results as applying the conventional approach of classifying nodes using their eigenvalues. The validity of the flux criterion has been demonstrated mathematically for a single-membrane, three-component system, and tested empirically for a two-membrane, four-component system. I hypothesize that the criterion extends to systems of any number of components and membranes, offering a rapid technique for determining the node properties of multi-membrane systems which would otherwise be computationally problematic.

5.5.2 Shortcut node classification with complex permeation

Earlier in this chapter I examined examples of M-RCMs and MM-RCMs with complex permeation. I will now re-examine those same examples to look into the relationship between total flux and node properties in systems with complex permeation. As was shown earlier in this chapter, flux depends on a number of physical features of the membranes present. These characteristics are not necessarily of interest when looking at permeation behaviour in a general sense. For this reason it is convenient to quantify flux relative to the reference component, in a manner similar to that which is used for α.

Flux can be given as a ratio of the total flux of all components through both membranes to the flux that would occur through membrane one if exposed to pure component B, which we are using as the reference component. In this way, total flux is given by a unitless quantity which is not dependent on the physical properties of the membranes.

The single-membrane system shown in Figure 5.1 has the following permeation properties: α = [10, 1, 0.1] and $\boldsymbol{\gamma_{C,B}}$ = 3. The flux at pure A is 10, the flux at pure B is 1 and the flux at pure C is 0.1. The system has an unstable node at pure A, and stable nodes and pure B and

pure C. The complex permeation behaviour gives rise to a Saddle node on the B-C axis at a composition of (0,0.7,0.3). The flux at this node is 1.

The two-membrane system shown in Figure 5.3 combines the same membrane with complex permeation with another membrane that does not exhibit complex permeation. Membrane one has the same permeation properties as in the above example, while membrane two has α = [0.1, 1, 0.3]. E is 1 in this example. This system has an unstable node at pure A, with a saddle node at a composition of (0, 0.53) and stable nodes at pure component B and pure component C. The flux at pure component A is 10.1, the flux at pure component B is 2, the flux at pure component C is 0.4 and the flux at the additional saddle node is 2.

Figure 5.5 shows another single-membrane system with complex permeation behaviour, with the following permeation properties: α = [0.1, 1, 0.3] and $\boldsymbol{\gamma_{A,C}}$ = 1, resulting in a binary saddle node at a composition of (0.8, 0), with an unstable node at pure B and stable nodes at pure A and pure C. The flux at pure A is 0.1, the flux at pure B is 1, the flux at C is 0.3, while the flux at the additional node is 0.3.

All of these examples exhibit an interesting common characteristic. In each case, the binary node occurs at a point on that binary axis where the flux is equal to the flux at one of the pure components that lie on the end-points of that axis.

Now, in systems without complex permeation, the flux varies monotonically along each binary axis. In instances of complex permeation where additional nodes occur, it is possible for the maximum or minimum flux along a binary axis to lie at some point on the axis and not at either of the pure component compositions. In fact, it appears that the presence of an additional node on a binary axis can sometimes be predicted based on whether or not there is an inflection point in the total flux along that binary axis.

Consider again the system first shown in Figure 5.1, an M-RCM for a membrane with α = [10, 1, 0.1] and $\gamma_{C,B}$ = 3. This M-RCM exhibits an additional saddle node at a composition of [0, 0.3, 0.7]. By plotting total flux along with composition along the B-C axis it is possible to glean further insight into the interrelationship between total flux and node properties for systems with complex permeation.

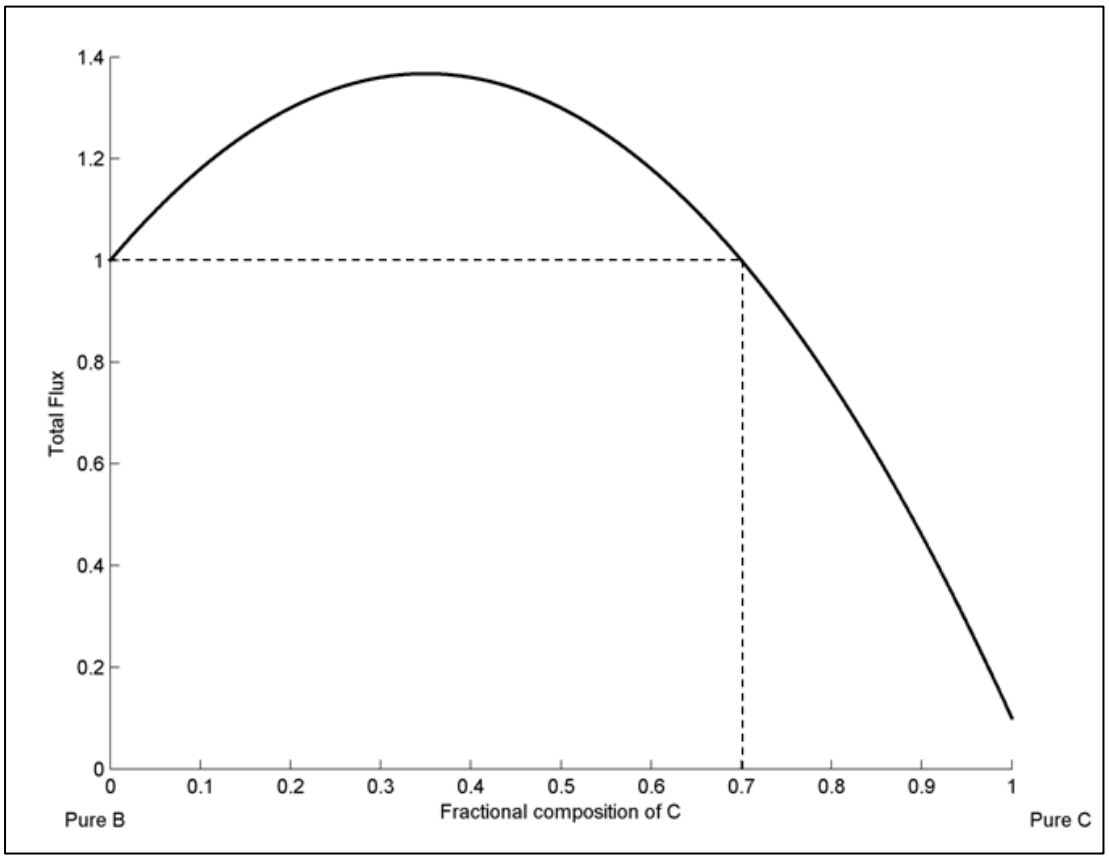


Figure 5.9: Total flux along B-C axis of a membrane permeation system with α = [10, 1, 0.1] and $\gamma_{C,B}$ = 3. Dashed lines to indicate location of additional node

My intuitive expectation was that the additional nodes would occur at the inflection point, at the local maximum or minimum flux on that binary axis. Figure 5.9 shows, however, that this additional node occurs instead at a point at which the flux is equal to that at one of the end-points. This proves that the flux criterion for node classification does not extend to complex permeation, since two nodes of different type end up with the same total flux. In other words,

those nodes cannot be distinguished on the basis of the total flux at those compositions, while they can be distinguished using the conventional approach of eigenvalue inspection.

Nevertheless, the observation is of interest and offers some additional insight into the relationship between topographical behaviour and total flux for systems with complex permeation. However, this is merely an observation based on limited examples, all using the same model for complex permeation. It is not possible to draw any firm conclusions based on these observations, though they are an interesting starting point for anyone seeking to undertake further research into the relationship between total flux and topographical behaviour in systems with complex permeation.

5.6 Discussion

In this chapter it has been demonstrated that the MM-RCM technique and node classification method can be extended to higher order systems and systems exhibiting complex permeation behaviour. It has also been shown that in instances where complex permeation behaviour is not present, nodes can be classified by inspection of the total quantity of material flux through all membranes, a method which is computationally much simpler than calculating the eigenvalues.

This offers a much more rapid method of classifying nodes along with an interesting insight into topographical behaviour in general. The observation that membrane separations tend to proceed from high flux to low flux fits an intuitive expectation that chemical systems proceed from states of high driving forces to states of lower driving forces.

This method of characterising nodes therefore makes M-RCMs more intuitively understandable when compared to the much more abstract approach of using eigenvalue

analysis. In this way, it promises to serve as a teaching tool for multi-membrane separation in much the same way that RCMs have for distillation.

This chapter served to demonstrate the broad applicability and usefulness of the node classification method and to provide a computational shortcut, simplifying node classification. The MM-RCM method and the node classification method dramatically simplify the synthesis and preliminary design of multi-membrane permeators.

Chapter 6. Concluding Remarks

This thesis set out to offer methods of reducing energy expenditure in separation processes by investigating alternatives to distillation. Of course, simple awareness of alternatives achieves nothing unless it is also possible to design and implement them.

Chapters 2 and 4 each highlighted one promising alternative separation method and demonstrated improved separation efficiency. Chapters 3 and 5 extended those concepts, demonstrating how to implement them in practical circumstances and showing their potential for further development.

6.1 Energy-efficient bioethanol recovery

This thesis has shown that the energy requirements of ethanol purification can be mitigated by blending a partially purified ethanol mixture directly into petrol as opposed to fully purifying the ethanol first.

In Chapter 2 this concept was verified using rigorous simulation based on phase equilibrium measurements taken from literature [25]. A process flowsheet was developed to illustrate this concept, and based on simulations a simple process using two-stage counter-current liquid-liquid extraction proved to be sufficient to produce a fuel mixture of desirable ethanol content, while recovering 98% of ethanol feed in the fuel phase.

This process represents a significant cost-saving when compared to conventional processes, since it foregoes the energy required for final purification. However, the process flowsheet from Chapter 2 does not necessarily constitute a fully optimized process. Further, the optimality of any particular version of the process is contingent on the circumstances in which it is implemented.

In light of this, Chapter 3 investigated the process in greater detail, examining the effects of various operating parameters and looking more deeply at the requirements of two different contexts for implementation: the South African market, where 2% ethanol blends have been mandated for use by new legislation and the United States market, where 10% ethanol blends are already in widespread use.

In that chapter, different versions of the bioethanol blending process were examined specifically for their suitability in those two contexts.

It must be very clearly noted, however, that the ethanol pre-blending concept creates a large optimization space for the design of bioethanol production processes, and this thesis has explored only a small portion of that optimization space. I am confident that there are a number of possible refinements to achieve better performance using this concept and to integrate it into other creative approaches to bioethanol separation.

One example of such a possibility is a setup resembling that of heteroazeotropic distillation where the phase split and distillation both occur within the same unit. Such a setup could potentially achieve a high recovery of ethanol into a fuel mixture, without prior partial purification as is necessary for the process presented in this thesis. Another exotic possibility is a reactive distillation unit with phase-split occurring within the column.

These and numerous other possibilities are yet to be investigated, and there may be other significant advantages to them. For instance, a process integrating the liquid-liquid phase split into another form of separation could potentially benefit from the phase split in terms of energy consumption, while still producing an under-saturated fuel mixture and thereby providing higher stability and avoiding the complications that result from dealing with a saturated mixture.

According to the South African Petroleum Industry Association [38], in 2009 national petrol useage was 11.3 billion liters, with steady increases in that figure expected. This means that the 2% ethanol content mandated by legislation corresponds to at least 226 million liters of ethanol to be blended per year. With the process presented in chapter 2 reducing energy useage per liter by between 0.916MJ and 2.13MJ that places the potential energy saving nationwide at between 2.07×10^8 MJ and 4.81×10^8 MJ per annum, approximately equivalent to the household electricity consumption of between ten and twenty thousand average households.

While this is a significant sum to a nation suffering an energy crisis, it is trivial in comparison to the potential implications in the United States and elsewhere in the world. This thesis has addressed the South African context, as that is where this university is situated and therefore is the market with the most immediacy and relevance. I have also considered the context of the United States not only because they are the single largest ethanol producer but also for reasons of convenience. Their biofuels legislation has established highly uniform ethanol content, which creates a clear target when synthesizing a new process such as that presented in Chapter 2. Brazil, for instance, permits wide-ranging ethanol content in fuel. Without a clear target for ethanol content, process viability is more difficult to assess, and optimization becomes more complex because of the additional degree of freedom. Having clear-cut targets for ethanol content allows for a straightforward demonstration of the viability and value of the proposed process.

That is not to say, however, that the concepts and flowsheets presented in this thesis are any less applicable elsewhere in the world. Flexibility in terms of ethanol content could in fact make our specific process more attractive. Any specified ethanol content more or less dictates the blending ratio that must be used in this process, constraining the design within narrow parameters. Being able to adjust blending ratio in order to maximize profit will allow a

designer the flexibility needed to best implement the concept of using phase equilibrium to assist separation.

Furthermore, the development of new processes using this concept need not adhere to any particular specification of ethanol content. Since the particulars of any such process will tend to be highly dependent on the required ethanol content, this flexibility offers a large design space for creative designs.

While our specific process design offers immediate benefits, the true potential of the core concept is yet to be explored. It is optimistic to believe that the implementation of this simple concept will change the face of the bioethanol industry, but the findings of this thesis suggest that it is possible.

6.2 Multi-membrane permeation design methodology

Chapter 4 demonstrated the potential benefits of multi-membrane permeation, achieving higher separability in a single unit using two different membranes than was achievable using two single-membrane units in series.

A two-membrane unit with from which only a single permeate and retentate stream are withdrawn would have essentially the same equipment costs as an ordinary single-membrane unit, but with the membrane material cost being some weighted average of the two membrane types. Being able to use a single unit to achieve better performance than is achievable in two normal units is therefore a significant result, since it reflects improved performance along with reduced cost.

Chapter 4 also derived a residue curve equation for multi-membrane permeators, and showed how MM-RCMs can be used to synthesize and design multi-membrane processes.

Membrane technology as a whole is somewhat under-utilized in the Chemical Engineering industry, but it is a maturing technology that is becoming increasingly commonplace. Multi-membrane processes, however, are rarely seen. The concept has been only shallowly explored in the past, and has been largely forgotten. Sengupta and Sirkar [33] previously concluded that multi-membrane permeators do not offer performance benefits when compared to conventional units, perhaps discouraging further research into multi-membrane permeation.

In this thesis I have aimed to add to the groundwork required to change that. By offering both a demonstration of their advantages and a simple methodology for evaluating their applicability and for conducting preliminary design, I believe that I have confirmed the viability of multi-membrane permeation as an alternative separation technique.

The specific cases where multi-membrane permeation can be implemented will depend on the availability of membrane materials. The case of the Nitrogen/Argon/Krypton/Xenon system examined in Chapter 5 is of interest in nuclear off-gas treatment, but there are of course numerous other possibilities to be investigated. As a general guideline, multi-membrane permeation is likely to be advantageous in achieving problematic separations if different membrane materials exhibit very different permeabilities for the chemical species to be separated.

In Chapter 5 I uncovered an interesting property of Membrane Residue Curve Maps, showing that in cases where only simple permeation occurs, nodes can be classified by comparing total material flux. This method is much less computationally intensive than determining eigenvalues to classify nodes, making it useful for designers optimizing from a range of possible configurations.

It also establishes an intuitive relationship between node behavior and physical properties, hopefully serving to make M-RCMs more readily understandable. This will facilitate teaching of the fundamentals of membrane separation, particularly at the undergraduate level. The notion that permeation proceeds from high flux toward low flux is easily grasped on an intuitive level, whereas the classification of nodes by eigenvalue inspection is unintuitive and mathematically complex.

Residue Curve Maps are an established tool in engineering education on the topic of distillation. M-RCMs can play the same role for membrane separation, expanding the pool of engineers equipped with expertise in the design and synthesis of membrane permeation operations.

References

[1] G. Hewitt, J. Quarini and M. Morell; "More Efficient Distillation" *The Chemical Engineer*, vol. 94, pp. 179-184, 1999.

[2] U.S. Energy Information Administration, "How much ethanol is produced, imported, and consumed in the United States?," 2014. [Online]. Available: http://www.eia.gov/tools/faqs/faq.cfm?id=90&t=4. [Accessed: 24-Sep-2014].

[3] M. Vasquez-Ojeda, J. G. Segovia-Hernandez, S. Hernandez, A. Hernandez-Aguirre, and A. A. Kiss, "Design and optimization of an ethanol dehydration process using stochastic methods," *Separation and Purification Technology*, vol. 105, pp. 90–97, 2013.

[4] A. A. Martinez, J. Saucedo-Lun, J. G. Segovia-Hernandez, S. Hernandez, F. I. Gomez-Castro, and A. J. Castro-Montoya, "Dehydration of Bioethanol by Hybrid Process Liquid-Liquid Extraction/Extractive Distillation," *Industrial & Engineering Chemistry Research*, vol. 51, pp. 5847–5855, 2012.

[5] P. Garcia-Herreros, J. M. Gomez, I. D. Gil, and G. Rodriguez, "Optimization of the Design and Operation of an Extractive Distillation System for the Production of Fuel Grade Ethanol Using Glycerol as Entrainer," *Industrial & Engineering Chemistry Research*, vol. 50, pp. 3977–3958, 2011.

[6] M. Errico, B.-G. Rong, G. Tola, and M. Spano, "Optimal Synthesis of Distillation Systems for Bioethanol Separation. Part 1:Extractive Distillation with Simple Columns," *Industrial & Engineering Chemistry Research*, vol. 52, pp. 1612–1619, 2013.

[7] D. Kunnakorn, T. Rirksomboon, K. Siemanond, P. Aungkavattana, N. Kuancertchoo, P. Chuntanalerg, K. Hemra, S. Kulprathipanja, R. James, and S. Wongkasemjit, "Techno-economic comparison of energy usage between azeoptropic distillation and hybrid system for water-ethanol separation," *Renewable Energy*, vol. 51, pp. 310–316, 2013.

[8] W. J. Koros and G. K. Fleming, "Membrane-based gas separation," *Journal of Membrane Science*, vol. 83, no. 1, pp. 1–80, 1993.

[9] J. Zaman and A. Chakma, "Inorganic membrane reactors," *Journal of Membrane Science*, vol. 92, pp. 1–28, 1994.

[10] P. M. Budd and N. B. McKeown, "Highly permeable polymers for gas separation membranes," *Polymer Chemistry*, vol. 1, no. 1, p. 63, 2010.

[11] M. F. Doherty and J. D. Perkins, "On the dynamics of distillation processes - II. The simple distillation of model solutions," *Chemical Engineering Science*, vol. 33, pp. 569–578, 1978.

[12] M. Peters, S. Kauchali, D. Hildebrandt, and D. Glasser, "Derivation and Properties of Membrane Residue Curve Maps," *Industrial and Engineering Chemistry Research*, vol. 45, no. 26, pp. 9080–9087, 2006.

[13] M. Peters, S. Kauchali, D. Hildebrandt, and D. Glasser, "Application of Membrane Residue Curve Maps to Batch and Continuous Processes," *Industrial and Engineering Chemistry Research*, vol. 47, no. 7, pp. 2361–2376, 2008.

[14] M. Doherty and J. D. Perkins, “On the dynamics of distillation processes—III The topological structure of ternary residue curve maps,” *Chemical Engineering Science*, vol. 34, no. 12, pp. 1401–1414, 1979.

[15] L. R. Lynd, J. H. Cushman, R. J. Nichols, and C. Wyman, “Fuel Ethanol from Cellulosic Biomass,” *Science*, vol. 251, pp. 1318–1323, 1991.

[16] A. Demirbas, “Bioethanol from Cellulosic Materials: A Renewable Motor Fuel from Biomass,” *Energy Sources*, vol. 27, pp. 327–337, 2005.

[17] Y. Lin and S. Tanaka, “Ethanol fermentation from biomass resources: current state and prospects,” *Appl Microbiol Biotechnol*, vol. 69, pp. 627–642, 2006.

[18] J. Goldemberg, “Ethanol for a sustainable energy future.,” *Science*, vol. 315, no. 5813, pp. 808–810, 2007.

[19] A. E. Farrell, R. J. Plevin, B. T. Turner, A. D. Jones, M. O’Hare, and D. M. Kammen, “Ethanol can contribute to energy and environmental goals.,” *Science*, vol. 311, no. 5760, pp. 506–508, 2006.

[20] D. S. Abrams and J. M. Prausnitz, “Statistical thermodynamics of liquid mixtures: a new expression for the excess Gibbs energy of partly or completely miscible systems,” *AIChE Journal*, vol. 21, no. 1, pp. 116–128, 1975.

[21] M. Rahman, M. Asadullah, M. Rahman, M. Nabi, and M. Azad, “Extraction of Gasohol Grade Ethanol from Aqueous Solution using Gasoline as a solvent,” *Bangladesh Journal of Scientific and Industrial Research*, vol. 42, no. 3, 2007.

[22] Editors, “The cleaner state,” *Nature*, vol. 497, no. 7448, pp. 157–158, 2013.

[23] M. Errico, B.-G. Rong, G. Tola, and M. Spano, "Optimal Synthesis of Distillation Systems for Bioethanol Separation. Part 1:Extractive Distillation with Simple Columns," *Industrial & Engineering Chemistry Research*, vol. 52, pp. 1612–1619, 2013.

[24] M. Vasquez-Ojeda, J. G. Segovia-Hernandez, S. Hernandez, A. Hernandez-Aguirre, and A. A. Kiss, "Design and optimization of an ethanol dehydration process using stochastic methods," *Separation and Purification Technology*, vol. 105, pp. 90–97, 2013.

[25] A. A. Martinez, J. Saucedo-Lun, J. G. Segovia-Hernandez, S. Hernandez, F. I. Gomez-Castro, and A. J. Castro-Montoya, "Dehydration of Bioethanol by Hybrid Process Liquid-Liquid Extraction/Extractive Distillation," *Industrial & Engineering Chemistry Research*, vol. 51, pp. 5847–5855, 2012.

[26] N. T. Stacey, M. Peters, D. Hildebrandt, and D. Glasser, "Synthesis of Two-Membrane Permeation Processes Using Residue Curve Maps and Node Classification," *Ind. Eng. Chem. Res.*, vol. 52, no. 41, pp. 14637–14646, 2013.

[27] Y. Huang, K. Sundmacher, Z. Qi, and E. Schlunder, "Residue curve maps of reactive membrane separation," *Chemical Engineering Science*, vol. 59, no. 14, pp. 2863–2879, 2004.

[28] A. Javaid, "Membranes for solubility-based gas separation applications," *Chemical Engineering Journal*, vol. 112, pp. 219–226, 2005.

[29] L. M. Robeson, B. D. Freeman, D. R. Paul, and B. W. Rowe, "An empirical correlation of gas permeability and permselectivity in polymers and its theoretical basis," *Journal of Membrane Science*, vol. 341, no. 1–2, pp. 178–185, Sep. 2009.

[30] B. D. Freeman, "Basis of Permeability/Selectivity Tradeoff Relations in Polymeric Gas Separation Membranes," *Macromolecules*, vol. 32, pp. 375–380, 1999.

[31] S. Alexander Stern, "Polymers for gas separations: the next decade," *Journal of Membrane Science*, vol. 94, no. 1, pp. 1–65, 1994.

[32] S. A. Stern, J. E. Perrin, and E. J. Naimon, "Recycle And Multimembrane Permeators For Gas Separations," *Journal of Membrane Science*, vol. 20, pp. 25–43, 1984.

[33] A. Sengupta and K. K. Sirkar, "Ternary Gas Mixtures Separation In Two-membrane Permeators," *AIChE Journal*, vol. 33, pp. 529–539, 1987.

[34] J. Wijmans and R. W. Baker, "The solution-diffusion model: a review," *Journal of Membrane Science*, vol. 107, no. 1–2, pp. 1–21, 1995.

[35] S. Kimura, T. Nomura, T. Miyauchi, and M. Ohno, "Separation of rare gases by membranes," *Radiochem. Radioanal. Lett.*, vol. 13, no. 5–6, pp. 349–354, 1973.

[36] M. Ohno, O. Ozaki, and H. Sato, "Radioactive Rare Gas Separation Using A Separation Cell with Two Kinds of Membrane Differing in Gas Permeability Tendency," *Journal of Nuclear Science and Technology*, vol. 14, no. 8, pp. 589–602, 1977.

[37] M. Ohno, T. Morisue, and O. Ozaki, “Comparison of Gas Membrane Separation Cascades Using COnventional Separation Cell and Two-Unit Separation Cells,” *Journal of Nuclear Science and Technology*, vol. 15, no. 5, pp. 376–386, 1978.

[38] South African Petroleum Industry Organisation, “Industry Overview - South African Fuel Industry,” 2009. [Online]. Available: http://www.tradingeconomics.com/south-africa/road-sector-gasoline-fuel-consumption-kt-of-oil-equivalent-wb-data.html. [Accessed: 22-Oct-2014].

Appendix A: Raw stream data

Table A1: Raw stream data for blending ratio analysis

number of stages	blending ratio	component	aqueous feed flowrate	hydrocarbon feed flowrate	hydrocarbon outlet flowrate	aqeous outlet flowrate
1	4	ETHANOL	0.95		0.51368824	0.43631189
		WATER	0.05		0.00748227	0.04251774
		C8H18-01	0	3.8	3.63038762	0.16961185
1	6	ETHANOL	0.95		0.67577919	0.27422082
		WATER	0.05		0.00975274	0.04024725
		C8H18-01	0	5.7	5.63897168	0.06102826
1	8	ETHANOL	0.95		0.77116116	0.1788389
		WATER	0.05		0.0109309	0.03906911
		C8H18-01	0	7.6	7.57897951	0.02102011
1	10	ETHANOL	0.95		0.82635647	0.12364353
		WATER	0.05		0.01146611	0.03853388
		C8H18-01	0	9.5	9.4924652	0.00753481
1	15	ETHANOL	0.95		0.88772213	0.06227787
		WATER	0.05		0.01175932	0.03824067
		C8H18-01	0	14.25	14.2491232	0.00087686
1	20	ETHANOL	0.95		0.91092272	0.03907727
		WATER	0.05		0.0117539	0.03824607
		C8H18-01	0	19	18.9998194	0.00018081
1	50	ETHANOL	0.95		0.93913031	0.01086968
		WATER	0.05		0.01289188	0.03710809
		C8H18-01	0	47.5	47.4999965	3.77E-06
2	4	ETHANOL	0.95	0	0.63	0.32
		WATER	0.05	0	0.01	0.04
		C8H18-01	0	3.8	3.72	0.08
2	6	ETHANOL	0.95	0	0.84	0.11
		WATER	0.05	0	0.01	0.04
		C8H18-01	0	5.7	5.69	0.01
2	8	ETHANOL	0.95	0	0.92	0.03
		WATER	0.05	0	0.01	0.04
		C8H18-01	0	7.5	7.50	0.00
2	10	ETHANOL	0.95	0	0.94	0.01

		WATER	0.05	0	0.01	0.04
		C8H18-01	0	9.5	9.50	0.00
2	15	ETHANOL	0.95	0	0.95	0.00
		WATER	0.05	0	0.01	0.04
		C8H18-01	0	14.25	0.00	14.25
2	20	ETHANOL	0.95	0	0.95	0.00
		WATER	0.05	0	0.01	0.04
		C8H18-01	0	19	19.00	0.00
2	50	ETHANOL	0.95	0	0.00	0.95
		WATER	0.05	0	0.04	0.01
		C8H18-01	0	47.5	0.00	47.50
16	4	ETHANOL	0.95	0	0.25627612	0.69372389
		WATER	0.05	0	0.04079378	0.00920621
		C8H18-01	0	3.8	4.98E-02	3.7502352
16	6	ETHANOL	0.95	0	7.96E-02	0.87040404
		WATER	0.05	0	0.03843498	0.01156501
		C8H18-01	0	4.7	0.00189078	4.69810922
16	8	ETHANOL	0.95	0	3.68E-19	0.95
		WATER	0.05	0	0.03722463	0.01277536
		C8H18-01	0	7.6	1.19E-07	7.59999988
16	10	ETHANOL	0.95	0.00E+00	5.34E-21	0.95
		WATER	0.05	0	0.03735459	0.0126454
		C8H18-01	0	9.5	1.19E-07	9.49999988
16	15	ETHANOL	0.95	0	5.93E-24	0.95
		WATER	0.05	0	0.03787394	0.01212605
		C8H18-01	0	14.25	1.21E-07	14.2499999
16	20	ETHANOL	0.95	0	5.95E-26	0.95
		WATER	0.05	0	0.03816652	1.18E-02
		C8H18-01	0	19	1.22E-07	1.90E+01
16	50	ETHANOL	0.95	0	3.06E-32	0.95
		WATER	0.05	0	0.03725759	1.27E-02
		C8H18-01	0	47.5	1.19E-07	4.75E+01

Table A2: Raw stream data for pressure analysis

Pressure	Blending Ratio		aqueous in	hydrocarbon in	hydrocarbon out	aqueous out
0.8	6	ETHANOL	0.95	0	0.83998772	0.1100123
		WATER	0.05	0	0.01133654	0.0386635
		C8H18-01	0	5.7	5.69481152	0.0051885
1	6		0.95	0	0.84150267	0.1084973

		ETHANOL				
		WATER	0.05	0	0.01135855	0.0386415
		C8H18-01	0	5.7	5.69502994	0.0049701
1.5	6	ETHANOL	0.95	0	0.84156248	0.1084375
		WATER	0.05	0	0.01135267	0.0386473
		C8H18-01	0	5.7	5.69503926	0.0049607
2	6	ETHANOL	0.95	0	0.83967123	0.1103288
		WATER	0.05	0	0.01132574	0.0386743
		C8H18-01	0	5.7	5.69475683	0.0052432
3	6	ETHANOL	0.95	0	0.83943957	0.1105604
		WATER	0.05	0	0.01132272	0.0386773
		C8H18-01	0	5.7	5.69472197	0.005278
5	6	ETHANOL	0.95	0	0.8393784	0.1106216
		WATER	0.05	0	0.01132186	0.0386781
		C8H18-01	0	5.7	5.69471235	0.0052876
10	6	ETHANOL	0.95	0	0.83975415	0.1102459
		WATER	0.05	0	0.01133154	0.0386685
		C8H18-01	0	5.7	5.69476945	0.0052305
0.8	8	ETHANOL	0.95	0	0.92082875	0.0291712
		WATER	0.05	0	0.01241985	0.0375801
		C8H18-01	0	7.6	7.59993117	6.88E-05
1	8	ETHANOL	0.95	0	0.92118001	0.02882
		WATER	0.05	0	0.0124243	0.0375757
		C8H18-01	0	7.6	7.59993412	6.59E-05
1.5	8	ETHANOL	0.95	0	0.92131797	0.028682
		WATER	0.05	0	0.01242179	0.0375782
		C8H18-01	0	7.6	7.59993512	6.49E-05
2	8	ETHANOL	0.95	0	0.92131767	0.0286823
		WATER	0.05	0	0.01242235	0.0375776
		C8H18-01	0	7.6	7.59993513	6.49E-05
3	8	ETHANOL	0.95	0	0.92131734	0.0286827
		WATER	0.05	0	0.01242235	0.0375776
		C8H18-01	0	7.6	7.59993513	6.49E-05
5	8	ETHANOL	0.95	0	0.92131728	0.0286827
		WATER	0.05	0	0.01242235	0.0375776
		C8H18-01	0	7.6	7.59993513	6.49E-05
10	8	ETHANOL	0.95	0	0.92131727	0.0286827
		WATER	0.05	0	0.01242235	0.0375776
		C8H18-01	0	7.6	7.59993513	6.49E-05

Table A3: Raw stream data for temperature analysis

Blending Ratio	Temperature (C)	component	Aqueous feed	Fuel feed	Fuel product	Aqueous product
6	-25	ETHANOL	0.95	0	0.4190248	0.5309752
		WATER	0.05	0	0.0016023	0.0483977
		C8H18-01	0	5.6999999	5.520788	0.1792119
6	-15	ETHANOL	0.95	0	0.4967557	0.4532443
		WATER	0.05	0	0.0025704	0.0474296
		C8H18-01	0	5.6999999	5.5655271	0.1344729
6	0	ETHANOL	0.95	0	0.6276873	0.3223127
		WATER	0.05	0	0.0048515	0.0451485
		C8H18-01	0	5.6999999	5.6314679	0.0685321
6	12	ETHANOL	0.95	0	0.7365422	0.2134578
		WATER	0.05	0	0.007564	0.042436
		C8H18-01	0	5.6999999	5.6724206	0.0275793
6	20	ETHANOL	0.95	0	0.8038479	0.1461521
		WATER	0.05	0	0.0098012	0.0401988
		C8H18-01	0	5.6999999	5.6890796	0.0109203
6	25	ETHANOL	0.95	0	0.8394889	0.1105111
		WATER	0.05	0	0.0113285	0.0386715
		C8H18-01	0	5.7	5.6947371	0.0052629
6	30	ETHANOL	0.95	0	0.8699285	0.0800715
		WATER	0.05	0	0.0128964	0.0371036
		C8H18-01	0	5.6999999	5.6978484	0.0021516
6	40	ETHANOL	0.95	0	0.8940509	0.0559491
		WATER	0.05	0	0.0285357	0.0214643
		C8H18-01	0	5.6999999	5.6976252	0.0023747
6	60	ETHANOL	0.95	0	0.9145821	0.0354179
		WATER	0.05	0	0.0314976	0.0185024
		C8H18-01	0	5.6999999	5.6991359	0.0008641
8	-25	ETHANOL	0.95	0	0.5559554	0.3940446
		WATER	0.05	0	0.0021392	0.0478608
		C8H18-01	0	7.6	7.5055715	0.0944285
8	-15	ETHANOL	0.95	0	0.6505145	0.2994855
		WATER	0.05	0	0.0034015	0.0465985
		C8H18-01	0	7.6	7.5477522	0.0522478
8	0	ETHANOL	0.95	0	0.7897128	0.1602872
		WATER	0.05	0	0.0062035	0.0437965
		C8H18-01	0	7.6	7.5887256	0.0112744
8	12	ETHANOL	0.95	0	0.8735214	0.0764787
		WATER	0.05	0	0.0090869	0.0409131
		C8H18-01	0	7.6	7.598635	0.001365
8	20	ETHANOL	0.95	0	0.9077754	0.0422246
		WATER	0.05	0	0.0111398	0.0388602
		C8H18-01	0	7.6	7.599785	0.000215

8	25	ETHANOL	0.95	0	0.9210141	0.0289859
		WATER	0.05	0	0.0124134	0.0375866
		C8H18-01	0	7.6	7.5999328	6.72E-05
8	30	ETHANOL	0.95	0	0.9297515	0.0202485
		WATER	0.05	0	0.0136723	0.0363277
		C8H18-01	0	7.6	7.5999763	2.37E-05
8	40	ETHANOL	0.95	0	0.9396101	0.0103899
		WATER	0.05	0	0.016161	0.033839
		C8H18-01	0	7.6	7.5999953	4.68E-06
8	60	ETHANOL	0.95	0	0.9463511	0.0036489
		WATER	0.05	0	0.0211908	0.0288092
		C8H18-01	0	7.6	7.599999	1.05E-06

Table A4: Raw stream data for temperature swing process with temperature intervals of 55° and 25°

Blending Ratio:		aqueous feed	fuel feed	fuel after 1st decanting	fuel out	aqueous from 1st decanting	aqueous product
4	ETHANOL	0.95	0	0.679523	0.578702	0.270477	0.10076694
	WATER	0.05	0	0.015986	0.008428	0.034014	0.00755131
	C8H18-01	0	3.8	3.712179	3.658681	0.087821	0.05348021
8	ETHANOL	0.95	0	0.858953	0.822078	0.091047	0.03687185
	WATER	0.05	0	0.018668	0.011737	0.031332	0.00693027
	C8H18-01	0	7.6	7.594707	7.589125	0.005293	0.00558184
10	ETHANOL	0.95	0	0.888428	0.864938	0.061572	0.02348979
	WATER	0.05	0	0.018696	0.012076	0.031304	0.0066204
	C8H18-01	0	9.5	9.498419	9.496681	0.001581	0.00173803
15	ETHANOL	0.95	0	0.919249	0.908518	0.030751	0.01073129
	WATER	0.05	0	0.018367	0.012064	0.031633	0.00630225
	C8H18-01	0	14.25	14.24984	14.24967	0.000159	0.00016754
50	ETHANOL	0.95	0	0.944294	0.941977	0.005706	0.00231684
	WATER	0.05	0	0.020792	0.012915	0.029208	0.00787621
	C8H18-01	0	47.5	47.5	47.5	1.98E-06	8.09E-07

Table A5: Raw stream data for temperature swing process with temperature intervals of 55°, 40° and 25°

Blending Ratio		aqueous feed	fuel feed	fuel after 1st decanting	fuel after 2nd decanting	fuel out	aqueous from 1st decanting	aqueous from 2nd decanting	aqueous product
4	ETHANOL	0.95	0	0.65339398	0.62898571	0.58324458	0.29660601	0.02440827	0.04574113
	WATER	0.05	0	0.01432248	1.19E-02	0.00849744	0.03567751	2.44E-03	0.00338983
	C8H18-01	0	3.8	3.70022923	3.69E+00	3.66566385	0.09977082	1.00E-02	0.02456676

8	ETHANOL	0.95	0	0.85895266	8.45E-01	0.82752609	0.09104732	1.35E-02	0.01791047
	WATER	0.05	0.00E+00	1.87E-02	1.51E-02	1.18E-02	3.13E-02	3.53E-03	0.00331332
	C8H18-01	0	7.60E+00	7.59E+00	7.59E+00	7.59E+00	5.29E-03	1.23E-03	0.00278303
10	ETHANOL	0.95	0	0.88842789	0.87966044	0.86836102	0.0615721	0.00876744	0.01129942
	WATER	0.05	0	0.01869603	0.01528629	0.01212973	0.03130396	0.00340974	0.00315655
	C8H18-01	0	9.5	9.49841866	9.49805172	9.49720146	0.00158137	0.00036695	0.00085027
15	ETHANOL	0.95	0	0.91924911	0.91512505	0.91003662	0.03075088	0.00412405	0.00508842
	WATER	0.05	0	0.01836651	0.01506579	0.01208697	0.03163346	0.00330071	0.00297882
	C8H18-01	0	14.25	14.249841	14.2498068	14.2497268	0.00015925	3.42E-05	8.00E-05
50	ETHANOL	0.95	0	0.94429434	0.94329771	0.94223293	0.00570566	0.00099662	0.00106478
	WATER	0.05	0	0.02079156	0.01653661	0.01291804	0.02920843	0.00425495	0.00361857
	C8H18-01	0	47.5	47.499998	47.4999977	47.4999973	1.98E-06	3.24E-07	3.72E-07